MATERIALS CHEMISTRY FRONTIERS

CCS 中国化学会 CHINESE CHEMICAL SOCIETY

ICCAS

ROYAL SOCIETY OF CHEMISTRY

Chemical Perspectives of Heteroanionic Compounds and a Potential Playground for Multiferroics

Journal:	*Materials Chemistry Frontiers*
Manuscript ID	QM-REV-05-2024-000454.R1
Article Type:	Review Article
Date Submitted by the Author:	05-Sep-2024
Complete List of Authors:	Prasad, Karishma; Wichita State University, Chemistry and Biochemistry Nguyen, Vivian; Wichita State University, Chemistry and Biochemistry Ji, Bingheng; Wichita State University, Department of Chemistry and Biochemistry Quah, Jasmine; Wichita State University, Chemistry and Biochemistry Goodwin, Danielle; Wichita State University, Chemistry and Biochemistry Wang, Jian; Wichita State University, Chemistry

Chemical Perspectives of Heteroanionic Compounds and a Potential Playground for Multiferroics

Karishma Prasad [#], Vivian Nguyen [#], Bingheng Ji [#], Jasmine Quah, Danielle Goodwin, Jian Wang [*]

Department of Chemistry and Biochemistry, Wichita State University, Wichita, Kansas 67260, United States

Abstract

Heteroanionic compounds, which host two or more different anions, have appeared as a huge family of functional materials. Different from polyanionic compounds, there is no direct connection between anions within heteroanionic compounds. The connectivity between anions and central atoms constitutes various distorted basic building units (BBU). The linkage between BBUs further promotes the structural flexibility of heteroanionic compounds. Considering the diverse bonding nature of anion-metal interactions, which originate from the various physical and chemical properties of anions, explains the existence of many important applications of heteroanionic compounds. In this short review, we summarize the synthesis, structure examples, and physical applications of selected heteroanionic compounds. From a synthesis perspective, a deep understanding of crystal growth mechanisms and a better-controlled growth process should be emphasized in future research. The interactions between distinct anions and other featured elements such as elements with lone electron pairs, d^0 and d^{10} transition metals, etc., or other systems such as high entropy systems would further promote more interesting applications. Heteroanionic compounds, which exhibit comparable structure features with known multiferroics, might be a new paradise for discovering multiferroics. Machine learning and quickly developed calculation capabilities can also aid the study of heteroanionic compounds by understanding growth mechanisms, searching for new compounds, and targeting specific properties.

Introduction

Heteroanionic compounds, which constitute two or more different anions, have attracted growing interest due to their chemical flexibility [1-15]. The chemical flexibility originates from structural flexibility due to the presence of multiple anions. The chemical properties of common anions are tabulated in **Table 1**. From a structural perspective, the incorporation of two or three distinct anions naturally introduces the probability of intriguing structures plus the flexible connectivity of distinct anions to central metals. The first aspect of flexibility comes from the different chemical properties

Table 1. Chemical properties of selected anions [16].

	N	P	O	S	Se	F	Cl	Br	I
Atomic number	7	15	8	16	34	9	17	35	53
Melting point/ °C	-210	44	-218	112	217	-220	-101	-7.3	114
Ionic radius/ Shannon-Prewitt, Å (C.N.)	1.32(4)	2.12(6) [17]	1.26(6)	1.70(6)	1.84(6)	1.19(6)	1.67(6)	1.82(6)	2.06(6)
Electron negativity (Pauling)	3.0	2.1	3.5	2.5	2.4	4.0	3.0	2.8	2.5
Electron affinity/ kJ mol^{-1}	0	-72	-141	-200	-195	-328	-349	-325	-295
Oxidation states (as anions)	-3	-3	-2	-2	-2	-1	-1	-1	-1
Charge density/unit charge/ Å	2.27	1.42	1.59	1.18	1.09	0.84	0.60	0.55	0.49

of anions such as ionic radius, electronegativity, oxidation state, charge density, etc., which is shown in **Table 1**. The distinct anions connect to identical atoms or different atoms with comparable or different chemical bonding pictures. Selected compounds are shown in **Figure 1** to elucidate the fundamental building units and bonding picture of heteroanionic compounds. A good example would be $Na_3PO_yS_z$. As shown in **Figures 1a-1c**, three units $[POS_3]$, $[PO_2S_2]$, and $[PO_3S]$ act as major building units for Na_3POS_3 [18], $Na_3PO_2S_2$ [19], and Na_3PO_3S [20], respectively. The flexible $[PO_yS_z]$ units account for the structure difference (centrosymmetric vs. noncentrosymmetric) and exotic optical properties of this system [21-23]. The connectivity of different anions to the central metals raises the first degree of freedom of chemical flexibility of heteroanionic compounds. The

ordering and tilting of heteroanionic units add additional degrees of freedom to the compounds [4, 24]. The variable bond distance increases the distortion of basic building units as shown in **Figure 1d**. The La-Br bonds are much longer than the La-O bonds of $[LaO_6Br_3]$ units in $LaBrMoO_4$ [13, 25]. In addition to the obvious bond length difference, the bonding pictures of La-O interactions and La-Br interactions are clearly distinguishable. As shown in **Figures 1e** and **1f**, the ICOHP of La-Br interactions is slightly higher than La-O interactions even though the La-O interactions are much shorter than La-Br interactions. The ELF simulations indicate the ionic nature of both La-Br interactions and La-O interactions with the absence of ELF maxima within two adjacent atoms. The ELF maxima around Br is spherical while ELF around O is not, where O atoms have higher electronegativity than Br atoms with smaller sizes. The charge density of O is almost double that of Br as shown in **Table 1**. Heteroanionic compounds combine all these chemical and structural features in a single lattice, which explains the fantastic physical properties of heteroanionic compounds.

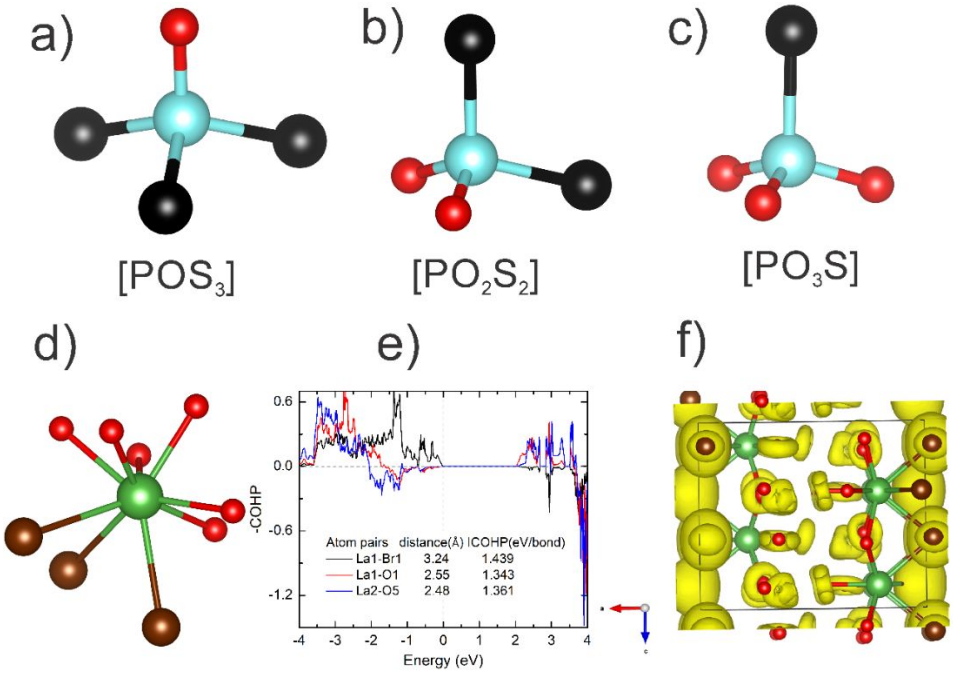

Figure 1. (a-c) $[POS_3]$ in Na_3POS_3($Cmc2_1$) [18], $[PO_2S_2]$ in $Na_3PO_2S_2$(*Pbca*) [19], and $[PO_3S]$ in Na_3PO_3S(*R*3*c*) [20], P: light blue, O: red, S: black; (d) $[LaO_6S_3]$ units in $LaBrMoO_4$, [13, 25] (e) crystal orbital Hamilton population (COHP) analysis of selected La-O and La-Br interactions; (f) electron localization function (ELF) of $LaBrMoO_4$ with η=0.6, La: green, O: red, Br: brown.

Heteroanionic compounds are different from polyanionic compounds, where there are anion-anion interactions existing within polyanionic clusters such as polyanionic $[AsO_4]^{3-}$ [2, 5, 26-31]. Heteroanionic compounds do not have direct anion-anion interactions. Heteroanionic compounds can be cataloged into two major groups: disordered heteroanionic compounds and ordered heteroanionic compounds. The disordered heteroanionic compounds refer to compounds having two or more anions jointly occupying the same atomic position such as Cd(SeTe) [32], SnO_2:F [33], and $LaFeAsO_{1-x}F_x$ [34]. The distinct anions occupy independent atomic positions within the ordered-heteroanionic compounds such as Na_3MoOF_3 [35], $LaGaOS_2$ [36], $KBe_2BO_3F_2$ [37], BiCuSeO [38],

CeZnSbO [39], etc. The different properties of various anions existing within one crystal lattice greatly enhance the structural flexibility of the heteroanionic compounds. The boundary of heteroanionic compounds was further extended recently via inserting H or C into known compounds such as $NdScSiC_x$ [40] and $CeTiGeH_x$ [41]. Furthermore, when heteroanionic building units interact with high entropy counterparts, high entropy heteroanionic compounds would be a new functional material family [42]. Heteroanionic compounds own many emerging physical properties including nonlinear optical (NLO) properties [37, 43-49], superconducting properties [34, 50-52], photoluminescent response [53-61] and thermoelectric properties [26-27, 62], etc., exist within heteroanionic compounds.

Hence, in this review, we plan to summarize the synthesis process and structural chemistry of many selected heteroanionic compounds. Important physical applications such as nonlinear optical (NLO) properties, superconducting properties, photoluminescent response, and thermoelectric properties were also summarized in this work. We hope to find some linkage from structural chemistry to the physical properties of heteroanionic compounds. We also want to provide an entry-level introduction to any researchers who are wanting to start to work on heteroanionic compounds. Many excellent review articles have been published recently to summarize various chemical properties of heteroanionic compounds [1, 2, 6, 63-69]. This review briefly summarizes the synthesis, structural chemistry, and applications including potential applications as multiferroics.

Synthesis perspective of heteroanionic compounds

Functionality arises from synthesis. The presence of more than one anion introduces structural flexibility into target systems while presenting more challenges for synthesis. One challenge is combining various anions within a single crystalline lattice using different sources of anions. Using the synthesis of oxyhalides as an example, oxides are a good source of incorporating oxygen anions. Sometimes carbonates can also be utilized as a source of oxides while taking into consideration the presence of CO_2. Halides are commonly employed to supply halogen anions. The distinct properties of oxides and halides such as melting temperature, vapor pressure, reactivity, etc., raise the difficulty of the synthesis process. Another difficulty in synthesizing heteroanionic compounds would be how to control the anion ratios within a single crystalline lattice, which is much harder. The anion ratios are one of the key components of the chemical properties of heteroanionic compounds. The growth of high-quality crystals of heteroanionic compounds is also not easy. The presence of distinct anions raises the difficulty of crystal growth. Hence, during the search for various heteroanionic compounds, many synthetic techniques were employed to target heteroanionic compounds. In this part, common synthetic methods of heteroanionic compounds are summarized.

2.1 Hydrothermal/solvothermal methods

Heating up mediums, which are used in a solvothermal reaction can utilize solvents such as water, alcohol, HF, etc., above their boiling point would generate a high-pressure environment. The presence of high pressure would enhance the solubility of many reactants such as oxides, which have limited solubility in many solvents under ambient conditions. In addition to increasing the solubility and reactivity of reactants, a solvothermal reaction will benefit the crystal growth and

the formation of heteroanionic compounds by controlling the temperature, pressure, reactants, type of mediums, etc. Hence, hydrothermal/solvothermal reactions are widely employed to grow heteroanionic compounds. In **Table S1** [70-74], some selected compounds represent the heteroanionic compounds synthesized by hydrothermal/solvothermal reactions. The broad applications of hydrothermal/solvothermal synthesis routes to synthesize heteroanionic compounds are also due to their capability of accessing metastable phases, which can be key for preparing heteroanionic compounds [75, 76].

2.2 High temperature flux methods

Flux methods were widely employed to grow inorganic solids, which can increase the contacting surface areas and improve the diffusion rates [77]. In addition to promoting chemical reactions, flux can also act as a reactant. For example, halide flux pairs usually have low eutectic temperatures, which are also good sources of halogen anions and flux. Oxides also commonly play a dual role of acting as flux and source of oxygen. Many factors should be considered such as solubility, inertness, melting temperature, toxicity, reaction vessel, price, etc., when choosing a flux [78]. We tabulated a few selected heteroanionic compounds in **Table S2** [79-83] which were grown by flux methods [84].

2.3 High temperature solid state methods

High temperature solid state reactions are another popular method to grow heteroanionic compounds. Solid state reactions have less chance of incorporating foreign elements compared to other methods. The selection of reactants is important for solid state reactions. Elements, binary or ternary compounds would dramatically affect final products due to the distinct properties of these reactants and different kinetic processes. The presence of low-melting reactants or reactants in small particle form would help speed up solid state reactions. One factor, which should be considered, would be the container of solid state reaction. Regular containers such as quartz tubes or carbonized quartz tubes do not tolerate high pressure. In the case of high pressure, sealed metal tubes such as tantalum tubes or niobium tubes would be a good choice. To further prevent possible contamination from metal tubes, a carbon crucible can be used. Sealing carbon crucibles in metal tubes with the protection of a quartz jacket can solve some problems. The sealed environment can efficiently prevent the oxidation of target compounds such as synthesizing oxychalcogenides. In this section, selected heteroanionic compounds grown by solid state method are summarized in **Table S3** [85-89]**.** In **Table S3**, some compounds are selected to represent the heteroanionic compounds synthesized by high temperature solid state methods.

2.4 Other methods and perspectives

Other methods can also be utilized to grow heteroanionic compounds such as chemical vapor transport (CVT) [90]. CVT process usually involves chemicals with high vapor pressure. Extreme conditions such as high pressure synthesis were also utilized to grow heteroanionic compounds such as $A_2NiO_2Ag_2Se_2$ (A=Sr, Ba) (7 GPa at 850 °C) [91] and $La_2B_2O_5(OH)_2$ (30 GPa and ~2,127 °C) [92]. Extreme conditions expand the synthesis boundary from the abovementioned methods. The topochemical reaction is also efficient to synthesize certain groups of heteroanionic compounds [93-95]. To gain a better understanding of the synthesis and crystal growth process of

heteroanionic compounds, in-situ study would be a powerful tool [26]. The rapid rise of computational power and the development of machine learning may be good assets for aiding the crystal growth of heteroanionic compounds [96-99].

Structural perspectives of heteroanionic compounds

Heteroanionic compounds are one of few inorganic groups, which exhibit super flexible and diverse structural chemistry. The crystal structure of heteroanionic compounds ranks from one-dimensional (1D) chains, two-dimensional (2D) layers, and three-dimensional (3D) frameworks. The basic building units of heteroanionic compounds are distorted and flexible due to the presence of two or more anions. The connectivity between these basic building units further promotes the structural diversity of heteroanionic compounds. In this part, we select some heteroanionic compounds to represent the diverse structure nature of each group. The basic building units are summarized. No comprehensive structure analysis and summary are present in this part. Many structure factors such as anion-order, anion-disorder, cation coordination environments (heteroleptic or homoleptic) are the dominant driving force for the chemical flexibility of heteroanionic compounds, which are summarized in many previous works [4, 29, 61, 100-102].

3.1 Oxohalides

Oxohalides are any compounds or molecules that constitute both oxygen and halogen atoms as anions, which include oxyfluorides, oxychlorides, oxybromides, and oxyiodides. In this part, some oxohalides were selected to present the diverse structural chemistry of oxohalides. More selected oxohalides were tabulated in **Table S4** [72-74, 85, 103-147] with an emphasis on basic building units.

$KBe_2(BO_3)F_2$ (KBBF). As the leading deep-ultraviolet nonlinear optical material, KBBF has kept sparking research interests [148]. KBBF crystallizes in the *R*32 (no.155) space group. The crystal structure of KBBF is shown in **Figure 2**. KBBF is alternatively constructed by [KF] layers and $[Be_2BO_3F]$ layers. The [KF] layers are made by $[KF_6]$ octahedron via sharing edges. The $[Be_2BO_3F]$ layers are built by planar $[BO_3]$ units and distorted $[BeO_3F]$ tetrahedron, which are interlinked by sharing vertices. The connectivity between two layers is by ionic K-F interactions, which makes the crystal growth of KBBF very challenging [149-152]. $KBe_2(BO_3)F_2$ has one independent K cation and one independent Be cation. K is homoleptic with six surrounding F atoms and Be is heteroleptic with three surrounding O atoms and one surrounding F atom.

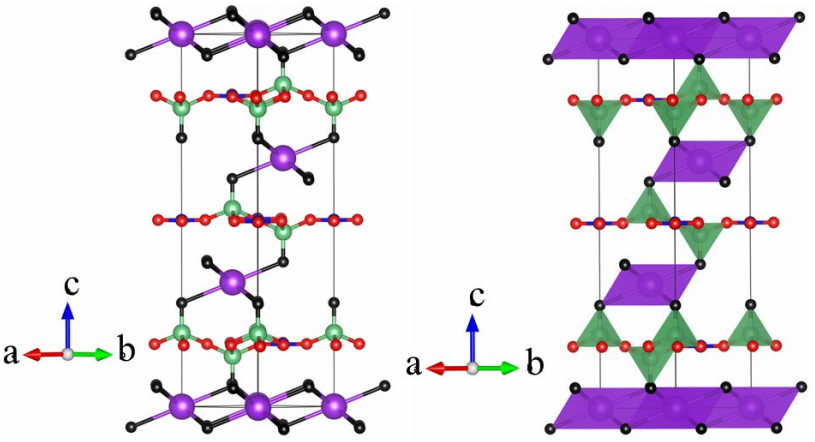

Figure 2. Ball-stick (left) and polyhedral (right) structural models of KBBF. K: purple, B: blue, Be: light green, O: red, F: black.

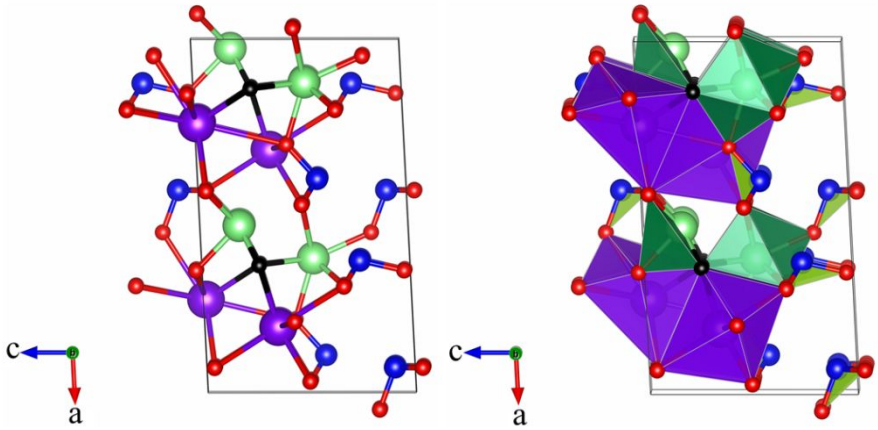

Figure 3. Ball-stick (left) and polyhedral (right) structural models of $Rb_2Bi_2(SeO_3)_3F_2$. Rb: purple, Bi: light green, Se: blue, O: red, F: black.

$Rb_2Bi_2(SeO_3)_3F_2$ crystallizes in the *Cm* (no. 8) space group [72]. The crystal structure of $Rb_2Bi_2(SeO_3)_3F_2$ is shown in **Figure 3**. The 3D framework of $Rb_2Bi_2(SeO_3)_3F_2$ is constructed by $[Bi_2O_9F_2]$ chains that are further interconnected by adjacent chains through bridging selenite groups. The basic building units would be $[SeO_3]$ pyramidal units, distorted $[BiO_6F_2]$, and $[BiO_5F_2]$ polyhedra. $Rb_2Bi_2(SeO_3)_3F_2$ exhibits a high second harmonic generation response of 14.4(2)× KH_2PO_4 (KDP). $Rb_2Bi_2(SeO_3)_3F_2$ has two independent Bi cations and two independent Rb cations. Bi1 is heteroleptic with six surrounding O atoms and two surrounding F atoms. Bi2 is heteroleptic with three surrounding O atoms and two surrounding F atoms. Rb1 and Rb2 are heteroleptic with eight surrounding O atoms and two surrounding F atoms.

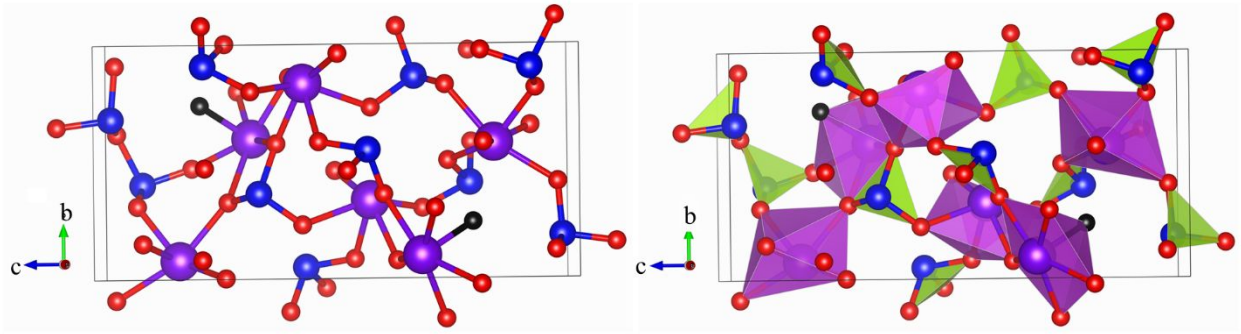

Figure 4. Ball-stick (left) and polyhedral (right) structural models of $Bi_3(SeO_3)_3(Se_2O_5)F$. Bi: purple, Se: blue, O: red, F: black.

$Bi_3(SeO_3)_3(Se_2O_5)F$ crystallizes in the $P2_1$ (no. 4) space group [73], which is shown in **Figure 4**. The 3D framework of $Bi_3(SeO_3)_3(Se_2O_5)F$ is constructed by $[BiO_7]$, $[BiO_6F]$, $[SeO_3]$, and $[Se_2O_5]$ units, where the connectivity between them are via vertices or edges. Both Bi^{3+} and Se^{4+} have stereoactive lone pairs, which significantly contribute to the SHG response. $Bi_3(SeO_3)_3(Se_2O_5)F$ exhibits a large SHG response of 8×KDP. $Bi_3(SeO_3)_3(Se_2O_5)F$ has three independent Bi cations. Bi1 is homoleptic with five surrounding O atoms. Bi2 is heteroleptic with five surrounding O atoms and one surrounding F atom. Bi3 is homoleptic with six linked O atoms.

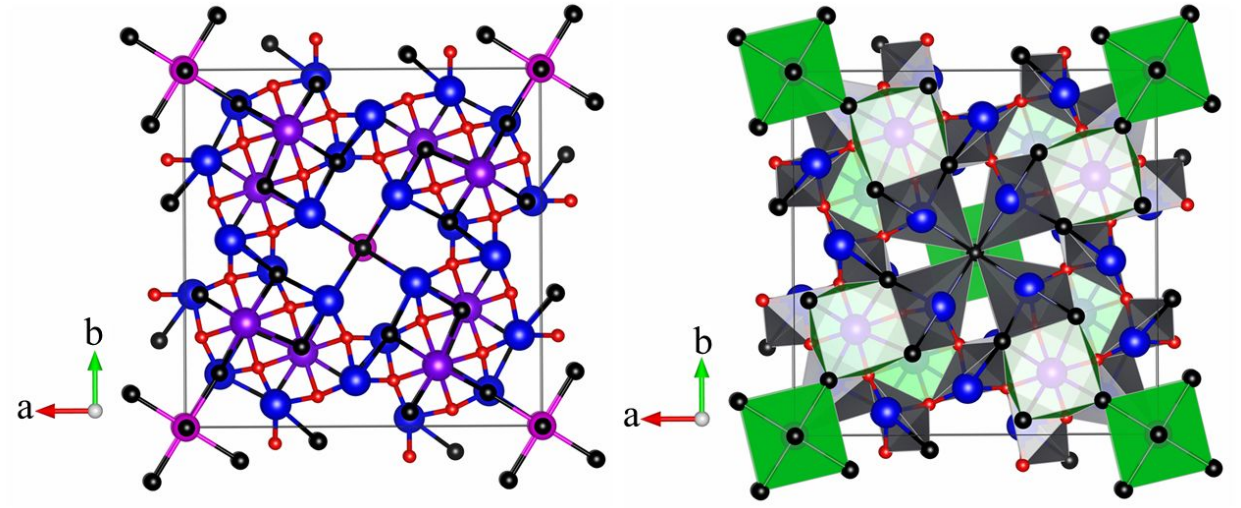

Figure 5. Ball-stick (left) and polyhedral (right) structural models of $Ba_8SrPb_{24}O_{24}Cl_{18}$. Ba: purple, Sr: pink, Pb: blue, O: red, Cl: black.

$Ba_8SrPb_{24}O_{24}Cl_{18}$ crystallizes in the $I4/m$ (no. 87) space group [153], which is shown in **Figure 5**. The complex 3D framework of $Ba_8SrPb_{24}O_{24}Cl_{18}$ is constructed by $[SrCl_6]$, $[BaO_4Cl_4]$, and $[Pb_3O_5]$ units. Another view of the crystal structure of $Ba_8SrPb_{24}O_{24}Cl_{18}$ would be the 2D multimember−ring layers sandwiched by $[SrCl_6]$ layers. The coexistence of alkali-earth metals Sr and Ba and SCALP cation Pb lead to rich structural chemistry here. As the first alkali-earth metal lead(II) oxyhalide, $Ba_8SrPb_{24}O_{24}Cl_{18}$ exhibits a moderate band gap of 3.09 eV and moderate

birefringence of 0.014@1064 nm. $Ba_8SrPb_{24}O_{24}Cl_{18}$ has one independent Ba cation, one independent Sr cation, and three independent Pb cations. Ba is heteroleptic with four surrounding O atoms and four surrounding Cl atoms. Sr is homoleptic with six surrounding Cl atoms. Pb1 is heteroleptic with two surrounding O atoms and three surrounding Cl atoms. Pb2 and Pb3 are heteroleptic with three surrounding O atoms and one surrounding Cl atom.

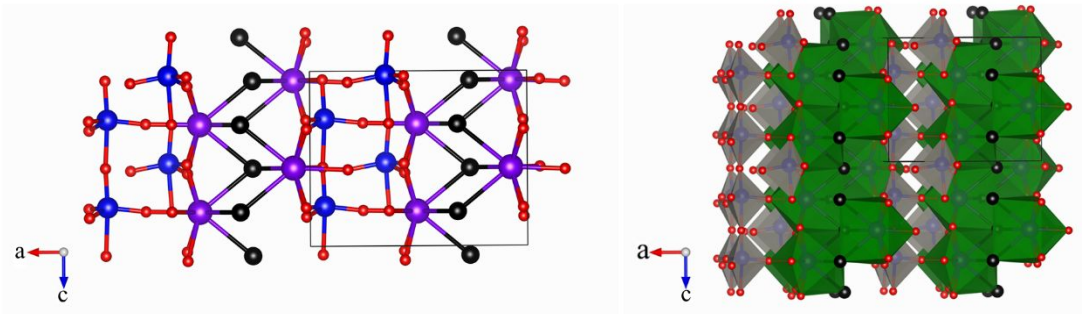

Figure 6. Ball-stick (left) and polyhedral (right) structural models of $CeBrWO_4$. Ce: purple, W: blue, O: red, Br: black.

$CeBrWO_4$ crystallizes in the *Pc* (no.7) space group, which is shown in **Figure 6** [12]. The 3D framework of $CeBrWO_4$ is made of two-dimensional (2D) $[CeBrO_4]^{6-}$ strips and one-dimensional (1D) $[WO_5]$ strands. The 1D $[WO_5]$ strands are built by distorted $[WO_5]$ trigonal bipyramids, which connect to each other via apical oxygen atoms and run along the [001] direction. The 2D $[CeBrO_4]^{6-}$ strips are built by distorted tetracapped trigonal prisms $[CeO_6Br_3]$, where six oxygen atoms and three bromine atoms surround the central Ce atoms. The presence of partially filled 4f orbitals of Ce set $CeBrWO_4$ is suitable for infrared nonlinear applications compared to isostructural $LaBrWO_4$, which is a good ultraviolet NLO material [13]. $CeBrWO_4$ has two independent Ce cations and two independent W cations. Ce1 and Ce2 are heteroleptic with six surrounding O atoms and three surrounding Br atoms. W1 and W2 are homoleptic with five surrounding O atoms.

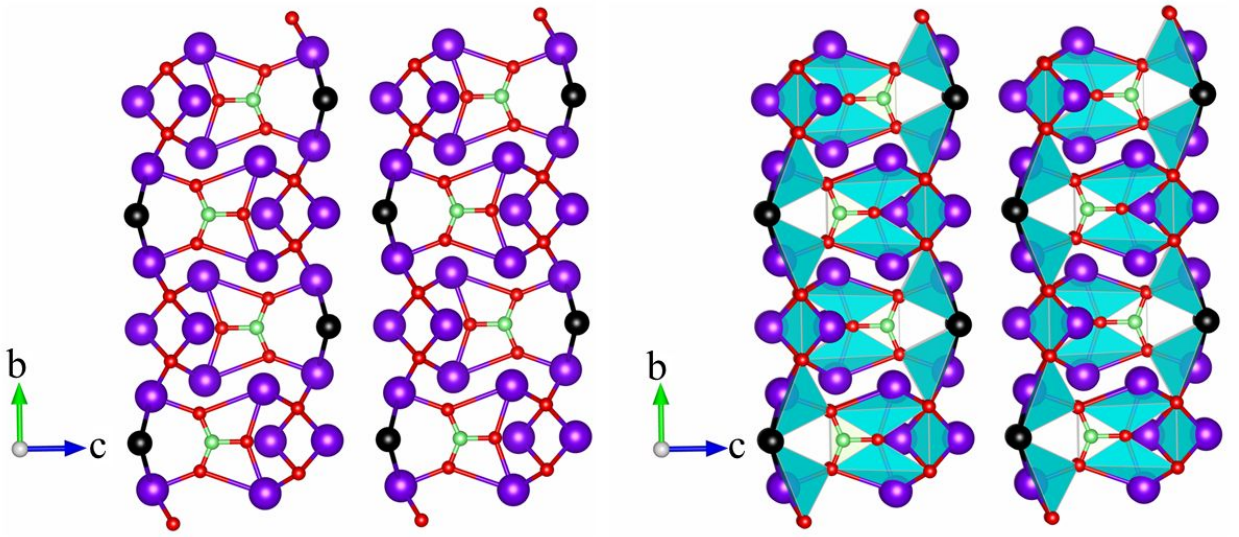

Figure 7. Ball-stick (left) and polyhedral (right) structural models of $(O_2Pb_3)_2(BO_3)I$. Pb: purple, B: light green, O: red, I: black.

$(O_2Pb_3)_2(BO_3)I$ crystallizes in the *Pmmn* space group (no. 59), which is shown in **Figure 7** [154]. $(O_2Pb_3)_2(BO_3)I$ is constructed by 1D $[O_2Pb_3]$ double chains, $[BO_3]$ units, and $[IPb_8]$ units. The 1D $[O_2Pb_3]$ double chains are made by $[O_2Pb_6]$ dimers, which are interconnected by two $[OPb_4]$ tetrahedra via edge-sharing. The 2D ($[O_2Pb_3][BO_3]$) layers are constructed by 1D $[O_2Pb_3]$ double chains interlinked by $[BO_3]$ units. The I^- ions, which are connected to Pb atoms, are located between 2D ($[O_2Pb_3][BO_3]$) layers. $(O_2Pb_3)_2(BO_3)I$ was predicted to exhibit moderate birefringence of about 0.072@1064 nm. $(O_2Pb_3)_2(BO_3)I$ has four independent Pb cations. Pb1, Pb3 and Pb4 are homoleptic with four surrounding O atoms, and Pb2 is heteroleptic with two surrounding O atoms and two surrounding I atoms.

3.2 Oxysulfides and Oxyselenides

Oxychalcogenides are any compounds or molecules that constitute both oxygen and chalcogen atoms as anions including oxysulfides and oxyselenides. Oxygen and other chalcogen elements have the same oxidation states with different atomic sizes or electronegativity, which still results in flexible structures. Selected compounds are presented herein to showcase the structures of oxychalcogenides. More compounds are listed in **Table S5** [91, 155-162].

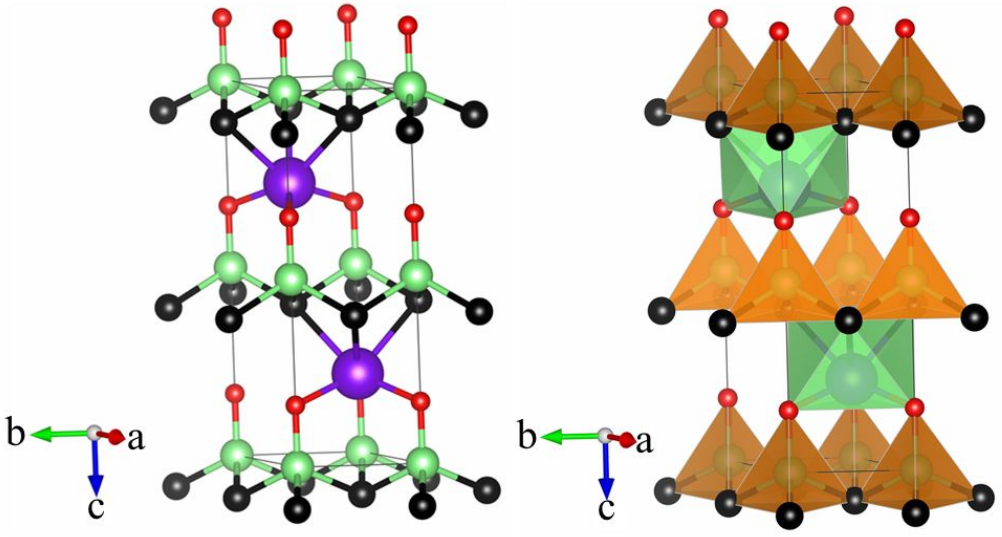

Figure 8. Ball-stick (left) and polyhedral (right) structural models of CaOFeS. Ca: purple, Fe: light green, O: red, S: black.

CaOFeS crystallizes in the $P6_3mc$ space group (no. 186), which is shown in **Figure 8** [163]. The 3D framework of CaOFeS is alternately constructed by layers of [CaO] and [FeS], which exhibit clear layered features. The basic building units are $[FeS_3O]$ tetrahedra and $[CaS_3O_3]$ octahedra. CaOFeS owns the existence of two-dimensional (2D) short-range ordering. Geometrically frustrated compound condenses into a partial long-range ordered state with AFM coupled Fe layers below Tn = 40.6 K. CaOFeS belongs to the CaOZnS structure family with many isostructural compounds known. CaOFeS has one independent Ca cation and one independent Fe cation. Ca is heteroleptic

with four surrounding S atoms and three surrounding O atoms, and Fe is heteroleptic with three surrounding S atoms and one surrounding O atom.

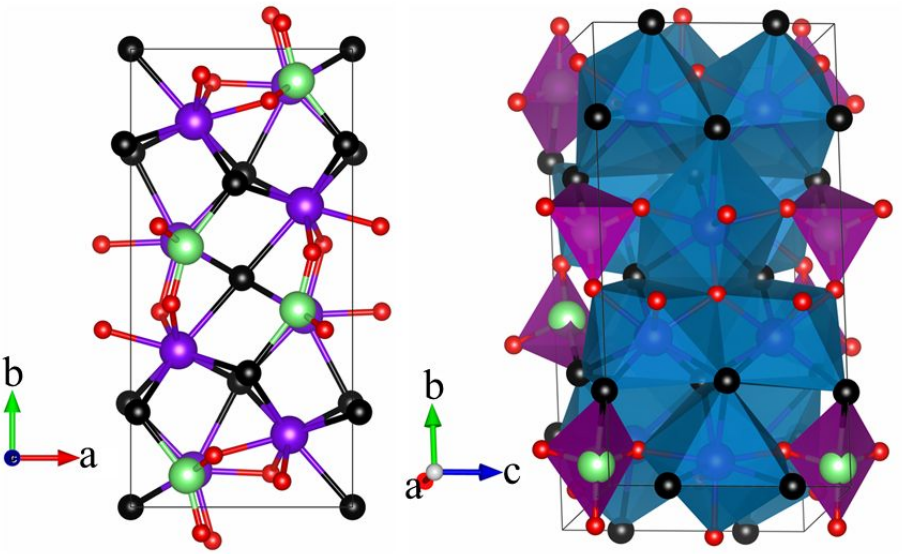

Figure 9. Ball-stick (left) and polyhedral (right) structural models of $Ce_3NbO_4S_3$. Ce: purple, Nb: light green, O: red, S: black.

$Ce_3NbO_4S_3$ crystallizes in the *Pbam* (no.55) space group, which is shown in **Figure 9** [164]. The 3D framework of $Ce_3NbO_4S_3$ is constructed by highly distorted $[NbO_3S_3]$ octahedra, $[CeO_3S_5]$ and $[CeO_4S_4]$ units. Certain oxygen and sulfur atoms are not connected to niobium but are exclusively surrounded by cerium. All polyhedron are connected to each other through the vertex. Magnetic susceptibility measurements indicated a weak antiferromagnetic coupling within $Ce_3NbO_4S_3$ with a Weiss-constant θp = - 12(1) K. No magnetic ordering was detected above 2 K. $Ce_3NbO_4S_3$ has two independent Ce atoms and one independent Nb atom. Ce1 is heteroleptic with five surrounding S atoms and three surrounding O atoms, and Ce2 is heteroleptic with four surrounding S atoms and four surrounding O atoms. Nb is heteroleptic with one S atom and three O atoms as coordination environment.

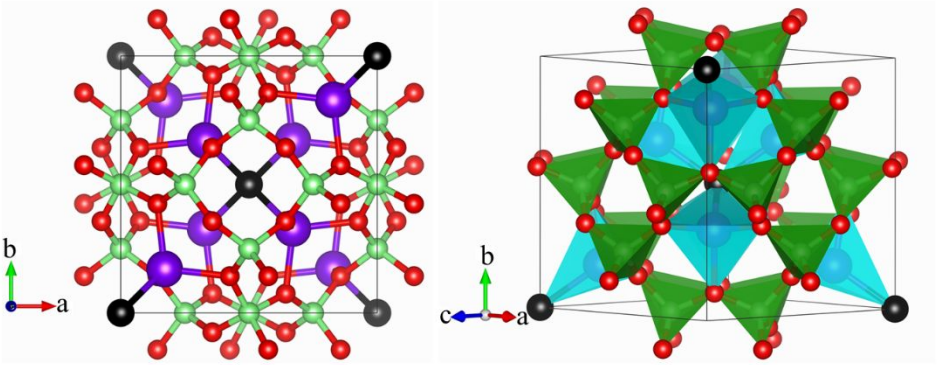

Figure 10. Ball-stick (left) and polyhedral (right) structural models of $Zn_4B_6O_{12}S$. Zn: purple, B: light green, O: red, S: black.

$Zn_4B_6O_{12}S$ crystallizes in *I*-43*m* (no. 217) space group, which belongs to the $Zn_4B_6O_{13}$ structure type as shown in **Figure 10** [81]. Tetrahedra are basic building units for $Zn_4B_6O_{12}S$. A truncated octahedron was constructed by the quadrangles and hexagons via sharing corners. All Zn atoms locate toward alternating hexagonal faces. $Zn_4B_6O_{12}S$ has a SHG around 1.9 × KDP at 1.604 μm, and its photo-current is 2.1 $\mu A/cm^2$. $Zn_4B_6O_{12}S$ has one independent Zn cation and one independent B cation. Zn is heteroleptic with one surrounding S atoms and three surrounding O atoms, and B is homoleptic with four surrounding O atoms.

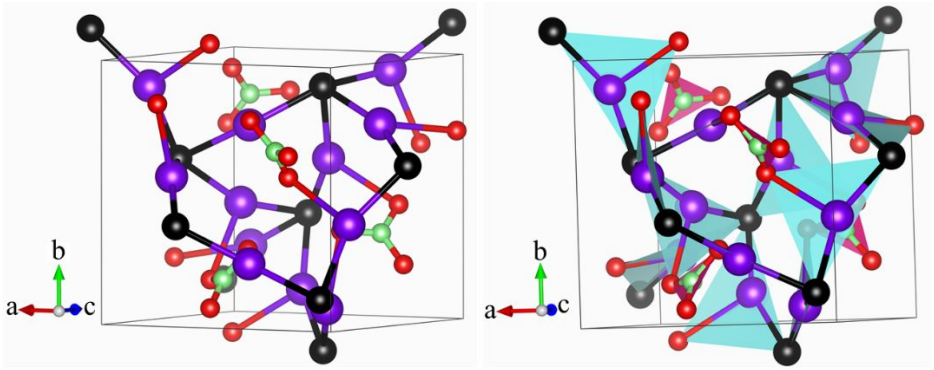

Figure 11. Ball-stick (left) and polyhedral (right) structural models of $Ag_3S(NO_3)$. Ag: purple, N: light green, O: red, S: black

$Ag_3S(NO_3)$ crystallizes in the $P2_13$ (no. 198) space group, which is shown in **Figure 11** [165]. The 3D positively-charged $[Ag_3S]^+$ frameworks were constructed by $[SAg_6]$ octahedron, where the $[NO_3]^-$ fills all cavities. The $[Ag_3S]^+$ cationic framework is formed by two crystallographically independent atoms, sulfur and silver. $Ag_3S(NO_3)$ shows semiconducting behavior with a band gap of ca. 1.2 eV. $Ag_3S(NO_3)$ has one independent Ag cation and one independent N cation. Ag is heteroleptic with two surrounding S atoms and one surrounding O atom, and N is homoleptic with three surrounding O atoms.

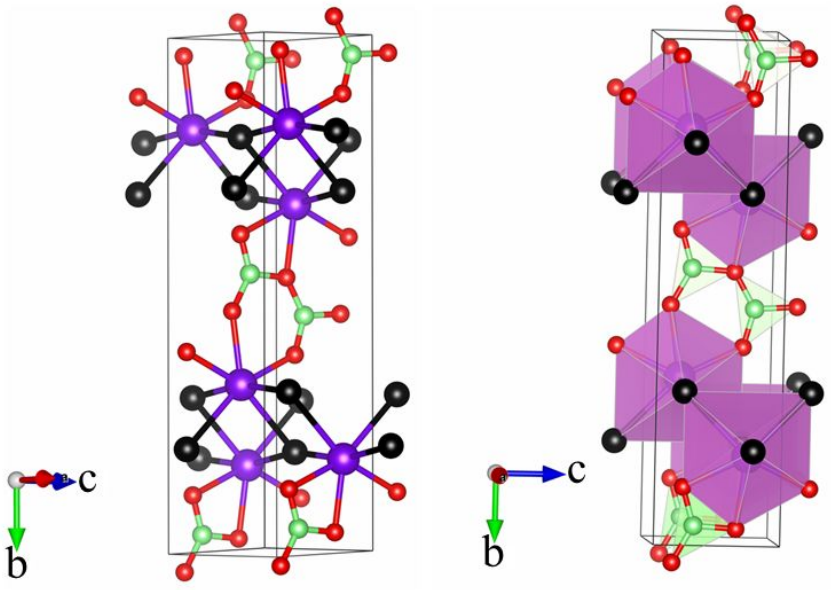

Figure 12. Ball-stick (left) and polyhedral (right) structural models of $YSeBO_2$. Y: purple, B: light green, O: red, Se: black

$YSeBO_2$ crystallizes in the *Cmc*2_1 (no. 36) space group, which is presented in **Figure 12** [161]. The 3D framework of $YSeBO_2$ is built by two basic building units, $[BO_3]^{3-}$ planar triangles and $[YO_3Se_4]^{11-}$ pentagonal bipyramids, which are interlinked via sharing edges. The structure feature is the $[YSeBO_2]_n$ planar belt. $YSeBO_2$ has a large bandgap of 3.45 eV. $YSeBO_2$ is a type-I phase matching material. $YSeBO_2$ has one independent Y cation and one independent B cation. Y is heteroleptic with four surrounding Se atoms and three surrounding O atoms, and B is homoleptic with three linked O atoms.

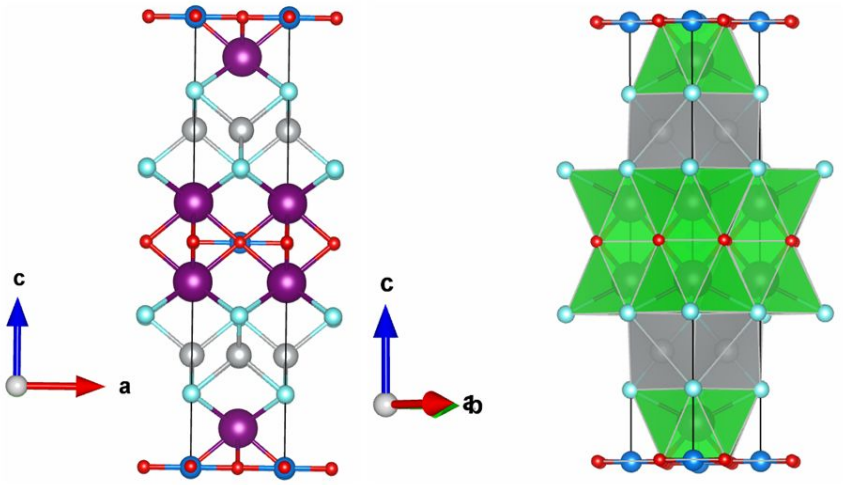

Figure 13. Ball-stick (left) and polyhedral (right) structural models of $Ba_2NiO_2Ag_2Se_2$. Ba: purple, Ni: blue, Ag: gray, O: red, Se: light blue.

$Ba_2NiO_2Ag_2Se_2$ crystallizes in the *I*4/*mmm* (no.139) space group, which is shown in **Figure 13** [91]. The 3D framework of $Ba_2NiO_2Ag_2Se_2$ contains clear layered features. The $[Ag_2Se_2]$ layers and $[NiO_2]$ layers are interconnected by Ba-Se and Ba-O interactions, which feature NiO_2 square net. Ba atoms are sandwiched between $[NiO_2]$ layer and $[Ag_2Se_2]$ layers. Each Ba is connected to four oxygen and four selenium atoms. $Ba_2NiO_2Ag_2Se_2$ exhibits a G-type spin order at 130 K and has strong in-plane antiferromagnetic interaction. $Ba_2NiO_2Ag_2Se$ has one independent Ba cation, one independent Ni cation, and one independent Ag cation. Ni is homoleptic with four surrounding O atoms, and Ag is homoleptic with four surrounding Se atoms.

3.3 Oxypnictides

Oxypnictides refers to compounds that constitute both oxygen and pnictogen elements as anions including anion groups of O-N, O-P, O-As, etc. Oxygen and other pnictogen elements have different oxidation states with different atomic sizes or electronegativity, which results in diverse structures. Selected compounds are presented herein to showcase the structures of oxypnictides. More compounds are listed in **Table S6** [82, 87, 89, 166-248].

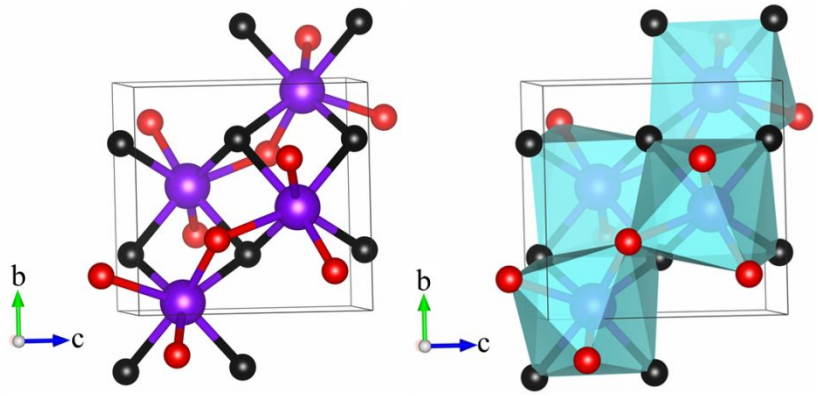

Figure 14. Ball-stick (left) and polyhedral (right) structural models of NbNO. Nb: purple, O: red, N: black.

NbON crystallizes in the $P2_1/c$ (no.14) space group, which is shown in **Figure 14** [249]. There is only one basic building unit of $[NbO_3N_4]$ within NbON. The $[NbO_3N_4]$ units connect to each other via sharing edges to form the 3D framework of NbON. NbON exhibits promising electrochemical behavior versus Li. The stabilized capacity was 250 $AhKg^{-1}$ with a cutoff potential of 0.05 V. NbON has one independent Nb cation, which is heteroleptic with three surrounding O and four surrounding N atoms.

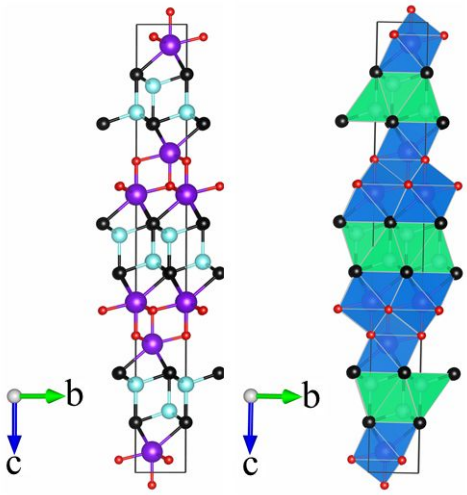

Figure 15. Ball-stick (left) and polyhedral (right) structural models of YZnPO. Y: purple, Zn: light blue, O: red, P: black

YZnPO crystallizes in the *R*-3*m* (no. 166) space group, which is shown in **Figure 15** [250]. The 3D framework of YZnPO is constructed by [ZnP] layers and [YO] layers. The basic building units within YZnPO are [ZnP_4] tetrahedron and [YO_4P_3] units. [ZnP] layers are made [ZnP_4] tetrahedra by edge-sharing and corner-sharing. Y atoms connect to oxygen atoms via edge-sharing and corner-sharing to form [YO] layers. Other isostructural compounds are REZnAsO (RE = Y, La–Nd, Sm, Gd–Er). YZnPO has one independent Y cation and one independent Zn cation. Y is heteroleptic with three surrounding P atoms and four surrounding O atoms. Zn is homoleptic with four connected P atoms.

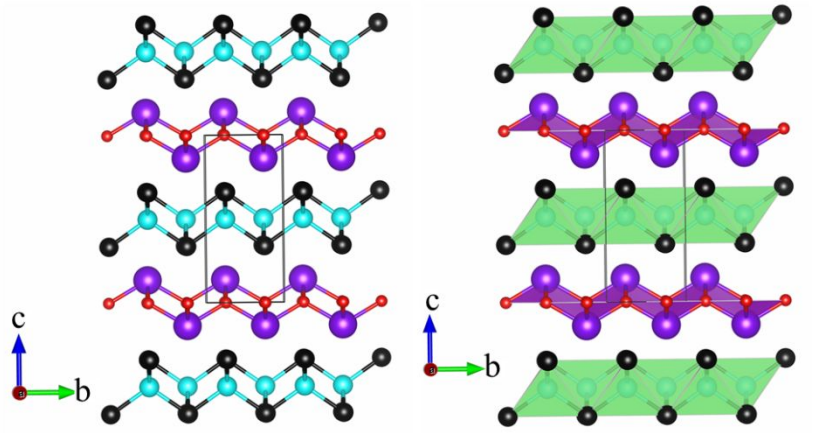

Figure 16. Ball-stick (left) and polyhedral (right) structural models of GdFeAsO. Gd: purple, Fe: light blue, O: red, As: black

GdFeAsO crystallizes in the *P*4/*nmm* (no. 129) space group, which is shown in **Figure 16** [182]. GdFeAsO belongs to the ZrCuSiAs structure type. GdFeAsO is built by two alternating layers of [ZnAs] layers and [GdO] layers. The square planar [GdO_4] units construct the [GdO] layers via edge-sharing. The [ZnAs] layers are constructed by [$ZnAs_4$] tetrahedra. The layer structural

features host very rich physical properties for many isostructural compounds such as (other compounds of this structure type are: ThFeAsN with superconducting properties [251]. LaCuSO with diamagnetic properties [252] and EuCuSF with optical properties [252]. GdFeAsO has one independent Gd cation and one independent Fe cation. Gd is homoleptic with four coordinated O atoms, and Fe is homoleptic with four coordinated As atoms.

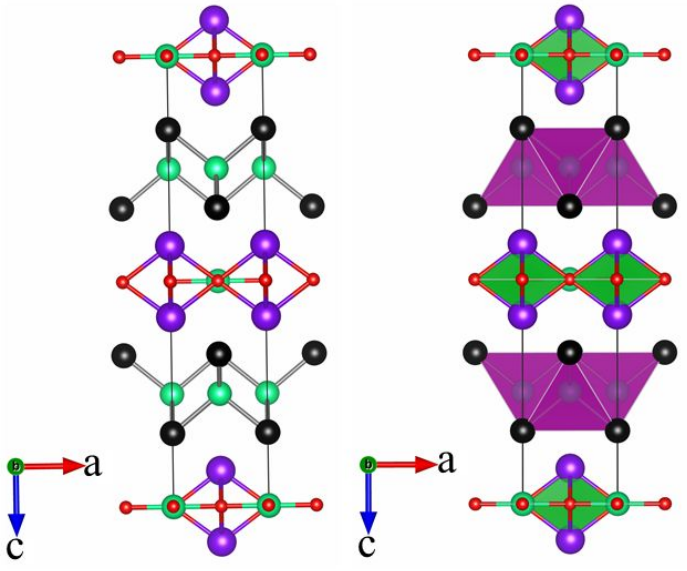

Figure 17. Ball-stick (left) and polyhedral (right) structural models of $Sr_2Mn_3Sb_2O_2$, Sr: purple, Mn: light green, O: red, Sb: black

$Sr_2Mn_3Sb_2O_2$ crystallizes in the *I*4/*mmm* (no. 139) space group, which is shown in F**igure 17** [187]**.** $Sr_2Mn_3Sb_2O_2$ contains a CuO_2-type layer created by square planar corner-sharing MnO_4 units. Mn forms a tetrahedra with four Sb atoms which are edge-sharing with three other tetrahedra to create a $BaAl_4$-type layer. These [MnO_2] and [Mn_2Sb_2] layers sandwich Sr atoms. $Sr_2Mn_3Sb_2O_2$ has one independent Sr cation and two independent Mn cations. Sr is homoleptic with four coordinated O atoms. Mn1 is homoleptic with four coordinated O atoms, and Mn2 is homoleptic with three coordinated Sb atoms.

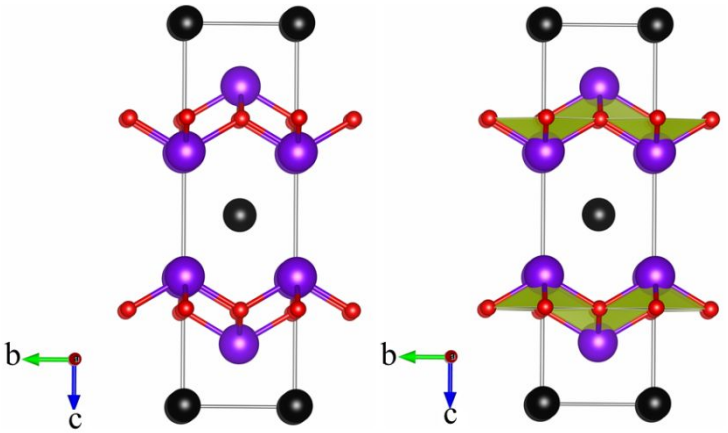

Figure 18. Ball-stick (left) and polyhedral (right) structural models of Ce_2O_2Bi, Ce: purple O: red, Bi: black

Ce_2O_2Bi crystallizes in in *I*4/*mmm* (no. 139) space group, which belongs to the Th_2TeN_2 structure type (anti-$ThCr_2Si_2$) [222] as shown in **Figure 18**. Ce is coordinated by four oxygen atoms in a distorted square planar geometry. These [CeO_4] units connect together by edge-sharing through O atoms which creates a CeO layer. CeO layers are separated by a Bi square net layer. Ce_2O_2Bi exhibited metallic properties. Ce_2O_2Bi has one independent Ce cation. Ce is homoleptic with four coordinated O atoms.

3.4. Other heteroanionic combinations (N-Cl, S-Cl, Se-Cl, P-Cl, P-Br, etc.)

As stated in the introduction, many possible combinations of various anions result in more heteroanionic compounds beyond oxygen-containing materials. In this part, we selected a few samples to present the flexible structural chemistry. Selected examples are shown in **Table S7** [79, 83, 253-289].

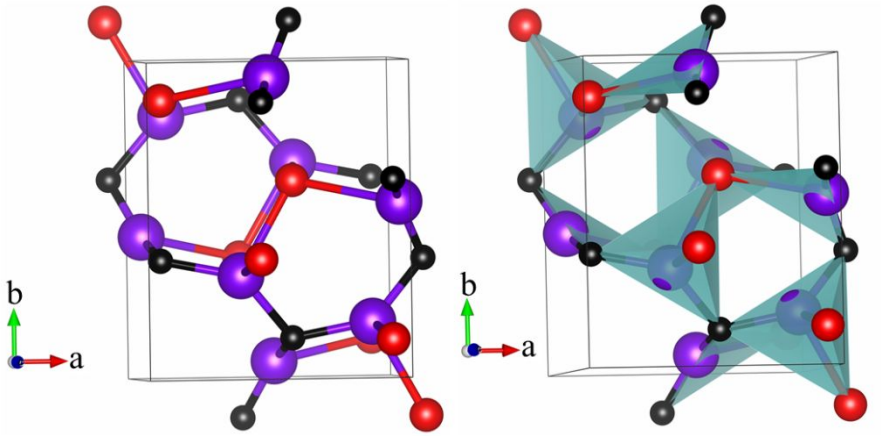

Figure 19. Ball-stick (left) and polyhedral (right) structural models of Zn_2NCl, Zn: purple, N: red, Cl: black

Zn_2NCl crystallizes in the *Pna*2_1 (no. 33) space group, which is shown in **Figure 19** [83, 290]. The basic building units of Zn_2NCl are distorted [ZnN_2Cl_2] tetrahedra. The highly distorted [ZnN_2Cl_2]

tetrahedra connect to each other via sharing N and Cl atoms to form the 3D framework. Zn_2NCl exhibits balanced NLO properties (bandgap: 3.21 eV, SHG: 0.9×AGS). Zn_2NCl has two independent Zn cations. Zn1 is heteroleptic with two surrounding N atoms and two surrounding Cl atoms, and Zn2 is heteroleptic with two surrounding N atoms and one surrounding Cl atom.

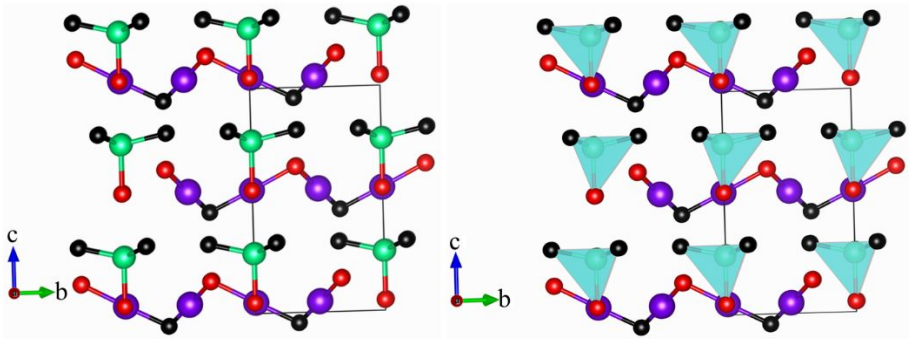

Figure 20. Ball-stick (left) and polyhedral (right) structural models of $Hg_3ZnS_2Cl_4$, Hg: purple, Zn: light green, S: red, Cl: black

$Hg_3ZnS_2Cl_4$ crystallizes in the *P*6$_3$*mc* (no. 186) space group, which is shown in **Figure 20** [79, 291]. $Hg_3ZnS_2Cl_4$ features a 2D layered structure. The 12-membered [$Hg_6S_3Cl_3$] rings are interconnected to form chair-like conformation 2D slabs. The 2D layers are adjacent to [$ZnSCl_3$] tetrahedra. The basic building units for $Hg_3ZnS_2Cl_4$ are linear [HgSCl] units and [$ZnSCl_3$] tetrahedra. $Hg_3ZnS_2Cl_4$ is a semiconductor with an experimentally measured bandgap of 2.65 eV. $Hg_3ZnS_2Cl_4$ has one independent Hg cation and one independent Zn cations. Hg is heteroleptic with one surrounding S atom and one surrounding Cl atom. Zn is heteroleptic with one surrounding S atom and three linked Cl atoms.

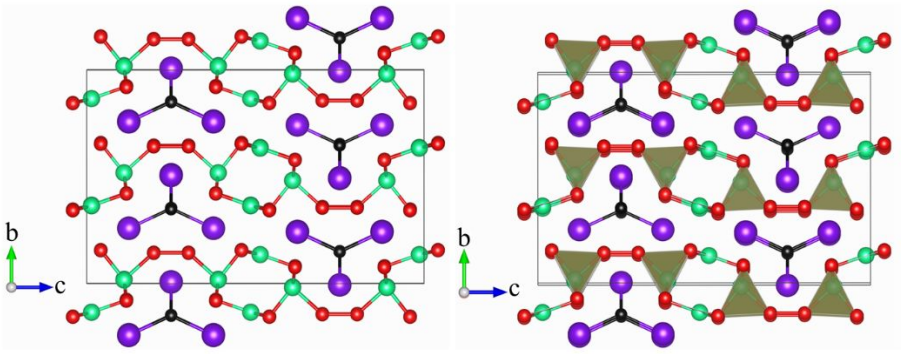

Figure 21. Ball-stick (left) and polyhedral (right) structural models of $La_3Zn_4P_6Cl$, La: purple, Zn: light green, P: red, Cl: black

$La_3Zn_4P_6Cl$ crystallizes in the orthorhombic space group *Cmcm* (no. 63), which is shown in **Figure 21** [272]. In $La_3Zn_4P_6Cl$, 2D [Zn_4P_6] layers sandwich 1D [La_3Cl] chains. 2D [Zn_4P_6] layers are constructed by 1D [Zn_4P_4] tubes linked to each other via homoatomic P-P bonds. $La_3Zn_4P_6Cl$ is constructed by trigonal planar [ZnP_3] units, [ZnP_4] tetrahedra, and [$ClLa_4$] tetrahedra. $La_3Zn_4P_6Cl$ is a small bandgap semiconductor of 0.24 eV. $La_3Zn_4P_6Cl$ has two independent La cations and two independent Zn cations. La1 is heteroleptic with six surrounding P atoms and one surrounding Cl

atom, and La2 is heteroleptic with six surrounding P atoms and two surrounding Cl atoms. Zn1 is homoleptic with four connected P atoms, and Zn2 is homoleptic with three surrounding P atoms.

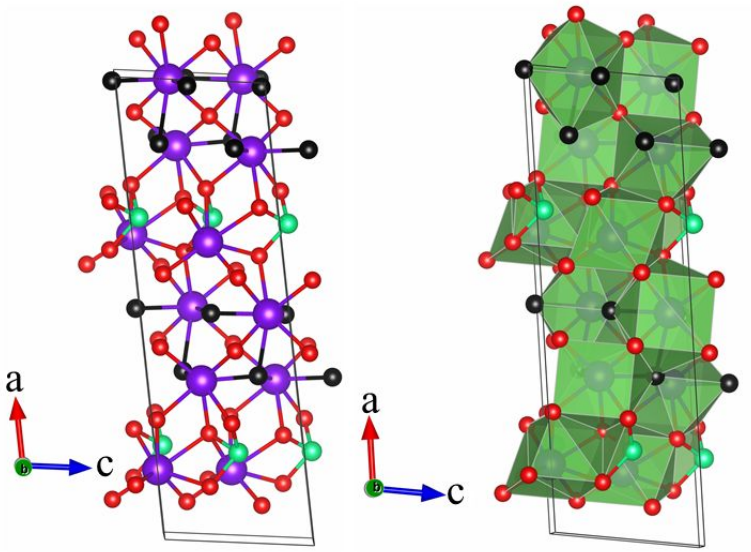

Figure 22. Ball-stick (left) and polyhedral (right) structural models of $La_3AsS_5Br_2$, La: purple, As: light green, S: red, Br: black

$La_3AsS_5Br_2$ crystallizes in the acentric monoclinic space group *Cc* (no. 9), which is shown in **Figure 22** [14]. The 3D framework of $La_3AsS_5Br_2$ is constructed by $[LaS_5Br_3]$ bicapped trigonal prisms, $[La_3S_7]$ capped trigonal prisms, and $[AsS_3]$ trigonal pyramids, which are linked to each other. $La_3AsS_5Br_2$ is a semiconductor of 2.83 eV with a moderate SHG response of 0.23× AGS for the sample of 150–200 μm particle size. $La_3AsS_5Br_2$ has three independent La cations and one independent As cation. La1 is heteroleptic with four surrounding S atoms and three surrounding Br atoms, La2 is heteroleptic with five surrounding S atoms and two surrounding Br atoms, La3 is homoleptic with seven surrounding S atoms. As is homoleptic with three surrounding S atoms.

Selected physical applications of heteroanionic compounds

4.1 Nonlinear optical (NLO) properties

One important way to expand the laser frequency is via the second harmonic generation (SHG) process, where two photons of the same frequency interact with nonlinear optical (NLO) materials to generate a new photon of doubled frequency. The NLO materials are the core materials for the SHG process. Based on the application spectrum range, NLO materials can be cataloged into deep-ultraviolet NLO materials, ultraviolet-visible NLO materials, infrared NLO materials, far-infrared NLO materials, etc. A good NLO material should balance a long list of properties such as a large second harmonic generation coefficient (SHG, d_{ij} >$AgGaS_2$ for infrared NLO materials), moderate birefringence (Δn) for phase matchability, high laser damage threshold (LDT >$AgGaS_2$), large bandgap for good transmission range at desired spectrum range and good thermal-, air-, and chemical stability. But most importantly, NLO materials should crystallize in noncentrosymmetric (NC) structures. The presence of distinct anions increases the degree of distortion of basic building units, which guarantees heteroanionic compounds to 'easily' form NC structures. In addition to

contributing to form NC structures, a higher degree of distortion also benefits the enhancement of SHG coefficients [15, 292-299]. The chemical properties difference among different anions makes the bandgap of heteroanionic compounds adjustable. For example, oxyhalides, especially oxyfluorides, are the best candidates for deep-ultraviolet NLO applications due to the presence of highly electronegative O^{2-} and F^-, which results in very large bandgap solids [300, 301]. As shown in **Figure 23**, the bandgap of oxyflourides span the largest range from ~2 eV to ~6.5 eV. Bandgap is an important parameter for many optical and optoelectronic applications. As shown in **Figure 23**, heteroanionic compounds exhibit variable bandgaps, which originate from structural flexibility. Employing proper strategies, the bandgap of heteroanionic compounds can be suppressed to be suitable for visible NLO materials or even IR NLO materials [293-299]. For example, one successful strategy to create good oxyhalide IR NLO materials is to incorporate heavy metals like Pb, such as $Pb_{18}O_8Cl_{15}I_5$ [302], $Pb_{13}O_6Cl_4Br_{10}$ [303], $Pb_{17}O_8Cl_{18}$ [304]. Another good method to employ oxyhalides as IR NLO materials is to add more anions such as $[Ba_2F_2][Ge_2O_3S_2]$ [305]. Our recent work of employing the partially filled 4f orbitals of cerium atoms also successfully makes the $CeHaVIO_4$ (Ha = Cl, Br; VI = Mo, W) system suitable for IR NLO materials [12]. The high chance of forming NC structures coupled with tunable band gaps keeps heteroanionic compounds appealing for NLO materials research. Moving forward, heteroanionic compounds can be advanced by interacting with other chemical strategies such as mixed-cation to further enlarge bandgaps or elements containing stereochemically active lone pairs to enhance SHG response [294-299].

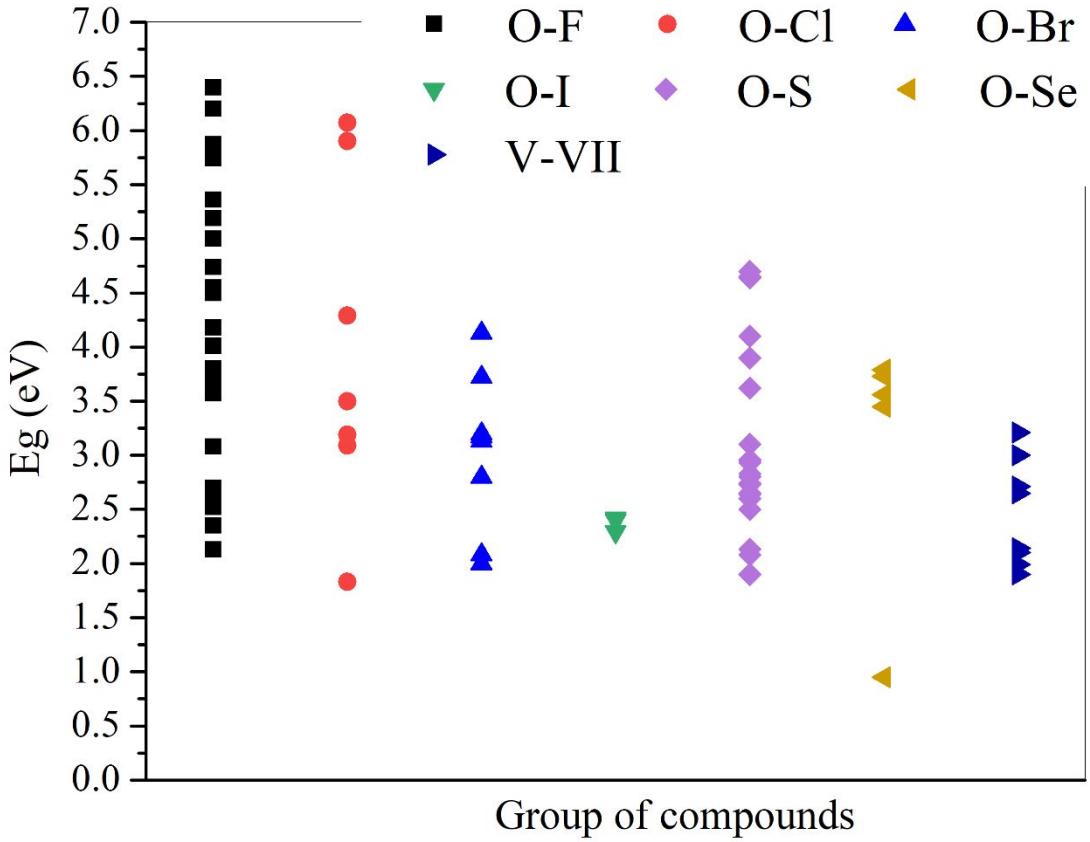

Figure 23. A summary of bandgap of seven groups of heteroanionic compounds, V-VII represents heteroanionic compounds constituting of main group five and main group seven elements.

4.2 Superconducting properties

Superconductors have been always an important research topic due to their scientific importance and potential applications [34, 51]. Superconductors were reported in a number of material systems including elements such as lead [306] and tin, [307] alloys such as Nb-Ti [308] and Ge-Nb, [309,310]organic compounds such as $(TMTSF)_2PF_6$ (TMTSF = tetramethyltetraselenafulvalene, P = 1.1 GPa) [311] and A_3C_{60} (A = K, Rb, Cs), [312,313]oxides such as $LiTi_2O_4$ [314] and YBCO, [315] superhydrides under high pressure such as LaH_{10}, [316] sulfide such as H_3S, [317] heteroanionic compounds and others. Among all of these compounds, heteroanionic compounds do not play a negligible role. Heteroanionic superconducting compounds belong to the unconventional superconductor family such as LaFePO [318] and REFeAsO (RE = rare earth), [34, 319,320] $(Sr_2VO_3)_2Fe_2As$, [321] $Ba_2Ti_2Fe_2As_4O$, [322] $(Sr_3Sc_2O_5)Fe_2As_2$, [323] etc. The well-studied LaFePO [318] and REFeAsO (RE = rare earth) compounds belong to the '1-1-1-1' phase system, which crystallizes in ZrCuSiAs structure type [34, 319, 320]. There were more than one hundred quaternary oxypnictides reported within the '1-1-1-1' phase system. Among the '1-1-1-1' phase system, the two-dimensional [FeAs] layers seem to be a common structure feature among these heteroanionic superconducting compounds. As shown in the structure section, there are more compounds containing 2D $[FePn]_{Pn=P,\ As}$ layers that wait for studies. Combining the $[FePn]_{Pn=P,\ As}$ tetrahedra with other heteroanionic building blocks may result in the discovery of new compounds that possess intriguing physical properties. The central element of $[TPn]_{T=\text{ transition metals},\ Pn=P,\ As}$ tetrahedra can also expand to other transition metals such as heteroanionic La_2NiO_3F, which also contain 2D $[NiO_3]$ layers.

4.3 Photoluminescent response

Photoluminescent (PL) materials emit light in response to higher energy light exposure. Based on how long emitting light lasts, there are two types of photoluminescent processes: fluorescence and phosphorescence. Phosphorescent material can continually emit light from less than a second to several hours after the removal of the light resource. Fluorescent materials immediately stop emission after the removal of the exiting light. The difference between fluorescence and phosphorescence originates from the different electron-transferring paths. PL materials have many important applications such as emissive displays, [324] LEDs, [325] and X-ray detection, [326] etc. For visible light emission from PL materials, ultraviolet light is the common excitation light resource. To absorb UV light, materials are required to have a large bandgap, which falls into the realm of many heteroanionic compounds. The combination of strong electronegative anions, such as O, S, F, Cl, etc., and metals can generate ionic metal-anion interactions. The ionic interaction can produce large bandgaps for many systems. Only a large bandgap is not sufficient. Many inorganic systems do not emit light without doping of "light emitting centers", which are normally rare earth or transition metals incorporated into crystal lattice [13]. A feasible structural feature would add additional benefits for an inorganic system to be selected as PL material. Good ambient stability of PL materials is also essential, which explains why many oxyhalides (**Table S4**) and oxynitrides (**Table S6**) were widely studied as PL materials. In the future, studying PL materials coupled with other physical properties would open new research directions. Among those applications, the use

of luminescence in biological systems is efficient to understand cellular structures and diagnose diseases. Uncovering new materials that own high PL efficiency, are biologically compatible, and the use of light in the regions where tissues and cells have low absorption would be the targets for the future [327-329]. The heteroanionic compounds are less commonly utilized for biological application, generally due to the presence of heavy elements. The high stability, and excellent PL properties of heteroanionic compounds still keep the door open for application for biological purposes. Constructing heteroanionic compounds with light elements or even organic heteroanionic compounds may be a good way to expand the boundary of heteroanionic compounds. The solid-state LEDs have been developed well for low-energy applications. While the high energy PL materials, which can be utilized for high-energy output applications such as lasers, are still underdeveloped [330-332]. The high energy output PL materials require high thermal stability and thermal conductivity of heteroanionic compounds, which can conduct heat out quickly. The three-dimensional crystal structure and the presence of light elements coupled with strong bonding interactions can guarantee the high thermal conductivity of heteroanionic compounds, which indicates that heteroanionic compounds are good candidates for high-energy out PL materials [330-332].

4.4 Thermoelectric properties

The increased need for clean energy sources continues to fuel the research of thermoelectric materials, which can convert heat flow into electrical power through the Seebeck effect or conversely change electrical power into heat flow *via* the Peltier effect [272]. The performance of a thermoelectric material is evaluated through the dimensionless figure-of-merit $zT = S^2T/\rho\kappa$, where S is the Seebeck thermopower, T is the absolute temperature, ρ is the electrical resistivity, and κ is the thermal conductivity. A state-of-the-art thermoelectric material should combine high Seebeck coefficients, high electrical conductivity, and low thermal conductivity. All three parameters are intrinsically correlated via carrier concentration and electronic structures [333]. Thermal conductivity arises from two components, lattice thermal conductivity and carrier thermal conductivity, $K_{total}=K_{lattice}+K_{carrier}$. The carrier thermal conductivity is determined by carrier concentration and carrier mobility [333]. The lattice thermal conductivity is independent of carrier concentration, which is the major target of research to reduce. Many strategies such as including heavy elements, the presence of rattling elements and defects, and reducing the dimensionality of crystal lattice have proved to be efficient in reducing lattice thermal conductivity. Some heteroanionic compounds such as BiCuSeO and LaZnSbO, which combine 2D crystal lattice with defects to tune electrical and thermal conductivity, achieve a high figure of merit [334-336]. As discussed in the structure part, there are more heteroanionic compounds that feature 2D layered structures. Even some known compounds, which crystallize in ZrCuSiS structure type, remain unexplored for thermoelectric applications. With the quick development of machine learning and calculation power, more thermoelectric materials may be mined.

4.5 Other applications

The flexible structural chemistry of heteroanionic compounds results in more applications such as photocatalysis applications[337], battery materials [338], etc., which are summarized in related papers.

Exploring new compounds with flexible structures, which result in important applications, is always exciting for research.

4.6 Can heteroanionic compounds be a new paradise for discovering multiferroics?

The data that is created daily in 2024 is about 2.5 quintillion (10^{18}) bytes [339]! More data are expected in the future. Processing and storing these huge amounts of data remains a big challenge. Developing more compact, faster, and secure storage methods is crucial for our society. Multiferroics are considered as good candidates for next-generation storage materials, which could be utilized to fabricate smaller, faster, and secure storage devices [340-345]. Multiferroics refer to materials that exhibit more than one ferroic order simultaneously as shown in **Figure 24**. In addition to data storage, multiferroics find applications such as sensors [346-350], energy devices [351-355], radio and high-frequency devices [356-358], etc. The broad applications of multiferroics require *single-phase* multiferroics with transition temperature above room temperature, which have become the bottleneck for implementing those materials in technology. Seeking multiferroics is challenging because multiferroics combine two or more ferroic states within a single lattice, where some ferroic states naturally oppose each other. Even though the concept of multiferroics was developed many years ago, only a limited number of chemical systems were found to be multiferroics. The physicists roll the ball back to the chemists. The chemistry question arises: which chemical systems can host multiferroic states? Alternatively, what is a good chemical methodology to discover new multiferroics? Finding new chemical systems, that own the same microscopic building units with known multiferroics and good chemical flexibility, should be a good strategy. The highly flexible heteroanionic compounds**,** that share common structure features with known multiferroics, might be a new paradise for discovering multiferroics.

The multiferroics refer to materials that exhibit the coexistence of two or more ferroic states (ferroelectricity (**Figures 24a** and **24d**), ferromagnetism (**Figures 24b** and **24e**), ferroelasticity, and ferrotoroidicity) [359-371]. Multiferroics were found in various forms including single-phase crystals mainly oxides[372-374], thin films [375-378], composite materials [379-381], organics [382], and organic-inorganic hybrid materials [383-385], etc. Multiferroics are not new to the research community. The study of multiferroics can date back to around 1974, which was studied by Aizu [386]. The study of magnetoelectric materials, which exhibit interplay between electric and magnetic properties, began much earlier [387]. Not all magnetoelectric materials can be cataloged into multiferroics. In rigid terms, the combination of ferroelectricity and ferromagnetism are multiferroics (**Figures 24c** and **24f**). The magnetoelectric effect refers to magnetization induced by an applied electric field or vice versa as the electric polarization induced by an applied magnetic field. Multiferroic materials reignited more and more research interests over the past few decades due to many exotic properties that originate from the combination of ferroic states [340-385]. The list of applications of multiferroics keeps growing [346-373].

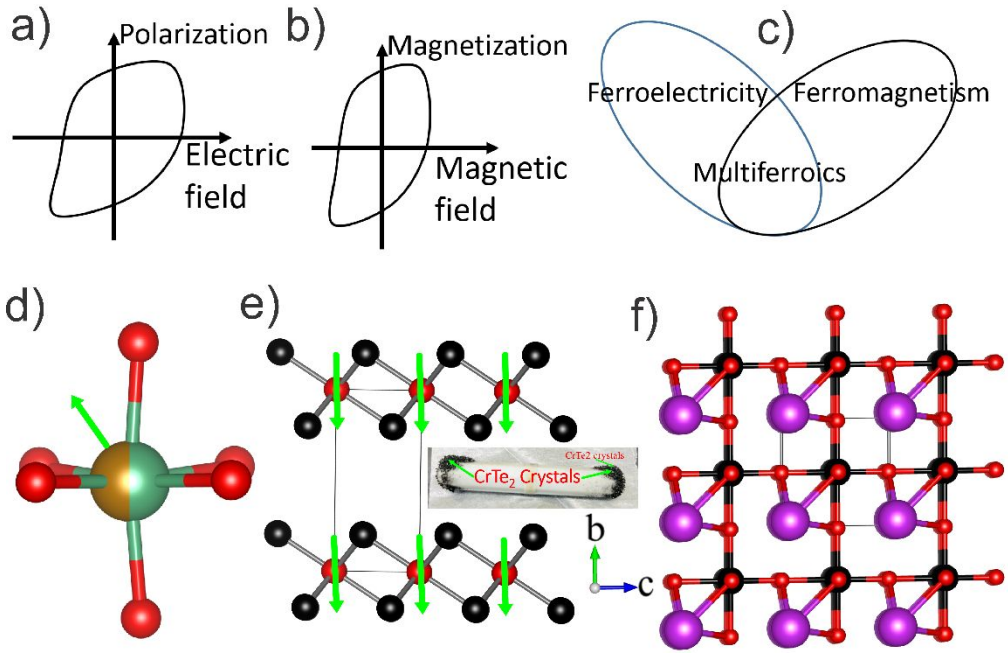

Figure 24. (a) Spontaneous polarization, which can be switched by an external electric field in ferroelectrics. (b) Spontaneous magnetization, which can be switched by an external magnetic field in ferromagnetic materials. (c) A Venn diagram of ferroelectricity and ferromagnetism combine to create multiferroics. (d) The $[d^0O_6]_{d0=Nb/Fe}$ octahedral within perovskites, the green arrow indicates the displacement of the central atom, O: red. (e) Crystal structure of 1T-$CrTe_2$, [388-390] a room-temperature ferromagnetic material (T_c= ~320K), the green arrows present the potential alignment of magnetic moments of Cr atoms, Cr: red, Te: black. The insert shows the 1T-$CrTe_2$ crystals grown in the PI's lab attracted to the magnetic stir bar at room temperature. (f) Crystal structure of $BiFeO_3$, [391,392] a well-known multiferroic compound, Bi: pink, Fe: black, O: red.

Why heteroanionic compounds are a good fit for multiferroics?

1) *Higher chance of forming acentric crystal structure*. Ferroelectricity can only be found within certain space groups [360]. Among these space groups, they should belong to one of ten polar point groups (1, 2, 3, 4, 6, m, mm2, 3m, 4mm, and 6mm). These 10 polar point groups also are subsets of 21 acentric point groups. Hence, an acentric crystal structure would be the first requirement to probe possible ferroelectrics. Macroscopic symmetry is determined by microscopic structures. Our previous study has found that distortion of tetrahedra [293, 393, 394], mixed-cations [297], and alignment of lone pairs [73] are useful strategies to form acentric crystal structures. The presence of distinct anions increases the degree of distortion of basic building units, which guarantees heteroanionic compounds to 'easily' form acentric structures [1-3].

2) *Highly distorted BBU without inversion center*. The acentric crystal structures cannot guarantee the presence of ferroelectricity. The presence of spontaneous polarization would be the key to achieving ferroelectricity. Understanding the origin of ferroelectricity from a chemical perspective, especially from a crystal structure viewpoint would help us find new materials. The ferroelectricity of perovskite materials originates from the 'off-center' movement of cations (usually d^0 metals) (**Figure 24d**), which is caused by the interactions between center cations and surrounding anions [360-371]. The presence and alignment of lone pairs of Bi^{3+} play a key role in contributing to the ferroelectricity of $BiFeO_3$ [391, 392]. Using the Valence Shell Electron Pair

Repulsion (VSEPR) theory, the lone pairs of Bi^{3+} can be treated as one domain. Bi^{3+} is also located in a highly distorted tetrahedral (**Figure 3c**). Nevertheless, in h-$YMnO_3$, the movement of [MnO_5] bipyramids, which result in the displacement of Y cations, is the dominant factor for its ferroelectricity (**Figure 3a**) [395, 396]. Distorted bipyramids are also common features for many compounds such as our recently discovered $REHaVIO_4$, where [WO_5] bipyramids are also present (**Figure 3b**) [12, 13]. The presence of various anions coupled with lone-pair active elements such as Sb^{3+}, Bi^{3+}, and Te^{4+} would introduce distinct distorted building units into the target system. The heteroanionic compounds share many comparable structure features with known multiferroics.

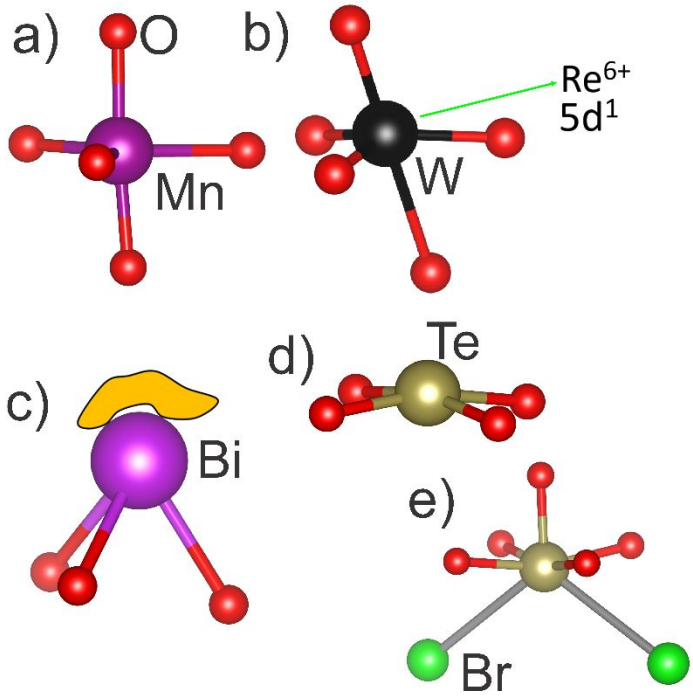

Figure 25. (a) [MnO_5] bipyramids in h-$RMnO_3$ [395, 396]. (b) [WO_5] bipyramids in $LaBrWO_4$ [12, 13], the arrow shows that W^{6+} can be replaced by Re^{6+}, where the unpaired $5d^1$ electron of Re^{6+} can introduce magnetic properties into the system. (c) [BiO_3] unit with lone pairs within $BiFeO_3$ [391, 392] (d) [TeO_4] unit and [TeO_5Br_2] unit within $Bi_4Te_2O_9Br_2$ [397]. O: red.

3) *Highly tunable crystal structure to adjust magnetic properties*. Ferromagnetic materials are primarily found among single elements like cobalt (Co) and iron (Fe), their alloys, and rare earth compounds such as neodymium iron boron (NdFeB). The transition temperature of a ferromagnetic material is mainly determined by crystal structure and its constituent magnetic elements. Recent studies on two-dimensional (2D) ferromagnetic materials have advanced our understanding of the origins and mechanisms of ferromagnetism [388-390]. As shown in **Figure 24e**, room-temperature 2D 1T-$CrTe_2$ features a simple crystal structure. Cr atoms are separated from adjacent Cr atoms by 4.0193 Å. Each Cr atom is surrounded by six Te atoms that form a close packing within the Cr layers. The Cr lattice accounts for the room-temperature ferromagnetic properties of bulk and thin-layer $CrTe_2$ samples. To be honest, how to find a new ferromagnetic material is a challenging question. A chemically flexible lattice, where multiple atomic positions can accommodate magnetic elements such as rare earth or transition metals, provides a promising foundation for discovering ferromagnetic materials. Heteroanionic compounds provide a good platform for chemical flexibility. Using a quaternary system A-B-C-D (A and B represent metals,

C and D are distinct anions), the presence of two metal atomic sites provides structural flexibility. Both A and/or B can be replaced by magnetic elements, which introduces magnetic properties into heteroanionic compounds. Within a heteroanionic compound lattice, the distances between magnetic elements can vary and are adjustable. One example would be our recent study of the $REHaVIO_4$ system, the RE atomic position can be occupied by magnetic 4f elements such as Ce-Yb. Another degree of flexibility comes from the substitution of group VI elements. The ionic sizes of Re^{6+} and W^{6+} are 74 pm and 69 pm, respectively, for a six-coordination environment. W^{6+} does not have any 5d electrons. Re^{6+} has one 5d electron ($5d^1$), which introduces magnetism into the target system (**Figure 25b**). As shown in **Figure 25c**, the lone pairs of Bi^{3+} and their alignment within $BiFeO_3$ are crucial for its ferroelectricity. Lone pair active elements are also common constituent elements for heteroanionic compounds. One of our proposed systems, $Bi_4Te_2O_9Br_2$ possesses two lone pair active elements, Bi^{3+} and Te^{4+}. The highly distorted $[TeO_4]$ unit and $[TeO_5Br_2]$ unit within $Bi_4Te_2O_9Br_2$ are shown in **Figures 25d** and **25e**. $Bi_4Te_2O_9Br_2$ was proven to show pyroelectric properties [397].

4). *High stability and chemical flexibility of heteroanionic compounds.* The three-dimensional structure constructed by strong chemical bonding will make heteroanionic compounds show very good water-, air- and chemical stability. One example would be our recent $REHaVIO_4$ system remaining unchanged in the air for many months. The crystals were collected after water treatment to remove salt flux [12,13]. The chemical properties difference among different anions makes the bandgap of heteroanionic compounds adjustable. For example, oxyhalides, especially oxyfluorides, have much bigger bandgaps than oxides, which makes them show good transmission of visible light or even deep-ultraviolet light [13]. Employing proper strategies, the bandgap of heteroanionic compounds can be suppressed to be suitable for the transmission of infrared radiation [12]. Adjustable bandgap adds another flexibility to the heteroanionic compounds since many physical processes are directly correlated to the bandgap of solids (**Figure 23**). Ferroelectricity typically exists within insulating materials characterized by a large bandgap, whereas ferromagnetic materials are often found in metals, which generally have no bandgap. This is another reason why it is extremely hard to combine both ferroic states within one lattice. In chemistry language: a polar crystal lattice with distorted building units is necessary to achieve ferroelectricity; A crystal lattice with magnetic elements interacting with tunable distances and coordination environments would be another prerequisite for ferromagnetic properties. Heteroanionic compounds satisfy both requirements. In summary, heteroanionic compounds are an ideal system for multiferroics and our preliminary results have demonstrated the high potential of heteroanionic compounds as multiferroics.

A brief history of research of heteroanionic compounds as multiferroics. Not too many multiferroic heteroanionic compounds have been discovered. But interestingly, the heteroanionic compound $Ni_3B_7O_{13}I$ was the first experimentally verified magnetic ferroelectric, which was discovered by Asher et al back in 1966 [398]. This system was further expanded later on [399]. Another heteroanionic CuO_2Cl_2 was discovered as a multiferroic material with ferroelectricity below 70K [400]. Theoretical studies also predicted that some heteroanionic compounds such as Eu_4Sb_2O [401] and $YCaFe_2O_5F$ [402] might be potential multiferroics, which are waiting for experimental studies. Since 1966, not too many heteroanionic compounds have been explored as multiferroics (or not too many successful examples). This project aims to recap and revisit some heteroanionic compounds as potential multiferroics.

Summary and outlook

In this review, we summarized the synthesis, selected crystal structures to present the diverse and feasible structural chemistry, and selected applications of heteroanionic compounds.

1. Synthesis. The incorporation of distinct anions introduces structure complexity into heteroanionic compounds, and in the, raises the difficulty of the synthesis process. Growing high-quality crystals still relies on a 'trial-and-error' model. Another challenge would be to control the ratio of different anions. Looking into the growth mechanisms of heteroanionic compounds via in-situ studies and theory simulation is becoming more and more important. The quickly developed AI techniques might also aid in helping the synthesis of heteroanionic compounds.
2. Structure perspective of heteroanionic compounds. As discussed in the second part, selected examples verify the diverse structural chemistry of heteroanionic compounds. The rich structural chemistry of heteroanionic compounds originates from flexible basic building units and their connecting manners. How these anions connect to central atoms is one important factor for the structures. Another factor would be the connectivity between these basic building units. Letting distinct anions interact with other structure features such as lone pair electrons, d^0 or d^{10} transition metals, not fully occupied 4f/5f orbitals might bring in a new realm for related research topics. Both new compounds and known compounds of heteroanionic compounds are worth expecting to be discovered and show exotic physical properties. Exploring new compounds can push the boundaries of heteroanionic compounds forward. Understanding the structure plus the controlled growth of many known heteroanionic compounds would also be a good add-on to solid-state chemistry.
3. Properties of heteroanionic compounds. As briefly discussed in section 3, heteroanionic compounds exhibit many intriguing physical properties. It seems heteroanionic compounds are naturally suitable for certain applications. Superconductive and thermoelectric materials favor layered structures, where many heteroanionic compounds find their place. The tunable bandgap of heteroanionic compounds also places them in a good position for NLO applications. Further, external stimuli such as high pressure or strain might introduce more important applications for heteroanionic compounds.
4. The research of new single-phase multiferroics are more and more crucial due to the important applications. The heteroanionic compounds, which own a high degree of chemical flexibility, might be a potential playground for studying multiferroics.

ASSOCIATED CONTENTS

Supporting Information

Synthesis details of selected heteroanionic compounds. Structural chemistry and physical properties of selected heteroanionic compounds.

Acknowledgments

This research was supported by the National Science Foundation (DMR-2316811).

Corresponding author

Jian Wang jian.wang@wichita.edu

Notes

# equally contributed

The authors declare no competing financial interest.

References

References

1. D. Hirai, Pinalites: Optical Properties and Quantum Magnetism of Heteroanionic $A_3MO_5X_2$ Compounds. *Inorg. Chem.*, 2024, **63**, 9, 4001–4010.
2. J. K. Harada, N. Charles, K. R. Poeppelmeier and J. M. Rondinelli, Heteroanionic Materials by Design: Progress Toward Targeted Properties. *Adv. Mater.*, 2019, **31**, 1805295.
3. S. Cui, H. Wu, X. Dong, Z. Hu, J. Wang, Y. Wu, K. R. Poeppelmeier and H. Yu, Chiral and Polar Duality Design of Heteroanionic Compounds: $Sr_{18}Ge_9O_5S_{31}$ Based on $[Sr_3OGeS_3]^{2+}$ and $[Sr_3SGeS_3]^{2+}$ Groups. *Adv. Sci.*, 2023,**11**, 2306825.
4. J. K. Harada, K. R. Poeppelmeier and J. M. Rondinelli, Heteroanionic Ruddlesden-Popper Ferroelectrics from Anion Order and Octahedral Tilts. *Phys. Rev. Mater.*, 2021, **5**,104404.
5. C. Zhang, J. He, R. McClain, H. Xie, S. Cai, L. N. Walters, J. Shen, F. Ding, X. Zhou, C. D. Malliakas, J. M. Rondinelli, M. G. Kanatzidis, C. Wolverton, V. P. Dravid and K. R. Poeppelmeier, Low Thermal Conductivity in Heteroanionic Materials with Layers of Homoleptic Polyhedra. *J. Am. Chem. Soc.*, 2022, **144**, 2569–2579.
6. H. Kageyama, K. Hayashi, K. Maeda, J. P. Attfield, Z. Hiroi, J. M. Rondinelli and K. R. Poeppelmeier, Expanding frontiers in materials chemistry and physics with multiple anions. *Nat. Commun.*, 2018, **9, 772.**
7. K. Maeda, F. Takeiri, G. Kobayashi, S. Matsuishi, H. Ogino, S. Ida, T. Mori, Y. Uchimoto, S. Tanabe, T. Hasegawa, N. Imanaka and H. Kageyama, Recent Progress on Mixed-Anion Materials for Energy Applications. *Bull. Chem. Soc. Jpn.*, 2022, **95**, 26–37.
8. Y.-Y. Li, W.-J. Wang, H. Wang, H. Lin and L.-M. Wu,Mixed-Anion Inorganic Compounds: A Favorable Candidate for Infrared Nonlinear Optical Materials. *Cryst. Growth & Des.*, 2019, **19**, 4172–4192.

9. G. Yadav and M. Ahmaruzzaman,Multi Anion-based Materials: Synthesis and Catalytic Applications. *Mater. Res. Bull.*, 2022, **152**, 111836.

10. J. jing Xu and K. Wu,Comprehensive review on multiple mixed-anion ligands, physicochemical performances and application prospects in metal oxysulfides. *Coord. Chem. Rev.*, 2023, **486**, 215139.

11. X. Zhang, L. Kang, P. Gong, Z. Lin and Y. Wu, Nonlinear Optical Oxythiophosphate Approaching the Good Balance with Wide Ultraviolet Transparency, Strong Second Harmonic Effect, and Large Birefringence. *Angew. Chem. Int. Ed.*, 2021, **60**, 6386-6390.

12. Z. Jiao, J. Quah, T. H. Syed, W. Wei, B. Zhang, F. Wang and J. Wang,Synthesis, crystal and electronic structures, linear and nonlinear optical properties, and photocurrent response of oxyhalides CeHaVIO$_4$ (Ha = Cl, Br; VI = Mo, W). *Dalton Trans.*, 2024, **53**, 2029-2038.

13. Z. Jiao, O. M. Mireles, K. Ensz, F. Wang, M. Liang, P. S. Halasyamani, B. Zhang, D. P. Rillema and J. Wang, Heteroanionic LaBrVIO$_4$ (VI = Mo, W): Excellence in Both Nonlinear Optical Properties and Photoluminescent Properties. *Chem. Mater.*, 2023, **35**(17), 6998–7010.

14. A. Cicirello, A. Swindle and J. Wang,Visualizing the alignment of lone pair electrons in La3AsS5Br2 and $La_5As_2S_9Cl_3$ to form an acentric or centrosymmetric structure. *CrystEngComm*, 2023, **25**, 6354-6360.

15. C. Cropek, B. Ji, A. Sarkar, F. Wang, T. H. Syed, W. Wei, S.-P. Guo and J. Wang,Revisiting two thiophosphate compounds constituting d^0 transition metal HfP_2S_6 and d^{10} transition metal α-$Ag_4P_2S_6$ as multifunctional materials for combining second harmonic generation response and photocurrent response. *CrystEngComm*, 2023, **25**, 1175-1185.

16. G. E. Rodgers, *Descriptive inorganic, coordination, and solid state chemistry*, Brooks/Cole, Cengage Learning, Belmont, CA, 3rd edn, 2012.

17. R. D. Shannon, Revised effective ionic radii and systematic studies of interatomic distances in halides and chalcogenides. *Acta Crystallogr. A*, 1976, **32** : 751–767.

18. M. Pompetzki and M. Jansen,Natriumtrithiophosphat(V): Kristallstruktur und Natriumionenleitfähigkeit. *Z. Fur Anorg. Und Allg. Chem.*, 2003, **629**, 1929–1933.

19. M. Pompetzki, R. E. Dinnebier and M. Jansen, Sodium dithiophosphate(V): Crystal structure, sodium ionic conductivity and dismutation. *Solid State Sci.*, 2003, **5**, 1439–1444.

20. M. Pompetzki and M. Jansen, Sodium monothiophosphate(V): Crystal structure and sodium ionic conductivity. *Z. Fur Anorg. Und Allg. Chem.*, 2002, **628**, 641–646.

21. P. Wei, W. Chen, Q. Jing, M.-H. Lee and Z. Chen, Effects of P_2O_7 clusters arrangement on second harmonic generation responses of pyrophosphates. *J. Alloy. Compd.*, 2020, **827**, 153922.

22. R. J. Harrison, A. Putnis and W. Kockelmann,Phase transition behaviour and equilibrium phase relations in the fast-ion conductor system Na_3PO_4–Na_2SO_4. *Phys. Chem. Chem. Phys.*, 2002, **4**, 3252–3259.

23. A. A. Belik, Structure and electric conductivity of Na_3PO_4 single crystals. *Crystallogr. Rep.*, 2000, **45**, 902.

24. A. T. Giddings , E. A.-S. Scott , M. C. Stennett , D. C. Apperley , C. Greaves , N. C. Hyatt and E. E. McCabe, Symmetry and the Role of the Anion Sublattice in Aurivillius Oxyfluoride $Bi_2TiO_4F_2$. *Inorg. Chem.,* 2021, **60** , 14105 —14115.

25. T. Schustereit, H. Henning, T. Schleid and I. Hartenbach, Syntheses and Crystal Structures of the Bromide-derivatized Lanthanoid(III) Ortho-Oxomolybdates(VI) LnBr[MoO_4] (Ln = Pr, Nd, Sm, Gd–Lu). *Z. Fur Naturforsch. B*, 2013, **68**, 616–624.

26. R. McClain, C. D. Malliakas, J. Shen, C. Wolverton and M. G. Kanatzidis,In Situ Mechanistic Studies of Two Divergent Synthesis Routes Forming the Heteroanionic BiOCuSe. *J. Am. Chem. Soc.*, 2021, **143**, 12090–12099.

27. H. Hiramatsu, H. Yanagi, T. Kamiya, K. Ueda, M. Hirano and H. Hosono,Crystal Structures, Optoelectronic Properties, and Electronic Structures of Layered Oxychalcogenides MCuOCh (M = Bi, La; Ch = S, Se, Te): Effects of Electronic Configurations of M^{3+} Ions. *Chem. Mater.*, 2008, **20**, 326–334.

28. S. J. Clarke, P. Adamson, S. J. C. Herkelrath, O. J. Rutt, D. R. Parker, M. J. Pitcher and C. F. Smura,Structures, Physical Properties, and Chemistry of Layered Oxychalcogenides and Oxypnictides. *Inorg. Chem.*, 2008, **47**, 8473–8486.

29. J. K. Harada, K. R. Poeppelmeier and J. M. Rondinelli, Predicting the Structure Stability of Layered Heteroanionic Materials Exhibiting Anion Order. *Inorg. Chem.*, 2019, **58**, 13229–13240.

30. N. Zapp, F. Oehler, M. Bertmer, H. Auer, D. Sheptyakov, C. Ritter and H. Kohlmann, Aliovalent anion substitution as a design concept for heteroanionic Ruddlesden–Popper hydrides. *Chem. Commun.*, 2022, **58**, 12971-12974.

31. C. Masquelier and L. Croguennec, Polyanionic (Phosphates, Silicates, Sulfates) Frameworks as Electrode Materials for Rechargeable Li (or Na) Batteries. *Chem. Rev.*, 2013, **113**, 6552–6591.

32. S. C. Selvaraj, S. Gupta, D. Caliste and P. Pochet, Passivation mechanism in CdTe solar cells: The hybrid role of Se. *Appl. Phys. Lett.*, 2021, **119**, 062105.

33. T. Karaman, A. u. R. Sherwani, M. M. Can, S. Shawuti and S. Kaneko, Synthesis and optical analyses of fluorine doped tin oxide (SnO_2) nanoparticles. *Eur. Phys. J. Appl. Phys.*, 2021, **95**, 20402.

34. Y. Kamihara, T. Watanabe, M. Hirano and H. Hosono, Iron-Based Layered Superconductor La[$O_{1-x}F_x$]FeAs (x = 0.05−0.12) with T_c = 26 K. *J. Am. Chem. Soc.*, 2008, **130**, 3296–3297.

35. F. J. Brink, L. Norén, D. J. Goossens, R. L. Withers, Y. Liu and C.-N. Xu, A combined diffraction (XRD, electron and neutron) and electrical study of $Na_3MoO_3F_3$. *J. Solid State Chem.*, 2003, **174**, 450–458.

36. S. Jaulmes,Oxysulfure de gallium et de lanthane $LaGaOS_2$. *Acta Cryst.logr. Sect. B Struct. Crystallogr. Crystal Chem.*, 1978, **34**, 2610–2612.

37. Y. Xia, C. Chen, D. Tang and B. Wu, New nonlinear optical crystals for UV and VUV harmonic generation. *Adv. Mater.*, 1995, **7**, 79–81.

38. L. N. Kholodkovskaya, L. G. Akselrud, A. M. Kusainova, V. A. Dolgikh and B. A. Popovkin, BiCuSeO: Synthesis and Crystal Structure. *Mater. Sci. Forum*, 1993, **133-136**, 693–696.

39. J. Liu, J. Wang, C.-l. Wang and S.-q. Xia, $Ce_{1-x}Sr_xZnSbO$: New thermoelectric materials formed between intermetallics and oxides. *J. Alloy. Compd.*, 2016, **688**, 849–853.

40. T. Mahon, E. Gaudin, A. Villesuzanne, B. Chevalier and S. Tencé,Effect of Carbon Insertion on the Structural and Magnetic Properties of NdScSi. *Inorg. Chem.*, 2019, **58**, 15255–15268.

41. T. Mahon, S. Tencé, R. Pöttgen, B. Chevalier and E. Gaudin, Study of the structural transition and hydrogenation of CeTiGe. *J. Alloy. Compd.*, 2019, **805**, 701–708.

42. P. Edalati, X.-F. Shen, M. Watanabe, T. Ishihara, M. Arita, M. Fuji and K. Edalati, High-entropy oxynitride as a low-bandgap and stable photocatalyst for hydrogen production. *J. Mater. Chem. A*, 2021, **9**, 15076–15086.

43. E. E. Oyeka, M. J. Winiarski, H. Świątek, W. Balliew, C. D. McMillen, M. Liang, M. Sorolla and T. T. Tran, $Ln_2(SeO_3)_2(SO_4)(H_2O)_2$ (Ln=Sm, Dy, Yb): A Mixed-Ligand Pathway to New Lanthanide(III) Multifunctional Materials Featuring Nonlinear Optical and Magnetic Anisotropy Properties. *Angew. Chem. Int. Ed.*, 2022, **61**, e202213499.

44. C. Hu, M. Cheng, W. Jin, J. Han, Z. Yang and S. Pan, A Cation-Driven Approach toward Deep-Ultraviolet Nonlinear Optical Materials. *Research*, 2023, **6**, 0053.

45. R. Wang, Y. Guo, X. Zhang, Y. Xiao, J. Yao and F. Huang, $Sr_5Ga_8O_3S_{14}$: A Nonlinear Optical Oxysulfide with Melilite-Derived Structure and Wide Band Gap. *Inorg. Chem.*, 2020, **59**, 9944–9950.

46. J. Wang, Y. Cheng, H. Wu, Z. Hu, J. Wang, Y. Wu and H. Yu, $Sr_3[SnOSe_3][CO_3]$: A Heteroanionic Nonlinear Optical Material Containing Planar π-conjugated $[CO_3]$ and Heteroleptic $[SnOSe_3]$ Anionic Groups. *Angew. Chem. Int. Ed.*, 2022, **61**, e202201616.

47. Y.-F. Shi, W.-B. Wei, X.-T. Wu, H. Lin and Q.-L. Zhu, Recent progress in oxychalcogenides as IR nonlinear optical materials. *Dalton. Trans.*, 2021, **50**, 4112–4118.

48. R. Wang, F. Liang, X. Liu, Y. Xiao, Q. Liu, X. Zhang, L.-M. Wu, L. Chen and F. Huang, Heteroanionic Melilite Oxysulfide: A Promising Infrared Nonlinear Optical Candidate with a Strong Second-Harmonic Generation Response, Sufficient Birefringence, and Wide Bandgap. *ACS Appl. Mater. & Interfaces*, 2022, **14** , 23645–23652.

49. S. Cui, H. Wu, Z. Hu, J. Wang, Y. Wu and H. Yu,The Antiperovskite-Type Oxychalcogenides $Ae_3Q[GeOQ_3]$ (Ae = Ba, Sr; Q = S, Se) with Large Second Harmonic Generation Responses and Wide Band Gaps. *Adv. Sci.*, 2023,**10**, 2204755.

50. H. Takahashi, H. Soeda, M. Nukii, C. Kawashima, T. Nakanishi, S. Iimura, Y. Muraba, S. Matsuishi and H. Hosono,Superconductivity at 52 K in hydrogen-substituted $LaFeAsO_{1-x}H_x$ under high pressure. *Sci. Rep.*, 2015, **5**, 7829.

51. D. Johrendt and R. Pöttgen,Pnictide Oxides: A New Class of High-T_C Superconductors. *Angew. Chem. Int. Ed.*, 2008, **47**, 4782–4784.

52. S. Baranets, G. M. Darone and S. Bobev,Structural diversity among multinary pnictide oxides: a minireview focused on semiconducting and superconducting heteroanionic materials. *Z. Fur Krist. - Cryst. Mater.*, 2022, **237**, 1–26.

53. L. H. Brixner, H. Y. Chen and C. M. Foris, Structure and luminescence of the orthorhombic $LnWO_4Cl$-type rare earth halo tungstates. *J. Solid State Chem.*, 1982, **45**, 80–87.

54. G. B. Ayer, V. V. Klepov, M. D. Smith, M. Hu, Z. Yang, C. R. Martin, G. Morrison and H.-C. zur Loye, $BaWO_2F_4$: a mixed anion X-ray scintillator with excellent photoluminescence quantum efficiency. *Dalton. Trans.*, 2020, **49**, 10734–10739.

55. T. Schustereit, P. Netzsch, H. A. Höppe and I. Hartenbach, Green Light: On $YCl[WO_4]$ as Host Material for Luminescence Active Tb^{3+} Cations. *Z. Fur Anorg. Und Allg. Chem.*, 2018, **644**, 1749–1753.

56. I. Hartenbach, S. Strobel, T. Schleid, K. W. Krämer and P. K. Dorhout, Chloride Derivatives of Lanthanide Ortho-Oxomolybdates: 1. Structural Comparison, Magnetic Properties, and Luminescence

of the LnCl[MoO_4] Representatives with the Smaller Lanthanides (Ln = Sm–Lu). *Z. Fur Anorg. Und Allg. Chem.*, 2009, **635**, 966–975.

57. T. Schleid, S. Strobel, P. K. Dorhout, P. Nockemann, K. Binnemans and I. Hartenbach,YF[MoO4] and YCl[MoO4]: Two Halide Derivatives of Yttrium ortho-Oxomolybdate: Syntheses, Structures, and Luminescence Properties. *Inorg. Chem.*, 2008, **47**, 3728–3735.

58. L. H. Brixner, H. y. Chen and C. M. Foris, Structure and luminescence of the monoclinic $LnWO_4Cl$-type rare earth halo tungstates. *Mater. Res. Bull.*, 1982, **17**, 1545–1556.

59. K. V. Dorn, B. Blaschkowski, P. Netzsch, H. A. Höppe and I. Hartenbach,Blue Excitement: The Lanthanide(III) Chloride Oxidomolybdates(VI) $Ln_3Cl_3[MoO_6]$ (Ln = La, Pr, and Nd) and Their Spectroscopic Properties. *Inorg. Chem.*, 2019, **58**, 8308–8315.

60. T. Schustereit, T. Schleid, H. A. Höppe, K. Kazmierczak and I. Hartenbach, Chloride derivatives of lanthanoid(III) ortho-oxidotungstates(VI) with the formula LnCl[WO_4] (Ln=Gd–Lu): Syntheses, crystal structures and spectroscopic properties. *J. Solid State Chem.*, 2015, **226**, 299–306.

61. N. Charles, R. J. Saballos and J. M. Rondinelli, Structural Diversity from Anion Order in Heteroanionic Materials. *Chem. Mater.*, 2018, **30**, 3528–3537.

62. G. Tan, L.-D. Zhao and M. G. Kanatzidis,Rationally Designing High-Performance Bulk Thermoelectric Materials. *Chem. Rev.*, 2016, **116**, 12123–12149.

63. J.-X. Zhang, P. Feng, M.-Y. Ran, X.-T. Wu, H. Lin and Q.-L. Zhu, Ga-based IR nonlinear optical materials: Synthesis, structures, and properties, *Coord. Chem. Rev.*, 2024, **502**, 215617.

64. M.-Y. Ran, S.-H. Zhou, W.-B. Wei, B.-X. Li, X.-T. Wu, H. Lin and Q.-L. Zhu, Rational design of a rare-earth oxychalcogenide $Nd_3[Ga_3O_3S_3][Ge_2O_7]$ with superior infrared nonlinear optical performance, *Small.*,2023,**19,**2300248.

65. M.-Y. Ran, S.-H. Zhou, X.-T. Wu, H. Lin and Q.-L. Zhu, The first Hg-based oxychalcogenide $Sr_2HgGe_2OS_6$: Achieving balanced IR nonlinear optical properties through synergistic cation and anion substitution, *Mater. Today Phys.*, 2024, **44**, 101442.

66. M. Orr, G. R. Hebberd, E. E. McCabe and R. T. Macaluso, Structural diversity of rare-earth oxychalcogenides, *ACS Omega.*, 2022, **7**, 8209–8218.

67. Y. Zhang, H. Wu, Z. Hu and H. Yu, Oxychalcogenides: A promising class of materials for nonlinear optical crystals with mixed-anion groups, *Chemistry.*, 2022,**29**,e202203597.

68. X. Chen and K. M. Ok, Metal oxyhalides: an emerging family of nonlinear optical materials, *Chem. Sci.*, 2022, **13**, 3942–3956.

69. Y. Pan, S.-P. Guo, B.-W. Liu, H.-G. Xue and G.-C. Guo, Second-order nonlinear optical crystals with mixed anions, *Coord. Chem. Rev.*, 2018, **374**, 464–496.

70. K. Li, A. Yalikun and Z. Su, $[O_2Pb_3]_2(BO_3)I$: a new lead borate iodide with $^1{}_\infty[O_2Pb_3]$ double chains.*Dalton Trans.*, 2020, **49**, 8985–8990.

71. W. Jeitschko, T. A. Bither and P. E. Bierstedt, Crystal structure and ionic conductivity of Li boracites. *Acta Crystallogr. B*, 1977, **33**, 2767–2775.

72. S. Shi, C. Lin, G. Yang, L. Cao, B. Li, T. Yan, M. Luo and N. Ye, $A_2Bi_2(SeO_3)_3F_2$ (A = K and Rb): Excellent Mid-Infrared Nonlinear Optical Materials with Both Strong SHG Responses and Large Band Gaps.*Chem. Mater.*, 2020, **32**, 7958–7964.

73. J. Y. Chung, H. Jo, S. Yeon, H. R. Byun, T.-S. You, J. I. Jang and K. M. Ok, $Bi_3(SeO_3)_3(Se_2O_5)F$: A Polar Bismuth Selenite Fluoride with Polyhedra of Highly Distortive Lone Pair Cations and Strong Second-Harmonic Generation Response. *Chem. Mater.*, 2020, **32**, 7318–7326.

74. L. Wang, F. Yang, X. Zhao, L. Huang, D. Gao, J. Bi, X. Wang and G. Zou, $Rb_3SbF_3(NO_3)_3$: an excellent antimony nitrate nonlinear optical material with a strong second harmonic generation response fabricated by a rational multi-component design.*Dalton Trans.*, 2019, **48**, 15144–15150.

75. S. Feng and R. Xu, New materials in hydrothermal synthesis, *Acc. Chem. Res.*, 2001, **34**, 239–247.

76. M. S. Whittingham, Hydrothermal synthesis of transition metal oxides under mild conditions, *Curr. Opin. Solid State Mater. Sci.*, 1996, **1**, 227–232.

77. J. Wang, P. Yox and K. Kovnir, Flux Growth of Phosphide and Arsenide Crystals. *Front. Chem.*, 2020, **8,** 186.

78. S. Atri and R. Tomar,A Review on the Synthesis and Modification of Functional Inorganic-Organic-Hybrid Materials via Microwave-Assisted Method. *ChemistrySelect*, 2021, **6**, 9351–9362.

79. W.-T. Chen, H.-M. Kuang and H.-L. Chen,Solid-state syntheses, crystal structures and properties of two novel metal sulfur chlorides—$Zn_6S_5Cl_2$ and $Hg_3ZnS_2Cl_4$. *J. Solid State Chem.*, 2010, **183**, 2411–2415.

80. Y. Chi, H.-G. Xue and S.-P. Guo,Designing Sulfide Borate as a Novel Type of Second-Order Nonlinear-Optical Material. *Inorg. Chem.*, 2020, **59**, 1547–1555.

81. W. Zhou, W.-D. Yao, R.-L. Tang, H. Xue and S.-P. Guo,Second-order nonlinear optical and photoelectric properties of $Zn_4B_6O_{12}S$ *J. Alloys Compd.*, 2021, **867**, 158879.

82. F. Nitsche, Th. Doert and M. Ruck, Tetragonal to orthorhombic phase transition of GdFeAsO studied by single-crystal X-ray diffraction.*Solid State Sci.*, 2013, **19**, 162–166.

83. X. Zhao, C. Lin, J. Chen, M. Luo, F. Xu, S. Yang, S. Shi, B. Li and N. Ye,Halonitrides Zn_2NX (X=Cl,Br): Novel Mid-Infrared Nonlinear Optical Materials. *Chem. Mater.*, 2021, **33**, 1462–1470.

84. M. G. Kanatzidis, R. Pöttgen and W. Jeitschko,The Metal Flux: A Preparative Tool for the Exploration of Intermetallic Compounds. *Angew. Chem. Int. Ed.*, 2005, **44**, 6996–7023.

85. W. Zhao, S. Pan, J. Han, Z. Zhou, X. Tian and J. Li, Synthesis, crystal structure and optical properties of a new lead fluoride borate with isolated $[B_9O_{21}]^{15-}$ unit. *Inorg. Chem. Commun.*, 2011, **14**, 566–568.

86. M. Cheng, W. Jin, Z. Yang and S. Pan, $Cs_3B_3O_3F_6$ with a Deep-Ultraviolet Cutoff Edge and a Suitable Birefringence as the Potential Zero-Order Waveplate Material. *Inorg. Chem.*, 2020, **59**, 13014–13018.

87. T. Yajima, K. Nakano, F. Takeiri, J. Hester, T. Yamamoto, Y. Kobayashi, N. Tsuji, J. Kim, A. Fujiwara and H. Kageyama, Synthesis and Physical Properties of the New Oxybismuthides $BaTi_2Bi_2O$ and $(SrF)_2Ti_2Bi_2O$ with a d^1 Square Net. *J. Phys. Soc. Jpn.*, 2013, **82**, 013703.

88. Q. Dong, P. Xiong, J. Yang, Y. Fu, W. Chen, F. Yang, Z. Ma and M. Peng,Bismuth activated blue phosphor with high absorption efficiency for white LEDs. *J. Alloys Compd.*, 2021, **885**, 160960.

89. A. Ablimit, Y.-L. Sun, H. Jiang, J.-K. Bao, H.-F. Zhai, Z.-T. Tang, Y. Liu, Z.-C. Wang, C.-M. Feng and G.-H. Cao,Synthesis, crystal structure and physical properties of a new oxypnictide $Ba_2Ti_2Cr_2As_4O$ containing $[Ti_2As_2O]^{2-}$ and $[Cr_2As_2]^{2-}$ layers. *J. Alloys Compd.*, 2017, **694**, 1149–1153.

90. D. Nowak, M. Valldor, B. Rubrecht, S. Froeschke, S. Eltoukhy, B. Büchner, S. Hampel and N. Gräßler, Crystal growth of the 2D Janus rhodium chalcohalide RhSeCl. *Inorg. Chem. Front.*, 2023, **10**, 2911-2916,

91. Y. Matsumoto, T. Yamamoto, K. Nakano, H. Takatsu, T. Murakami, K. Hongo, R. Maezono, H. Ogino, D. Song, C. M. Brown, C. Tassel and H. Kageyama, High-Pressure Synthesis of $A_2NiO_2Ag_2Se_2$ (A=Sr, Ba) with a High-Spin Ni^{2+} in Square-Planar Coordination. *Angew. Chem. Int. Ed.*, 2019, **58**, 756–759.

92. O. Ibragimova, L. Vaquero, Z. Hussein, V. Drozd, S. Chariton, V. Prakapenka and I. Chuvashova, The synthesis of novel lanthanum hydroxyborate at extreme conditions. *Front. Chem*. 2023, **11**, 1259000.

93. S. Sasaki, M. T. Caldes, C. Guillot-Deudon, I. Braems, G. Steciuk, L. Palatinus, E. Gautron, G. Frapper, E. Janod, B. Corraze, S. Jobic and L. Cario, Design of metastable oxychalcogenide phases by topochemical (de)intercalation of sulfur in $La_2O_2S_2$, *Nat. Commun.*,2021,**12**,3605.

94. R. Zhang, M. S. Senn and M. A. Hayward, Directed lifting of inversion symmetry in ruddlesden–popper oxide–fluorides: Toward ferroelectric and multiferroic behavior, *Chem. Mater.*, 2016, **28**, 8399–8406.

95. E. E. McCabe and C. Greaves, Fluorine insertion reactions into pre-formed metal oxides, *J. Fluor. Chem.*, 2007, **128**, 448–458.

96. H. Tao, T. Wu, M. Aldeghi, T. C. Wu, A. Aspuru-Guzik and E. Kumacheva,Nanoparticle synthesis assisted by machine learning. *Nat. Rev. Mater.*, 2021, **6**, 701–716.

97. M. Lu, H. Ji, Y. Zhao, Y. Chen, J. Tao, Y. Ou, Y. Wang, Y. Huang, J. Wang and G. Hao, Machine Learning-Assisted Synthesis of Two-Dimensional Materials. *ACS Appl. Mater. & Interfaces*, 2023, **15**, 1871-1878.

98. D. G. Gulevich, I. R. Nabiev and P. S. Samokhvalov,Machine learning–assisted colloidal synthesis: A review. *Mater. Today Chem.*, 2024, **35**, 101837.

99. Y. Wu, C.-F. Wang, M.-G. Ju, Q. Jia, Q. Zhou, S. Lu, X. Gao, Y. Zhang and J. Wang, Universal machine learning aided synthesis approach of two-dimensional perovskites in a typical laboratory. *Nat. Commun.*, 2024, **15**, 138.

100. S. D. Young, J. Chen, W. Sun, B. R. Goldsmith and G. Pilania, Thermodynamic stability and anion ordering of perovskite oxynitrides, *Chem. Mater.*, 2023, **35**, 5975–5987.

101. G. Pilania, A. Ghosh, S. T. Hartman, R. Mishra, C. R. Stanek and B. P. Uberuaga, Anion order in oxysulfide perovskites: origins and implications, *Npj Comput. Mater.*,2020,**6**,71.

102. C. Legein, B. J. Morgan, A. G. Squires, M. Body, W. Li, M. Burbano, M. Salanne, T. Charpentier, O. J. Borkiewicz and D. Dambournet, Correlated anion disorder in heteroanionic cubic $TiOF_2$, *J. Am. Chem. Soc.*, 2024, **146**, 21889–21902.

103. Z. Žák and M. Kosička, The crystal structure of lithium fluorosulphate $LiSO_3F$. *Acta Crystallogr. B*, 1978, **34**, 38–40.

104. H. B. Yahia, M. Shikano, S. Koike, K. Tatsumi, H. Kobayashi, H. Kawaji, M. Avdeev, W. Miiller, C. D. Ling, J. Liu and M.-H. Whangbo,Synthesis and Characterization of the Crystal Structure and Magnetic Properties of the New Fluorophosphate $LiNaCo[PO_4]F$. *Inorg. Chem.*, 2012, **51**, 8729–8738.

105. R. Guo, X. Liu, C. Tao, C. Tang, M. Xia, L. Liu, Z. Lin and X. Wang, $BaZnBe_2(BO_3)_2F_2$: a novel zinc-beryllium borate with SBBO-type structure overcoming the polymorphism problem. *Dalton Trans.*, 2021, **50**, 2138–2142.

106. L. Lin, X. Jiang, C. Wu, Z. Lin, Z. Huang, M. G. Humphrey and C. Zhang, First chiral fluorinated lead vanadate selenite $Pb_2(V_2O_4F)(VO_2)(SeO_3)_3$ with five asymmetric motifs and large optical properties. *Dalton Trans.*, 2021, **50**, 7238–7245.

107. X. Huang, M. Zhang, J. Li, Z. Zhao and Z. He,Synthesis, crystal structures and physical properties of two new sulfates $KYb(SO_4)_2{\cdot}H_2O$ and $KYb(SO_4)F_2$. *J. Solid State Chem.*, 2021, **294**, 121822.

108. C. Kutahyali Aslani, V. V. Klepov and H.-C. zur Loye,Flux crystal growth of a new $BaTa_2O_6$ polymorph, and of the novel tantalum oxyfluoride salt inclusion phase $[Ba_3F]Ta_4O_{12}F$: Flux dependent phase formation. *J. Solid State Chem.*, 2021, **294**, 121833.

109. S. C. Manna, P. Sandineni and A. Choudhury, Low temperature hydrothermal synthesis of $Na_3Fe_2(PO_4)_2F_3$ and its cathode electrochemistry in Na- and Li-ion batteries. *J. Solid State Chem.*, 2021, **295**, 121922.

110. Y. Chen, W. Zhang, D. An, M. Abudoureheman, Z. Chen and H. Mi,New Polymorphism for $Ba_3Zn_2(BO_3)_3F$ with Two Polymorphs Exhibiting Anomalous Phase Transition. *Eur. J. Inorg. Chem.*, 2021, **2021**, 1117–1121.

111. B. Scheibe, A. J. Karttunen, F. Weigend and F. Kraus,Photochemistry with Chlorine Trifluoride: Syntheses and Characterization of Difluorooxychloronium(V) Hexafluorido(non)metallates(V), $[ClOF_2][MF_6]$ (M=V, Nb, Ta, Ru, Os, Ir, P, Sb). *Chem. – Eur. J.*, 2021, **27**, 2381–2392.

112. S. Novikov, R. Bagum, Z. B. Yan, J. P. Clancy and Y. Mozharivskyj, Two new magnesium and magnesium-lead fluorogermanates and revision of the $Mg_{28}Ge_{7.5}O_{38}F_{10}$ phase.*J. Solid State Chem.*, 2021, **293**, 121741.

113. C. Wu, L. Li, L. Lin, Z. Huang, M. G. Humphrey and C. Zhang, Enhancement of Second-Order Optical Nonlinearity in a Lutetium Selenite by Monodentate Anion Partial Substitution. *Chem. Mater.*, 2020, **32**, 3043–3053.

114. J. C. Hancock, M. L. Nisbet, W. Zhang, P. S. Halasyamani and K. R. Poeppelmeier,Periodic Tendril Perversion and Helices in the $AMoO_2F_3$ (A = K, Rb, NH_4, Tl) Family. *J. Am. Chem. Soc.*, 2020, **142**, 6375–6380.

115. Q. Ding, X. Liu, S. Zhao, Y. Wang, Y. Li, L. Li, S. Liu, Z. Lin, M. Hong and J. Luo,Designing a Deep-UV Nonlinear Optical Fluorooxosilicophosphate. *J. Am. Chem. Soc.*, 2020, **142**, 6472–6476.

116. M. Ding, J. Xu, H. Wu, H. Yu, Z. Hu, J. Wang and Y. Wu, $Li_3CaB_2O_5F$: a unique sandwich-like structure with diverse and wide Li ion diffusion pathways. *Dalton Trans.*, 2020, **49**, 12184–12188.

117. W. Zhang, Z. Wei, Z. Yang and S. Pan,Two new ammonium/alkali-rare earth metal difluorophosphates $ALa(PO_2F_2)_4$ (A = NH_4 and K) with moderate birefringence and short cutoff edges. *Dalton Trans.*, 2020, **49**, 11591–11596.

118. C. Wu, X. Jiang, L. Lin, Z. Lin, Z. Huang, M. G. Humphrey and C. Zhang, $AGa_3F_6(SeO_3)_2$ (A = Rb, Cs): A New Type of Phase-Matchable Hexagonal Tungsten Oxide Material with Strong Second-Harmonic Generation Responses *Chem. Mater.*, 2020, **32**, 6906–6915.

119. W. Zhang, W. Jin, Z. Yang and S. Pan, $K_4(PO_2F_2)_2(S_2O_7)$: first fluorooxophosphorsulfate with mixed-anion $[S_2O_7]^{2-}$ and $[PO_2F_2]^-$ groups. *Dalton Trans.*, 2020, **49**, 17658–17664.

120. M.-L. Liang, Y.-X. Ma, C.-L. Hu, F. Kong and J.-G. Mao, $Ba(MoO_2F)_2(QO_3)_2$ (Q = Se, Te): Partial Fluorination of MoO_6 Octahedra Enabling Two Polar Solids with Strong and Phase Matchable SHG Response. *Chem. Mater.*, 2020, **32**, 9688–9695.

121. L. Lin, X. Jiang, C. Wu, L. Li, Z. Lin, Z. Huang, M. G. Humphrey and C. Zhang,$Ba(MoO_2F)_2(XO_3)_2$ (X = Se and Te): First Cases of Noncentrosymmetric Fluorinated Molybdenum Oxide Selenite/Tellurite Through Unary Substitution for Enlarging Band Gaps and Second Harmonic Generation. *ACS Appl. Mater. Interfaces*, 2020, **12**, 49812–49821.

122. M. A. Kirsanova, A. S. Akmaev, D. A. Aksyonov, S. V. Ryazantsev, V. A. Nikitina, D. S. Filimonov, M. Avdeev and A. M. Abakumov, Monoclinic α-Na_2FePO_4F with Strong Antisite Disorder and Enhanced Na^+ Diffusion. *Inorg. Chem.*, 2020, **59**, 16225–16237.

123. J. Zhou, Y. Liu, H. Wu, H. Yu, Z. Lin, Z. Hu, J. Wang and Y. Wu,$CsZn_2BO_3X_2$ (X_2=F_2, Cl_2, and FCl): A Series of Beryllium-Free Deep-Ultraviolet Nonlinear-Optical Crystals with Excellent Properties. *Angew. Chem. Int. Ed.*, 2020, **59**, 19006–19010.

124. Y. Deng, L. Huang, X. Dong, L. Wang, K. M. Ok, H. Zeng, Z. Lin and G. Zou, $K_2Sb(P_2O_7)F$: Cairo Pentagonal Layer with Bifunctional Genes Reveal Optical Performance. *Angew. Chem. Int. Ed.*, 2020, **59**, 21151–21156.

125. R. C. Vincent, P. Vishnoi, M. B. Preefer, J.-X. Shen, F. Seeler, K. A. Persson and R. Seshadri, $Li_5VF_4(SO_4)_2$: A Prototype High-Voltage Li-Ion Cathode. *ACS Appl. Mater. Interfaces*, 2020, **12**, 48662–48668.

126. R. E. Stene, B. Scheibe, A. J. Karttunen, W. Petry and F. Kraus, Synthesis and Characterization of $A[W_2O_2F_9]$ (A = Li – Cs). *Eur. J. Inorg. Chem.*, 2020, **2020**, 2260–2269.

127. P.-F. Li, F. Kong and J.-G. Mao, $M^{II}_2M_3^{III}F_3(Te_6F_2O_{16})$ (M^{II} = Pb, Ba; M^{III} = Al, Ga): New mixed anionic tellurites with isolated Te_6 coplanar rings. *J. Solid State Chem.*, 2020, **286**, 121288.

128. Y. Xie, Z. He, W. Zhang, Z. Zhao, M. Zhang and X. Huang,A new 3d-4f heterometallic selenite chloride with a distorted Shastry-Sutherland lattice. *J. Solid State Chem.*, 2020, **286**, 121315.

129. C. Stoll, M. Seibald, D. Baumann and H. Huppertz, K_2SnOF_4 and $K_2WO_3F_2$ – different but similar. *Z. Für Naturforschung B*, 2020, **75**, 833–841.

130. C. Stoll, M. Seibald and H. Huppertz, Synthesis and characterization of $K_5Sn_2OF_{11}$. *Z. Für Naturforschung B*, 2020, **75**, 83–90.

131. M. Shang and P. S. Halasyamani, Synthesis and electrical transport properties of $Lu_{2+x}Ti_{2-x}O_{7-x/2}$ oxide-ion conductors, *J. Solid State Chem.*, 2020, **282**, 121121.

132. T. Shi, F. Zhang, Y. Li, L. Gao, Z. Yang and S. Pan, Structural Diversity of Molybdate Iodate and Fluoromolybdate: Syntheses, Structures, and Calculations on $Na_3(MoO_4)(IO_3)$ and $Na_3Cs(MoO_2F_4)_2$, Inorg. Chem., 2020, **59**, 3034–3041.

133. Y. Wang, J. Han, J. Huang, Z. Yang and S. Pan, $Al_8(BO_3)_4(B_2O_5)F_8$: A F-Containing Aluminum Borate Featuring Two Types of Isolated B-O Groups, *Inorg. Chem.*, 2020, **59**, 810–817.

134. S. Han, M. Mutailipu, A. Tudi, Z. Yang and S. Pan, $PbB_5O_7F_3$: A High-Performing Short-Wavelength Nonlinear Optical Material, *Chem. Mater.*, 2020, **32**, 2172–2179.

135. H. Grossholz, C. Buyer, S. M. A. Lotter, S. Wolf and T. Schleid, About Lanthanoid Fluoride Selenide Oxoselenotantalates with the Composition $Ln_3F_2Se_2TaO_4$ (Ln = La – Nd), *Z. Für Anorg. Allg. Chem.*, 2020, **646**, 1588–1594.

136. J. T. Goettel, M. R. Bortolus, D. G. Stuart, H. P. A. Mercier and G. J. Schrobilgen, Chromium Oxide Tetrafluoride and Its Reactions with Xenon Hexafluoride; the $[XeF_5]^+$ and $[Xe_2F_{11}]^+$ Salts of the $[Cr^{VI}OF_5]^-$, $[Cr^{IV}F_6]^{2-}$, $[Cr^{V}OF_5]^{2-}$, and $[Cr^{V}_2O_2F_8]^{2-}$ Anions, *Chem. – Eur. J.*, 2019, **25**, 15815–15829.

137. R. E. Stene, B. Scheibe, A. J. Karttunen, W. Petry and F. Kraus, Lewis Acidic Behavior of $MoOF_4$ towards the Alkali Metal Fluorides in Anhydrous Hydrogen Fluoride Solutions, *Eur. J. Inorg. Chem.*, 2019, **2019**, 3672–3682.

138. G. Morrison, B. O. Wilkins, N. R. Spagnuolo, M. D. Smith and H.-C. zur Loye, Rare earth silicates and germanates crystallizing in the wadeite and related structure types, *J. Solid State Chem.*, 2019, **269**, 51–55.

139. Q. Ding, S. Zhao, L. Li, Y. Shen, P. Shan, Z. Wu, X. Li, Y. Li, S. Liu and J. Luo, Abrupt Structural Transformation in Asymmetric $ABPO_4F$ (A = K, Rb, Cs), *Inorg. Chem.*, 2019, **58**, 1733–1737.

140. N. Jiang and H. S. La Pierre, Frustrated Magnetism in a 2-D Ytterbium Fluoride, *Inorg. Chem.*, 2019, **58**, 12152–12156.

141. S. Shi, M. Luo, C. Lin and N. Ye, A cation size effect on the framework structures in $ABi_2SeO_3F_5$ (A = K and Rb): first examples of alkali metal bismuth selenite fluorides, *Dalton Trans.*, 2018, **47**, 6598–6604.

142. H. Li, H. Wu, X. Su, H. Yu, S. Pan, Z. Yang, Y. Lu, J. Han and K. R. Poeppelmeier, $Pb_3B_6O_{11}F_2$: the first non-centrosymmetric lead borate fluoride with a large second harmonic generation response, *J. Mater. Chem. C*, 2014, **2**, 1704–1710.

143. M. Mutailipu, M. Zhang, B. Zhang, Z. Yang and S. Pan, The first lead fluorooxoborate PbB_5O_8F: achieving the coexistence of large birefringence and deep-ultraviolet cut-off edge, *Chem. Commun.*, 2018, **54**, 6308–6311.

144. M. Luo, F. Liang, Y. Song, D. Zhao, N. Ye and Z. Lin, Rational Design of the First Lead/Tin Fluorooxoborates $MB_2O_3F_2$ (M = Pb, Sn), Containing Flexible Two-Dimensional $[B_6O_{12}F_6]_\infty$ Single Layers with Widely Divergent Second Harmonic Generation Effects, *J. Am. Chem. Soc.*, 2018, **140**, 6814–6817.

145. S. G. Jantz, M. Dialer, L. Bayarjargal, B. Winkler, L. van Wüllen, F. Pielnhofer, J. Brgoch, R. Weihrich and H. A. Höppe, $Sn[B_2O_3F_2]$—The First Tin Fluorooxoborate as Possible NLO Material, *Adv. Opt. Mater.*, 2018, **6**, 1800497.

146. W. Zhao, S. Pan, J. Han, J. Yao, Y. Yang, J. Li, M. Zhang, L. H. Zhang and Y. Hang, Synthesis, crystal structure and optical properties of the new lead fluoride borate—Pb_2BO_3F, *J. Solid State Chem.*, 2011, **184**, 2849–2853.

147. W. Zhao, S. Pan, X. Dong, J. Li, X. Tian, X. Fan, Z. Chen and F. Zhang, Synthesis, crystal structure and properties of a new lead fluoride borate, Pb_3OBO_3F, *Mater. Res. Bull.*, 2012, **47**, 947–951.

148. N. Ye and D. Tang, Hydrothermal growth of $KBe_2BO_3F_2$ crystals, *J. Cryst. Growth*, 2006, **293**, 233–235.

149. G. Yang, P. Gong, Z. Lin and N. Ye, $AZn_2BO_3X_2$(A = K, Rb, NH_4; X = Cl, Br): New Members of KBBF Family Exhibiting Large SHG Response and the Enhancement of Layer Interaction by Modified Structures, *Chem. Mater.*, 2016, **28**, 9122–9131.

150. L. Mei, X. Huang, Y. Wang, Q. Wu, B. Wu and C. Chen, Crystal structure of $KBe_2BO_3F_2$. *Z. Fur Krist.*, 1995, **210**, 93–95.

151. Y. Sang, D. Yu, M. Avdeev, R. Piltz, N. Sharma, N. Ye, H. Liu and J. Wang, X-ray and neutron diffraction studies of flux and hydrothermally grown nonlinear optical material $KBe_2BO_3F_2$, *CrystEngComm*, 2012, **14**, 6079.

152. J. Yu, L. Liu, S. Jin, H. Zhou, X. He, C. Zhang, W. Zhou, X. Wang, X. Chen and C. Chen, Superstructure and stacking faults in hydrothermal-grown $KBe_2BO_3F_2$ crystals, *J. Solid State Chem.*, 2011, **184**, 2790–2793.

153. Z. Li, S. Zhang, W. Xing, Z. Lin, J. Yao and Y. Wu, $Ba_8SrPb_{24}O_{24}Cl_{18}$: the first alkali-earth metal lead(ii) oxyhalide with an intriguing multimember-ring layer, *Dalton. Trans.*, 2020, **49**, 3667–3671.

154. K. Li, A. Yalikun and Z. Su, $[O_2Pb_3]_2(BO_3)I$: a new lead borate iodide with $^1{}_\infty[O_2Pb_3]$ double chains, *Dalton. Trans.*, 2020, **49**, 8985–8990.

155. S. Azuma, T. Kadoguchi, Y. Eguchi, H. Hirabaru, H. Ota, M. Sadakane, K. Yanagisawa, T. Hasegawa and T. Ueda, *Dalton. Trans.*, 2020, **49**, 2766–2770.

156. T. Zhu, S. Lee, X. Zhang, H. Yang, Y. Jin, Y. Jin, K.-Y. Choi and M. Lü, Variable Structures and One-Dimensional-Canting Antiferromagetism Found in Fluoride Selenates, $A_2Mn(SeO_4)F_3$ (A = K, Rb, Cs), *Inorg. Chem.*, 2021, **60**, 13707–13717.

157. P. Poltarak, V. Komarov, Y. Gayfulin, S. Artemkina and V. Fedorov, New O-centered titanium chalcohalide: synthesis and structure of $Ti_4O(Se_2)_4Br_6$, *Z. Für Anorg. Allg. Chem.*, 2021, **647**, 1729–1734.

158. B. C. Sheath, S. J. Cassidy and S. J. Clarke, Cation site preferences in layered oxide chalcogenides, synthesis, structures and magnetic ordering in $Sr_{3-x}Ca_xFe_2O_5Cu_2Ch_2$ (Ch = S, Se; x = 1, 2), *J. Solid State Chem.*, 2021, **293**, 121761.

159. Z.-H. Shi, Y. Chi, M. Yang, W. Liu and S.-P. Guo, A Series of Chalcogenide Borates $RE_6Ta_2MgQB_8O_{26}$ (RE = Sm, Eu, Gd; Q = S, Se) Featuring a B_4O_{10} Cluster, *Inorg. Chem.*, 2020, **59**, 3532–3536.

160. H. Kabbour, E. Janod, B. Corraze, M. Danot, C. Lee, M.-H. Whangbo and L. Cario, Structure and Magnetic Properties of Oxychalcogenides $A_2F_2Fe_2OQ_2$ (A = Sr, Ba; Q = S, Se) with Fe_2O Square Planar Layers Representing an Antiferromagnetic Checkerboard Spin Lattice, *J. Am. Chem. Soc.*, 2008, **130**, 8261–8270.

161. Z.-T. Lu, W.-J. Fan, Z.-Q. Wang, N. Gu, Z.-H. Yue, H.-G. Xue and S.-P. Guo, Second-Order Nonlinear-Optical-Active Selenide Borate $YSeBO_2$: Featuring a $[YSeBO_2]_n$ Planar Belt, *Inorg. Chem.*, 2020, **59**, 7905–7909.

162. X. Zhang, Y. Xiao, R. Wang, He, D. Wang, K. Bu, G. Mu and F. Huang, Synthesis, Crystal Structure, and Physical Properties of Layered *Ln*$CrSe_2O$ (Ln = Ce-Nd), *Inorg. Chem.* 2019, **58**, 14, 9482–9489.

163. C. Delacotte, O. Pérez, A. Pautrat, D. Berthebaud, S. Hébert, E. Suard, D. Pelloquin and A. Maignan, Magnetodielectric Effect in Crystals of the Noncentrosymmetric CaOFeS at Low Temperature, *Inorg. Chem.*, 2015, **54**, 6560–6565.

164. S. Altmannshofer and D. Johrendt, Synthesis, Crystal Structure and Magnetism of the New Oxysulfide $Ce_3NbO_4S_3$, *Z. Fur Anorg. Und Allg. Chem.*, 2008, **634**, 1361–1364.

165. T. A. Shestimerova, A. N. Kuznetsov and A. V. Shevelkov, Silver-chalcogen frameworks: crystal and electronic structure of $[Ag_3S](NO_3)$ and a comparison with $[Ag_4Te](SO_4)$, *Struct. Chem.*, 2018, **30**, 443–450.

166. J. R. Rea and E. Kostiner, The crystal structure of copper fluorophosphate, $Cu_2(PO_4)F$, *Acta Crystallogr. B*, 1976, **32**, 1944–1947.

167. M. J. Collins, R. J. Gillespie and J. F. Sawyer, Preparation and Crystal Structures of $(Te_2Se_8)(AsF_6)_2$, $(Te_{4.5}Se_{5.5})(AsF_6)_2$, and $(Te_2Se_6)(Te_2Se_8)(AsF_6)_4(SO_2)_2$, *Inorg. Chem.*, 1987, **26**, 1476–1481.

168. P. Boldrini, I. D. Brown, R. J. Gillespie, P. R. Ireland, W. Luk, D. R. Slim and J. E. Vekris, Preparation and crystal structures of ditellurium octaselenium bis(hexafluoroarsenate)-sulfur dioxide $Te_2Se_8(AsF_6)_2{\cdot}SO_2$, and "tetratellurium hexaselenium" bis(hexafluoroarsenate) $Te_{3.7}Se_{6.3}(AsF_6)_2$, *Inorg. Chem.*, 1976, **15**, 765–770.

169. J. R. Rea, J. B. Anderson and E. Kostiner, The crystal structures of copper chloroarsenate and cobalt chloroarsenate, $Cu_2(AsO_4)Cl$ and $Co_2(AsO_4)Cl$, *Acta Crystallogr. B*, 1977, **33**, 975–979.

170. Y. Wang, L. D. Calvert, E. J. Gabe and J. B. Taylor, Europium arsenic oxide Eu4As2O: a filled La_2Sb structure and its relation to the K_2NiF_4 and GeTeU types, *Acta Crystallogr. B*, 1977, **33**, 3122–3125.

171. R. Frankovsky, A. Marchuk, R. Pobel and D. Johrendt, Synthesis of $LaO_{1-x}F_xFeAs$ (x = 0–0.15) via solid state metathesis reaction*Solid State Commun.*, 2012, **152**, 632–634.

172. J. Karpinski, N. D. Zhigadlo, S. Katrych, Z. Bukowski, P. Moll, S. Weyeneth, H. Keller, R. Puzniak, M. Tortello, D. Daghero, R. Gonnelli, I. Maggio-Aprile, Y. Fasano, Ø. Fischer, K. Rogacki and B. Batlogg, Single crystals of $LnFeAsO_{1-x}F_x$ (Ln=La, Pr, Nd, Sm, Gd) and $Ba_{1-x}Rb_xFe_2As_2$: Growth, structure and superconducting properties, *Phys. C Supercond.*, 2009, **469**, 370–380.

173. N. Qureshi, Y. Drees, J. Werner, S. Wurmehl, C. Hess, R. Klingeler, B. Büchner, M. T. Fernández-Díaz and M. Braden, Crystal and magnetic structure of the oxypnictide superconductor $LaFeAsO_{1-x}F_x$: A neutron-diffraction study, *Phys. Rev. B*, 2010, **82**, 184521.

174. J. Kim, A. Fujiwara, T. Sawada, Y. Kim, K. Sugimoto, K. Kato, H. Tanaka, M. Ishikado, S. Shamoto and M. Takata, Evidence of electronic polarization of the As ion in the superconducting phase of F-doped LaFeAsO, *IUCrJ*, 2014, **1**, 155–159.

175. G. Cametti, M. Nagashima and S. V. Churakov, Role of lone-pair electron localization in temperature-induced phase transitions in mimetite, *Acta Crystallogr. Sect. B Struct. Sci. Cryst. Eng. Mater.*, 2022, **78**, 618–626.

176. H. Okudera, Relationships among channel topology and atomic displacements in the structures of $Pb_5(BO_4)_3Cl$ with B = P (pyromorphite), V (vanadinite), and As (mimetite), *Am. Mineral.*, 2013, **98**, 1573–1579.

177. J. Sejkora, J. Plasil, I. Cisarova, R. Skoda, J. Hlousek, F. Veselovsky and I. Jebava, Interesting supergene Pb-rich mineral association from the Rovnost mining field, Jáchymov (St. Joachimsthal), Czech Republic, *J. Geosci.*, 2011, **56**, 257–271.

178. J. Flis, O. Borkiewicz, T. Bajda, M. Manecki and J. Klasa, Synchrotron-based X-ray diffraction of the lead apatite series $Pb_{10}(PO_4)_6Cl_2$-$Pb_{10}(AsO_4)_6Cl_2$, *J. Synchrotron Radiat.*, 2010, **17**, 207–214.

179. Z. Yang, K. Ding, J. de Fourestier and H. Li, The crystal structure of mimetite-2M, a new polymorph of mimetite from Xianghualing tin-polymetallic orefield, Hunan Province, P. R. China, *Neues Jahrb. Für Mineral. - Abh.*, 2013, **190,** 229–235.

180. H. Effenberger and F. Pertlik, The crystal structure of finnemanite, $Pb_5Cl(AsO_3)_3$, with a comparison to the structure-type of chlorapatite, $Ca_5Cl(PO_4)_3$, *Mineral. Petrol.*, 1979, **26**, 95–107.

181. P. Quebe, L. J. Terbüchte and W. Jeitschko, Quaternary rare earth transition metal arsenide oxides RTAsO (T = Fe, Ru, Co) with ZrCuSiAs type structure, *J. Alloys Compd.*, 2000, **302**, 70–74.

182. F. Nitsche, A. Jesche, E. Hieckmann, Th. Doert and M. Ruck, Structural trends from a consistent set of single-crystal data of *R*FeAsO (*R*=La, Ce, Pr, Nd, Sm, Gd, and Tb), *Phys. Rev. B*, 2010, **82**, 134514.

183. R. H. Liu, Y. A. Song, Q. J. Li, J. J. Ying, Y. J. Yan, Y. He and X. H. Chen, Structure and Physical Properties of the Layered Pnictide-Oxides: $(SrF)_2Ti_2Pn_2O$ (Pn = As, Sb) and $(SmO)_2Ti_2Sb_2O$, *Chem. Mater.*, 2010, **22**, 1503–1508.

184. T. Watanabe, H. Yanagi, Y. Kamihara, T. Kamiya, M. Hirano and H. Hosono, Nickel-based layered superconductor, LaNiOAs, *J. Solid State Chem.*, 2008, **181**, 2117–2120.

185. T. Bartsch, R.-D. Hoffmann and R. Pöttgen, The quaternary arsenide oxides $Ce_9Au_{5-x}As_8O_6$ and $Pr_9Au_{5-x}As_8O_6$, *Z. Für Naturforschung B*, 2016, **71**, 1245–1252.

186. K. Bu, M. Luo, R. Wang, X. Zhang, J. He, D. Wang, W. Zhao and F. Huang, Enhanced Photoelectric $SrOCuSbS_2$ of a [SrO]-Intercalated $CuSbS_2$ Structure, *Inorg. Chem.*, 2019, **58**, 69–72.

187. S. L. Brock, N. P. Raju, J. E. Greedan and S. M. Kauzlarich, The magnetic structures of the mixed layer pnictide compounds $Sr_2Mn_3Pn_2O_2$, *J. Alloys Compd.*, 1996, **237**, 9–19.

188. J. Nuss and M. Jansen, Reticular merohedral twinning within the $La_9Sb_5O_5$ structure family: structure of $Pr_9Sb_5O_5$, $Sm_9Sb_5O_5$ and Dy_9Sb_5O, *Acta Crystallogr. B*, 2007, **63**, 843–849.

189. P. Wang, S. Forbes, T. Kolodiazhnyi, K. Kosuda and Y. Mozharivskyj, Synthesis, Crystal and Electronic Structures of New Narrow-Band-Gap Semiconducting Antimonide Oxides RE_3SbO_3 and $RE_8Sb_{3-\delta}O_8$, with RE = La, Sm, Gd, and Ho, *J. Am. Chem. Soc.*, 2010, **132**, 8795–8803.

190. B. Saparov and S. Bobev, Pentaeuropium dicadmium pentaantimonide oxide, Eu5Cd2Sb5O. Acta Crystallogr E. 2011, **67**, i11.

191. A. Pfitzner and P. Pohla, Syntheses and Crystal Structures of $PbSbO_2Br$, $PbSbO_2I$, and $PbBiO_2Br$, *Z. Für Anorg. Allg. Chem.*, 2009, **635**, 1157–1159.

192. J. F. Ackerman, The structures of Bi_3PbWO_8Cl and Bi_4NbO_8Cl and the evolution of the bipox structure series, *J. Solid State Chem.*, 1986, **62**, 92–104.

193. L. N. Kholodkovskaya, L. G. Akselrud, A. M. Kusainova, V. A. Dolgikh and B. A. Popovkin, BiCuSeO: Synthesis and Crystal Structure, *Mater. Sci. Forum*, 1993, **133–136**, 693–696.

194. A. P. Richard, J. A. Russell, A. Zakutayev, L. N. Zakharov, D. A. Keszler and J. Tate, Synthesis, structure, and optical properties of BiCuOCh (Ch=S, Se, and Te), *J. Solid State Chem.*, 2012, **187**, 15–19.

195. H. Hiramatsu, H. Yanagi, T. Kamiya, K. Ueda, M. Hirano and H. Hosono, Crystal Structures, Optoelectronic Properties, and Electronic Structures of Layered Oxychalcogenides MCuOCh (M = Bi, La; Ch = S, Se, Te): Effects of Electronic Configurations of M^{3+} Ions, *Chem. Mater.*, 2008, **20**, 326–334.

196. A. M. Kusainova, P. S. Berdonosov, L. G. Akselrud, L. N. Kholodkovskaya, V. A. Dolgikh and B. A. Popovkin, New Layered Compounds with the General Composition (MO) (CuSe), Where M = Bi, Nd, Gd, Dy, and BiOCuS: Syntheses and Crystal Structure, *J. Solid State Chem.*, 1994, **112**, 189–191.

197. R. H. C. Gil, J. Nuss, Y. Grin, W. Hönle and H. G. von Schnering, Crystal structure of tetraeuropium diantimonide oxide, Eu_4Sb_2O. *Z. Für Krist. - New Cryst. Struct.*, 1998, **213**, 14–14.

198. C. Hadenfeldt and H. O. Vollert, Darstellung und kristallstruktur der calciumpnictidoxide Ca_4P_2O und Ca_4As_2O, *J. Common Met.*, 1988, **144**, 143–151.

199. D. Kaczorowski, J. H. Albering, H. Noël and W. Jeitschko, Crystal structure and complex magnetic behaviour of a novel uranium oxyphosphide UCuPO, *J. Alloys Compd.*, 1994, **216**, 117–121.

200. H. Sakai, N. Tateiwa, T. D. Matsuda, T. Sugai, E. Yamamoto and Y. Haga, Crystal Structure and Physical Properties of Uranium–Copper Oxyphosphide UCuPO, *J. Phys. Soc. Jpn.*, 2010, **79**, 074721.

201. D. M. Wells, E. Ringe, D. Kaczorowski, D. Gnida, G. André, R. G. Haire, D. E. Ellis and J. A. Ibers, Structure, properties, and theoretical electronic structure of UCuOP and NpCuOP, *Inorg. Chem.*, 2011, **50**, 576–589.

202. T. Watanabe, H. Yanagi, T. Kamiya, Y. Kamihara, H. Hiramatsu, M. Hirano and H. Hosono, Nickel-Based Oxyphosphide Superconductor with a Layered Crystal Structure, LaNiOP, *Inorg. Chem.*, 2007, **46**, 7719–7721.

203. M. Tegel, D. Bichler and D. Johrendt, Synthesis, crystal structure and superconductivity of LaNiPO, *Solid State Sci.*, 2008, **10**, 193–197.

204. B. Lorenz, K. Sasmal, R. P. Chaudhury, X. H. Chen, R. H. Liu, T. Wu and C. W. Chu, Effect of pressure on the superconducting and spin-density-wave states of $SmFeAsO_{1-x}F_x$, *Phys. Rev. B*, 2008, **78**, 012505.

205. I. Schellenberg, T. Nilges and R. Pöttgen, Structural and ^{121}Sb Mössbauer Spectroscopic Investigations of the Antimonide Oxides REMnSbO (RE = La, Ce, Pr, Nd, Sm, Gd, Tb) and REZnSbO (RE = La, Ce, Pr), *Z. Für Naturforschung B*, 2008, **63**, 834–840.

206. Q. Zhang, C. M. N. Kumar, W. Tian, K. W. Dennis, A. I. Goldman and D. Vaknin, Structure and magnetic properties of *Ln*MnSbO (*Ln*=La and Ce), *Phys. Rev. B*, 2016, **93**, 094413.

207. H. Lincke, R. Glaum, V. Dittrich, M. Tegel, D. Johrendt, W. Hermes, M. H. Möller, T. Nilges and R. Pöttgen, Magnetic, Optical, and Electronic Properties of the Phosphide Oxides REZnPO (RE = Y, La–Nd, Sm, Gd, Dy, Ho), *Z. Für Anorg. Allg. Chem.*, 2008, **634**, 1339–1348.

208. B. I. Zimmer, W. Jeitschko, J. H. Albering, R. Glaum and M. Reehuis, The rare earth transition metal phosphide oxides LnFePO, LnRuPO and LnCoPO with ZrCuSiAs type structure, *J. Alloys Compd.*, 1995, **229**, 238–242.

209. X. Xu, M. A. Jones, S. J. Cassidy, P. Manuel, F. Orlandi, M. Batuk, J. Hadermann and S. J. Clarke, Magnetic Ordering in the Layered Cr(II) Oxide Arsenides $Sr_2CrO_2Cr_2As_2$ and $Ba_2CrO_2Cr_2As_2$, *Inorg. Chem.*, 2020, **59**, 15898–15912.

210. H. Jiang, J.-K. Bao, H.-F. Zhai, Z.-T. Tang, Y.-L. Sun, Y. Liu, Z.-C. Wang, H. Bai, Z.-A. Xu and G.-H. Cao, Physical properties and electronic structure of $Sr_2Cr_3As_2O_2$ containing CrO_2 and Cr_2As_2 square-planar lattices, *Phys. Rev. B*, 2015, **92**, 205107.

211. B. C. Sheath, X. Xu, P. Manuel, J. Hadermann, M. Batuk, J. O'Sullivan, R. S. Bonilla and S. J. Clarke, Structures and Magnetic Ordering in Layered Cr Oxide Arsenides $Sr_2CrO_2Cr_2OAs_2$ and Sr_2CrO_3CrAs, *Inorg. Chem.*, 2022, **61**, 12373–12385.

212. R. Nath, V. O. Garlea, A. I. Goldman and D. C. Johnston, Synthesis, structure, and properties of tetragonal $Sr_2M_3As_2O_2$ (M_3=Mn_3, Mn_2Cu, and $MnZn_2$) compounds containing alternating CuO2-type and FeAs-type layers, *Phys. Rev. B*, 2010, **81**, 224513.

213. M. Tegel, F. Hummel, S. Lackner, I. Schellenberg, R. Pöttgen and D. Johrendt, The Layered Iron Arsenide Oxides Sr_2CrO_3FeAs and Ba_2ScO_3FeAs, *Z. Für Anorg. Allg. Chem.*, 2009, **635**, 2242–2248.

214. T. Ozawa, M. M. Olmstead, S. L. Brock, S. M. Kauzlarich and D. M. Young, Synthesis and Characterization of a New Compound with Alternating MnO_2^{2-} and $Zn_2As_2^{2-}$ Layers: $Ba_2MnZn_2As_2O_2$, *Chem. Mater.*, 1998, **10**, 392–396.

215. Y.-L. Sun, H. Jiang, H.-F. Zhai, J.-K. Bao, W.-H. Jiao, Q. Tao, C.-Y. Shen, Y.-W. Zeng, Z.-A. Xu and G.-H. Cao, $Ba_2Ti_2Fe_2As_4O$: A New Superconductor Containing Fe_2As_2 Layers and Ti_2O Sheets, *J. Am. Chem. Soc.*, 2012, **134**, 12893–12896.

216. Y. Liu, W. E. Straszheim, P. Das, F. Islam, T. W. Heitmann, R. J. McQueeney and D. Vaknin, Synthesis and characterization of Ca-doped LaMnAsO, *Phys. Rev. Mater.*, 2018, **2**, 054410.

217. E. J. Wildman, N. Emery and A. C. Mclaughlin, Electronic and magnetic properties of $Nd_{1-x}Sr_xMnAsO$ oxyarsenides, *Phys. Rev. B*, 2014, **90**, 224413.

218. A. Marcinkova, E. Suard, A. N. Fitch, S. Margadonna and J. W. G. Bos, Response of the Crystal Structure and Electronic Properties to Calcium Substitution in NdFeAsO, *Chem. Mater.*, 2009, **21**, 2967–2972.

219. D. Kaczorowski, M. Potel and H. Noël, Crystal Structure of the First Uranium Oxyarsenide $U_2Cu_2As_3O$, *J. Solid State Chem.*, 1994, **112**, 228–231.

220. S. Amano and H. Yamane, Synthesis and crystal structure analysis of titanium bismuthide oxide, Ti_8BiO_7, *J. Alloys Compd.*, 2016, **675**, 377–380.

221. L. Qiao, J. Chen, B. Lv, X. Yang, J. Wu, Y. Cui, H. Bai, M. Li, Y. Li, Z. Ren, J. Dai and Z. Xu, Antiferromagnetic Kondo lattice compound Ce_2O_2Bi with anti-$ThCr_2Si_2$-type structure, *J. Alloys Compd.*, 2020, **836**, 155229.

222. J. Nuss and M. Jansen, Syntheses, structures and properties of the pnictide oxides R_2PnO_2 (R = Ce, Pr; Pn = Sb, Bi), *J. Alloys Compd.*, 2009, **480**, 57–59.

223. R. Benz, Ce_2O_2Sb and Ce_2O_2Bi crystal structure. *Acta Crystallogr. B*, 1971, **27**, 853–854.

224. H. Mizoguchi and H. Hosono, A Metal−Insulator Transition in R_2O_2Bi with an Unusual Bi^{2-} Square Net (R = Rare Earth or Y). *J. Am. Chem. Soc.*, 2011, **133**, 2394–2397.

225. S. Saha, S. Chanda, A. Dutta, U. Kumar, R. Ranjan and T. P. Sinha, Dielectric relaxation and anti-ferromagnetic coupling of $BiEuO_3$ and $BiGdO_3$. *J. Magn. Magn. Mater.*, 2014, **360**, 80–86.

226. J. Nuss, U. Wedig and M. Jansen, Geometric Variations and Electron Localizations in Intermetallics: The Case of La_2Sb Type Compounds. *Z. Für Anorg. Allg. Chem.*, 2011, **637**, 1975–1981.

227. S.-Q. Xia and S. Bobev, Dibarium tricadmium bismuthide(-I,-III) oxide, $Ba_2Cd_{3-\delta}Bi_3O$. *Acta Crystallogr.. E*, 2010, **66**, i81–i81.

228. S. Forbes, F. Yuan, K. Kosuda, T. Kolodiazhnyi and Y. Mozharivskyj, Synthesis, crystal structure, and physical properties of the Gd_3BiO_3 and $Gd_8Bi_3O_8$ phases. *J. Solid State Chem.*, 2016, **233**, 252–258.

229. M. Markov, L. Alaerts, H. P. C. Miranda, G. Petretto, W. Chen, J. George, E. Bousquet, P. Ghosez, G.-M. Rignanese and G. Hautier, Ferroelectricity and multiferroicity in anti–Ruddlesden–Popper structures. *Proc. Natl. Acad. Sci.*, 2021, **118**, e2026020118.

230. M. Boss, F. Pickhard, M. Zumdick and C. Röhr, Barium antimonide oxide, Ba_3Sb_2O. *Acta Crystallogr. C*, 2001, **57**, 503–504.

231. M. Boss, D. Petri, F. Pickhard, P. Zönnchen and C. Röhr, Neue Barium-Antimonid-Oxide mit den Zintl-Ionen $[Sb]^{3-}$, $[Sb_2]^{4-}$ und $^1{}_\infty[Sb_n]^{n-}$. *Z. Für Anorg. Allg. Chem.*, 2005, **631**, 1181–1190.

232. G. Derrien, M. Tillard, L. Monconduit and C. Belin, Potassium barium bismuth oxide. *Acta Crystallogr. C*, 2000, **56**, iuc0000138-e232.

233. B. Eisenmann and U. Rössler, Crystal structure of potassium tetrabarium tribismutide oxide, KBa_4Bi_3O. *Z. Für Krist. - New Cryst. Struct.*, 2000, **215**, 349–350.

234. H. Lincke, T. Nilges and R. Pöttgen, Dimorphic CeZnPO and PrZnPO. *Z. Für Anorg. Allg. Chem.*, 2006, **632**, 1804–1808.

235. R. J. Cava, H. W. Zandbergen, J. J. Krajewski, T. Siegrist, H. Y. Hwang and B. Batlogg, $Ln_3Cu_4P_4O_2$: A New Lanthanide Transition Metal Pnictide Oxide Structure Type. *J. Solid State Chem.*, 1997, **129**, 250–256.

236. H. Kotegawa, T. Kawazoe, H. Tou, K. Murata, H. Ogino, K. Kishio and J. Shimoyama, Contrasting Pressure Effects in $Sr_2VFeAsO_3$ and $Sr_2ScFePO_3$. *J. Phys. Soc. Jpn.*, 2009, **78**, 123707.

237. Y. Tojo, T. Shibuya, T. Nakamura, K. Shoji, H. Fujioka, M. Matoba, S. Yasui, M. Itoh, S. Iimura, H. Hiramatsu, H. Hosono, S. Hirai, W. Mao, S. Kitao, M. Seto and Y. Kamihara, Superconducting transition temperatures in the electronic and magnetic phase diagrams of $Sr_2VFeAsO_{3-\delta}$, a superconductor. *J. Phys. Condens. Matter*, 2019, **31**, 115801.

238. M. Tegela, I. Schellenberg, F. Hummel, R. Pöttgen and D. Jorendt, Low-temperature Crystal Structure and ^{57}Fe Mössbauer Spectroscopy of $Sr_3Sc_2O_5Fe_2As_2$. *Z. Für Naturforschung B*, 2009, **64**, 815–820.

239. D. Chen, T.-T. Zhang, Z.-D. Song, H. Li, W.-L. Zhang, T. Qian, J.-L. Luo, Y.-G. Shi, Z. Fang, P. Richard and H. Ding, New phase transition in $Na_2Ti_2As_2O$ revealed by Raman scattering. *Phys. Rev. B*, 2016, **93**, 140501.

240. J. Nuss and M. Jansen, New Ternary La_2Sb-Type Compounds, ScRESb (RE = La, Ce, Pr, Nd, Sm, Tb), and the Oxygen Stuffed Variant $Sc_4Yb_4Sb_4O$. *Z. Für Anorg. Allg. Chem.*, 2014, **640**, 713–718.

241. T. Yajima, K. Nakano, Y. Nozaki and H. Kageyama, Superconducting properties of $BaTi_2Pn_2O$ (Pn = Sb, Bi). *Phys. C Supercond. Its Appl.*, 2014, **504**, 36–38.

242. T. Yamamoto, T. Yajima, Z. Li, T. Kawakami, K. Nakano, T. Tohyama, T. Yagi, Y. Kobayashi and H. Kageyama, Pressure-Induced Collapse Transition in $BaTi_2Pn_2O$ (Pn = As, Sb) with an Unusual Pn–Pn Bond Elongation. *Inorg. Chem.*, 2021, **60**, 2228–2233.

243. K. Nakano, K. Hongo and R. Maezono, Phonon dispersions and Fermi surfaces nesting explaining the variety of charge ordering in titanium-oxypnictides superconductors. *Sci. Rep.*, 2016, **6**, 29661.

244. G. M. Darone and S. Bobev, $Ba_5Cd_2Sb_4O_2$—A New Antimonide Oxide with a Complex Structure. *Crystals*, 2011, **1**, 206–214.

245. T. Bartsch, O. Niehaus, D. Johrendt, Y. Kobayashi, M. Seto, P. M. Abdala, M. Bartsch, H. Zacharias, R.-D. Hoffmann, B. Gerke, U. C. Rodewald and R. Pöttgen, New quaternary arsenide oxides with square planar coordination of gold(I) – structure, ^{197}Au Mössbauer spectroscopic, XANES and XPS characterization of $Nd_{10}Au_3As_8O_{10}$ and $Sm_{10}Au_3As_8O_{10}$. *Dalton Trans.*, 2015, **44**, 5854–5866.

246. T. Bartsch, O. Niehaus, R.-D. Hoffmann, M. Bartsch, H. Zacharias, D. Johrendt and R. Pöttgen, Palladium pnictide oxides $Nd_{10}Pd_3As_8O_{10}$ and $Sm_{10}Pd_3As_8O_{10}$ – low temperature structural phase transition and physical properties. *J. Mater. Chem. C*, 2016, **4**, 6727–6741.

247. T. Bartsch, T. Wiegand, J. Ren, H. Eckert, D. Johrendt, O. Niehaus, M. Eul and R. Pöttgen, Phosphide Oxides RE_2AuP_2O (RE = La, Ce, Pr, Nd): Synthesis, Structure, Chemical Bonding, Magnetism, and ^{31}P and ^{139}La Solid State NMR. *Inorg. Chem.*, 2013, **52**, 2094–2102.

248. M. Eul, M. H. Möller, R.-D. Hoffmann, W. Jeitschko and R. Pöttgen, A Further Extension of Pnictide Oxide Chemistry – Synthesis and Structure of La_2AuP_2O. *Z. Für Anorg. Allg. Chem.*, 2012, **638**, 331–335.

249. X.-J. Wang, F. Krumeich, M. Wörle, R. Nesper, L. Jantsky and H. Fjellvåg, Niobium(V) Oxynitride: Synthesis, Characterization, and Feasibility as Anode Material for Rechargeable Lithium-Ion Batteries. *Chem. - Eur. J.*, 2012, **18**, 5970–5978.

250. H. Lincke, R. Glaum, V. Dittrich, M. Tegel, D. Johrendt, W. Hermes, M. H. Möller, T. Nilges and R. Pöttgen, Magnetic, Optical, and Electronic Properties of the Phosphide Oxides REZnPO (RE = Y, La–Nd, Sm, Gd, Dy, Ho). *Z. Fur Anorg. Und Allg. Chem.*, 2008, **634**, 1339–1348.

251. C. Wang, Z.-C. Wang, Y.-X. Mei, Y.-K. Li, L. Li, Z.-T. Tang, Y. Liu, P. Zhang, H.-F. Zhai, Z.-A. Xu and G.-H. Cao, A New ZrCuSiAs-Type Superconductor: ThFeAsN. *J. Am. Chem. Soc.*, 2016, **138**, 2170–2173.

252. R. Pöttgen and D. Johrendt, Materials with ZrCuSiAs-type Structure. *Z. Fur Naturforsch. B*, 2008, **63**, 1135–1148.

253. S. Yamanaka, T. Yasunaga, K. Yamaguchi and M. Tagawa, Structure and superconductivity of the intercalation compounds of TiNCl with pyridine and alkali metals as intercalant. *J. Mater. Chem.*, 2009, **19**, 2573–2582.

254. S. Yamanaka, H. Kawaji, K. Hotehama and M. Ohashi, A new layer-structured nitride superconductor. Lithium-intercalated β-zirconium nitride chloride, Li_xZrNCl. *Adv. Mater.*, 1996, **8**, 771–774.

255. R. Juzatr and H. Friedrichsen, Die Kristallstruktur von β-ZrNCl und β-ZrNBr. *Z. Für Anorg. Allg. Chem.*, 1964, **332**, 173–178.

256. R. Juza and J. Heners, Über Nitridhalogenide des Titans und Zirkons. *Z. Für Anorg. Allg. Chem.*, 1964, **332**, 159–172.

257. X. Liu, D.-Y. Liu, T.-T. Li, D.-M. Chen and L.-J. Zou, Investigation on the interlayer coupling and bonding in layered nitride-halides ThNF and ThNCl. *RSC Adv.*, 2021, **11**, 28698–28703.

258. S. Yamanaka, K. Hotehama and H. Kawaji, Superconductivity at 25.5 K in electron-doped layered hafnium nitride. *Nature*, 1998, **392**, 580–582.

259. J. Strähle, Die Kristallstruktur von Molybdännitridchlorid, $MoNCl_3$. *Z. Für Anorg. Allg. Chem.*, 1970, **375**, 238–254.

260. A. J. D. Barnes, T. J. Prior and M. G. Francesconi, Zeolite-like nitride–chlorides with a predicted topology. *Chem. Commun.*, 2007, **44** ,4638-4640.

261. W. Schnick and J. Lücke, $Zn_7[P_{12}N_{24}]Cl_2$ — ein Sodalith mit einem Phosphor-Stickstoff-Grundgerüst. *Angew. Chem.*, 1992, **104**, 208–209.

262. M. Ströbele, K. Eichele and H.-J. Meyer, Phosphorus-Centered and Phosphinidene-Capped Tungsten Chloride Clusters. *Eur. J. Inorg. Chem.*, 2011, **2011**, 4063–4068.

263. J.-A. Dolyniuk, N. Tran, K. Lee and K. Kovnir, Sr_2P_7X (X = Cl, Br, and I): Synthesis, Crystal and Electronic Structures of Double Zintl Salts Containing Heptaphosphanortricyclane, P_7^{3-}. *Z. Für Anorg. Allg. Chem.*, 2015, **641**, 1422–1427.

264. W. Harrison and J. Trotter, Crystal and molecular structure of nitrilohexaphosphonitrilic chloride [2,2,3a,5,5,6a,8,8,9a-nonachloro-2,2,5,5,8,8-hexahydro-1,3,4,6,7,9,9b-hepta-aza-2,3a,5,6a,8,9a-hexaphospha(3a,6a,9a,-PV)phenalene]. *J. Chem. Soc. Dalton Trans.*, 1972, **5**, 623-626.

265. W. Haubold, W. Keller and G. Sawitzki, Das erste *closo*-Diphosphahexaboran $P_2B_4Cl_4$. *Angew. Chem.*, 1988, **100**, 958–959.

266. H. Preiss, Die Kristallstrukturen der Verbindungen PCl_5NbCl_5 und PCl_5TaCl_5. *Z. Für Anorg. Allg. Chem.*, 1971, **380**, 56–64.

267. P. H. Collins and M. Webster, The crystal and molecular structure of the 1:1 compound formed between phosphorus pentachloride and tellurium tetrachloride, Cl_9PTe. *Acta Crystallogr. B*, 1972, **28**, 1260–1264.

268. J. Shamir, S. Luski, A. Bino, S. Cohen and D. Gibson, Reactions of phosphorus pentachloride with tin tetrachloride. Tetrachlorophosphonium salts with hexachlorostannate(2-), decachlorodistannate(2-), and pentachlorostannate(1-) anions: preparation and structure by vibrational spectra and x-ray crystallography. *Inorg. Chem.*, 1985, **24**, 2301–2309.

269. M. A. Kraft, S. P. Culver, M. Calderon, F. Böcher, T. Krauskopf, A. Senyshyn, C. Dietrich, A. Zevalkink, J. Janek and W. G. Zeier, *J. Am. Chem. Soc.*, 2017, **139**, 10909–10918.

270. H.-J. Deiseroth, S.-T. Kong, H. Eckert, J. Vannahme, C. Reiner, T. Zaiß and M. Schlosser, Influence of Lattice Polarizability on the Ionic Conductivity in the Lithium Superionic Argyrodites Li_6PS_5X (X = Cl, Br, I). *Angew. Chem. Int. Ed.*, 2008, **47**, 755–758.

271. A. V. Olenev, A. V. Shevelkov and B. A. Popovkin, Crystal Structure of $Hg_2PCl_2$and Electronic Structure of Its Main "Building Unit"—The (P_2Hg6) Octahedron. *J. Solid State Chem.*, 1999, **142**, 14–18.

272. J. Wang, D. Kaseman, K. Lee, S. Sen and K. Kovnir, Enclathration of X@La_4 Tetrahedra in Channels of Zn–P Frameworks in $La_3Zn_4P_6X$ (X = Cl, Br). *Chem. Mater.*, 2016, **28**, 4741–4750.

273. A. V. Olenev, A. I. Baranov, A. V. Shevelkov and B. A. Popovkin, A New Family of Supramolecular Complexes with 3D Cationic Hg/Z Frameworks, SnX_3^- Guest Anions (Z = P, As, Sb; X = Cl, Br, I): Crystal Structures and Host−Guest Interactions. *Eur. J. Inorg. Chem.*, 2002, **2002**, 547–553.

274. P. de Santis, E. Giglio and A. Ripamonti, The crystal structure of trimeric phosphonitrilic bromide. *J. Inorg. Nucl. Chem.*, 1962, **24**, 469–474.

275. H. Menke and H. G. von Schnering, Die Käfigverbindungen $Ge_{38}A_8X_8$mit A = P, As. Sb und X = Cl, Br, J. *Z. Für Anorg. Allg. Chem.*, 1973, **395**, 223–238.

276. O. Oeckler, H. Mattausch and A. Simon, Einige Phosphidhalogenide des Lanthans und verwandte Verbindungen/ Some Phosphide Halides of Lanthanum and Related Compounds. *Z. Für Naturforschung B*, 2007, **62**, 1377–1382.

277. K. A. Kovnir, J. V. Zaikina, L. N. Reshetova, A. V. Olenev, E. V. Dikarev and A. V. Shevelkov, Unusually High Chemical Compressibility of Normally Rigid Type-I Clathrate Framework: Synthesis and Structural Study of $Sn_{24}P_{19.3}Br_xI_{8-x}$ Solid Solution, the Prospective Thermoelectric Material. *Inorg. Chem.*, 2004, **43**, 3230–3236.

278. M. G. B. Drew and R. Mandyczewsky, Crystal and molecular structures of tungsten(VI) sulphide tetrachloride and tungsten(VI) sulphide tetrabromide. *J. Chem. Soc. Inorg. Phys. Theor.*, 1970, **0**, 2815-2818.

279. M. F. Groh, U. Müller, E. Ahmed, A. Rothenberger and M. Ruck, Substitution of Conventional High-temperature Syntheses of Inorganic Compounds by Near-room-temperature Syntheses in Ionic Liquids. *Z. Für Naturforschung B*, 2013, **68**, 1108–1122.

280. S. Toso, Q. A. Akkerman, B. Martín-García, M. Prato, J. Zito, I. Infante, Z. Dang, A. Moliterni, C. Giannini, E. Bladt, I. Lobato, J. Ramade, S. Bals, J. Buha, D. Spirito, E. Mugnaioli, M. Gemmi and L. Manna, Nanocrystals of Lead Chalcohalides: A Series of Kinetically Trapped Metastable Nanostructures. *J. Am. Chem. Soc.*, 2020, **142**, 10198–10211.

281. Z. Liu, T. Zinkevich, S. Indris, X. He, J. Liu, W. Xu, J. Bai, S. Xiong, Y. Mo and H. Chen, $Li_{15}P_4S_{16}Cl_3$, a Lithium Chlorothiophosphate as a Solid-State Ionic Conductor. *Inorg. Chem.*, 2020, **59**, 226–234.

282. M. Smith and G. J. Miller, Ta_3SBr_7—A New Structure Type in the M_3QX_7 Family (M=Nb, Ta;Q=S, Se, Te;X=Cl, Br, I) *J. Solid State Chem.*, 1998, **140**, 226–232.

283. S. Pohl, $Ge_4S_6Br_4$ – das erste Sulfidhalogenid des Germaniums. *Angew. Chem.*, 1976, **88**, 162–163.

284. T. Sakuma and S. Hoshino, The Phase Transition and the Structures of Superionic Conductor Ag_3SBr. *J. Phys. Soc. Jpn.*, 1980, **49**, 678–683.

285. W. Zhou, Z.-H. Shi, W. Liu and S.-P. Guo, Noncentrosymmetric chalcohalide $K_2Ba_3Ge_3S_9Cl_2$: A new nonlinear optical material with remarkable laser-induced damage threshold. *J. Alloys Compd.*, 2022, **895**, 162602.

286. A. G. Mikolaĭchuk, N. V. Moroz and P. Yu. Demchenko, Synthesis and electrical conductivity of a new $Ag_6SnS_4Br_2$ superionic compound. *Phys. Solid State*, 2010, **52**, 237–240.

287. P. Schwarz, J. Wachter and M. Zabel, Novel Coordination Modes for E4S3 Cage Molecules (E = P, As) in Unprecedented Quaternary $As_4S_3(CuCl)_n$ (n = 1,2) Solid-State Phases. *Eur. J. Inorg. Chem.*, 2008, **2008**, 5460–5463.

288. K. Feng, W. Yin, Z. Lin, J. Yao and Y. Wu, Five New Chalcohalides, Ba_3GaS_4X (X = Cl, Br), Ba_3MSe_4Cl (M = Ga, In), and $Ba_7In_2Se_6F_8$: Syntheses, Crystal Structures, and Optical Properties. *Inorg. Chem.*, 2013, **52**, 11503–11508.

289. H.-J. Zhao and P.-F. Liu, Synthesis, crystal and electronic structure, and optical property of the pentanary chalcohalide $Ba_3KSb_4S_9Cl$. *J. Solid State Chem.*, 2015, **232**, 37–41.

290. X. Liu, C. Wessel, F. Pan and R. Dronskowski, Synthesis and single-crystal structure determination of the zinc nitride halides Zn_2NX (X=Cl, Br, I). *J. Solid State Chem.*, 2013, **203**, 31–36.

291. G. Zhang, W.-W. Xiong, L. Nie and Q. Zhang. Synthesis, crystal structure and optical property of a novel metal chalcohalide: $ZnHg_3Se_2Cl_4$. *J. Solid State Chem.*, 2015, **230**, 182-185.

292. C.-Y. Zhang, X.-N. Niu, Y.-F. Wei, S.-X. Zhou, D.-Q. Yang, Y. Wang, J. Wang and B.-B. Zhang, $ZnGa_2S_4$: an infrared nonlinear optical material with large second-harmonic generation response and wide band gap. *Rare Met.*, 2024, 43,395-401.

293. B. Ji, F. Wang, K. Wu, B. Zhang and J. Wang, $Ba_6(Cu_xZ_y)Sn_4S_{16}$ (Z = Mg, Mn, Zn, Cd, In, Bi, Sn): High Chemical Flexibility Resulting in Good Nonlinear-Optical Properties. *Inorg. Chem.*, 2022, **61**, 2640–2651.

294. C. Cropek, V. Nguyen, S. K. Chhetri, J. Hu, S. Guo and J. Wang, Synthesis, Crystal and Electronic Structures, Nonlinear Optical Properties, and Magnetic Properties of Two Thiophosphates: $KInP_2S_7$ and $KCrP_2S_7$. *Crystals*, 2022, **12**, 1505.

295. S. Bardelli, Z. Ye, F. Wang, B. Zhang and J. Wang, Synthesis, Crystal and Electronic Structures, and Nonlinear Optical Properties of $Y_4Si_3S_{12}$. *Z. Fur Anorg. Und Allg. Chem.*, 2022, **648**, e202100388..

296. B. Ji, A. Sarkar, K. Wu, A. Swindle and J. Wang, $A_2P_2S_6$ (A = Ba and Pb): a good platform to study the polymorph effect and lone pair effect to form an acentric structure. *Dalton. Trans.*, 2022, **51**, 4522–4531.

297. V. Nguyen, B. Ji, K. Wu, B. Zhang and J. Wang, Unprecedented mid-infrared nonlinear optical materials achieved by crystal structure engineering, a case study of $(KX)P_2S_6$ (X = Sb, Bi, Ba). *Chem. Sci.*, 2022, **13**, 2640–2648.

298. F. Hou, D. Mei, Y. Zhang, F. Liang, J. Wang, J. Lu, Z. Lin and Y. Wu, $SrZnSnSe_4$: A quaternary selenide with large second harmonic generation and birefringence. *J. Alloy. Compd.*, 2022, **904**, 163944.

299. G. Cicirello, K. Wu, B. Zhang and J. Wang, Applying Band Gap Engineering to Tune Linear Optical and Nonlinear Optical Properties of Noncentrosymmetric Chalcogenides $La_4Ge_3Se_xS_{12-x}$ (x = 0, 2, 4, 6, 8, 10). Inorg. Chem. Front. 2021, **8**, 4914–4923.

300. Y. Cheng, H. Wu, H. Yu, Z. Hu, J. Wang and Y. Wu, Rational design of a promising oxychalcogenide infrared nonlinear optical crystal. *Chem. Sci.*, 2022, **13**, 5305-5310. .

301. Y.-F. Shi, S.-H. Zhou, B. Li, Y. Liu, X.-T. Wu, H. Lin and Q.-L. Zhu, $Ba_5Ga_2SiO_4S_6$: a Phase-Matching Nonlinear Optical Oxychalcogenide Design via Structural Regulation Originated from Heteroanion Introduction. *Inorg. Chem.*, 2023, **62**, 464-473.

302. X. Chen, Q. Jing and K. M. Ok, $Pb_{18}O_8Cl_{15}I_5$: A Polar Lead Mixed Oxyhalide with Unprecedented Architecture and Excellent Infrared Nonlinear Optical Properties. *Angew. Chem., Int. Ed.*, 2020, **59**, 20323–20327.

303. X. Chen, H. Jo and K. M. Ok, Inside Cover: Lead Mixed Oxyhalides Satisfying All Fundamental Requirements for High-Performance Mid-Infrared Nonlinear Optical Materials (Angew. Chem. Int. Ed. 19/2020). *Angew. Chem. Int. Ed.*, 2020, **59**, 7274.

304. H. Zhang, M. Zhang, S. Pan, X. Dong, Z. Yang, X. Hou, Z. Wang, K. B. Chang and K. R. Poeppelmeier, $Pb_{17}O_8Cl_{18}$: A Promising IR Nonlinear Optical Material with Large Laser Damage Threshold Synthesized in an Open System. *J. Am. Chem. Soc.*, 2015, **137**, 8360–8363.

305. H. Liu, Z. Song, H. Wu, Z. Hu, J. Wang, Y. Wu and H. Yu, $[Ba_2F_2][Ge_2O_3S_2]$: An Unprecedented Heteroanionic Infrared Nonlinear Optical Material Containing Three Typical Anions. *ACS Mater. Lett.*, 2022, **4**, 1593–1598.

306. H. K. Mao, Y. Wu, J. F. Shu, J. Z. Hu, R. J. Hemley and D. E. Cox, High-pressure phase transition and equation of state of lead to 238 GPa. *Solid State Commun.*, 1990, **74**, 1027–1029.

307. A. Salamat, R. Briggs, P. Bouvier, S. Petitgirard, A. Dewaele, M. E. Cutler, F. Corà, D. Daisenberger, G. Garbarino and P. F. McMillan, High-pressure structural transformations of Sn up to 138 GPa: Angle-dispersive synchrotron x-ray diffraction study. *Phys. Rev. B*, 2013, **88** ,104104.

308. S. Banumathy, R. K. Mandal and A. K. Singh, Structure of orthorhombic martensitic phase in binary Ti–Nb alloys. *J. Appl. Phys.*, 2009, **106**, 093518.

309. G. Arrhenius, E. Corenzwit, R. Fitzgerald, G. W. Hull, H. L. Luo, B. T. Matthias and W. H. Zachariasen, SUPERCONDUCTIVITY OF NB_3(Al, Ge) ABOVE 20.5°K. *Proc. National Acad. Sci.*, 1968, **61**, 621–628.

310. B. T. Matthias, T. H. Geballe, R. H. Willens, E. Corenzwit, and G. W. Hull, Jr., Superconductivity of Nb_3Ge. Phys. Rev. 139, A1501.

311. D. Jérome, A. Mazaud, M. Ribault and K. Bechgaard, Superconductivity in a synthetic organic conductor $(TMTSF)_2PF_6$. *J. Phys. Lett.*, 1980, **41**, 95–98.

312. P. W. Stephens, L. Mihaly, P. L. Lee, R. L. Whetten, S.-M. Huang, R. Kaner, F. Deiderich and K. Holczer, Structure of single-phase superconducting K_3C_{60}. *Nature*, 1991, **351**, 632–634.

313. O. Zhou and D. E. Cox, Structures of C_{60} intercalation compounds. *J. Phys. Chem. Solids*, 1992, **53**, 1373–1390.

314. S. Ren, J. Liu, D. Wang, J. Zhang, X. Ma, M. Knapp, L. Liu and H. Ehrenberg, Dielectric relaxation behavior induced by lithium migration in $Li_4Ti_5O_{12}$ spinel. *J. Alloy. Compd.*, 2019, **793**, 678–685.

315. S. G. Titova, A. V. Lukoyanov, S. V. Pryanichnikov, L. A. Cherepanova and A. N. Titov, Crystal and electronic structure of high temperature superconducting compound $Y_{1-x}Ca_xBa_2Cu_3O_y$ in the temperature interval 80–300 K. *J. Alloy. Compd.*, 2016, **658**, 891–897.

316. Z. M. Geballe, H. Liu, A. K. Mishra, M. Ahart, M. Somayazulu, Y. Meng, M. Baldini and R. J. Hemley, Synthesis and Stability of Lanthanum Superhydrides. *Angew. Chem. Int. Ed.*, 2018, **57**, 688–692.

317. V. S. Minkov, V. B. Prakapenka, E. Greenberg and M. I. Eremets, A Boosted Critical Temperature of 166 K in Superconducting D_3S Synthesized from Elemental Sulfur and Hydrogen. *Angew. Chem. Int. Ed.*, 2020, **59**, 18970–18974.

318. M. Tegel, I. Schellenberg, R. Pöttgen and D. Johrendt, A ^{57}Fe Mössbauer Spectroscopy Study of the 7 K Superconductor LaFePO. *Z. Fur Naturforsch. B*, 2008, **63**, 1057–1061.

319. J. Zhao, Q. Huang, C. de la Cruz, S. Li, J. W. Lynn, Y. Chen, M. A. Green, G. F. Chen, G. Li, Z. Li, J. L. Luo, N. L. Wang and P. Dai, Structural and magnetic phase diagram of $CeFeAsO_{1-x}F_x$ and its relation to high-temperature superconductivity. *Nat. Mater.*, 2008, 7, 953–959.

320. P. Quebe, L. J. Terbüchte and W. Jeitschko, Quaternary rare earth transition metal arsenide oxides RTAsO (T=Fe, Ru, Co) with ZrCuSiAs type structure. *J. Alloy. Compd.*, 2000, **302**, 70–74.

321. A. J. Corkett, D. G. Free, S. J. Cassidy, S. Ramos and S. J. Clarke, Control of the superconducting properties of $Sr_{2-x}Ca_xVO_3FeAs$ through isovalent substitution. *J. Solid State Chem.*, 2014, **216**, 91–98.

322. Y.-L. Sun, H. Jiang, H.-F. Zhai, J.-K. Bao, W.-H. Jiao, Q. Tao, C.-Y. Shen, Y.-W. Zeng, Z.-A. Xu and G.-H. Cao, $Ba_2Ti_2Fe_2As_4O$: A New Superconductor Containing Fe_2As_2 Layers and Ti_2O Sheets. *J. Am. Chem. Soc.*, 2012, **134**, 12893–12896.

323. H. Ogino, Y. Katsura, S. Horii, K. Kishio and J.-i. Shimoyama, New iron-based arsenide oxides $(Fe_2As_2)(Sr_4M_2O_6)$(M = Sc, Cr). *Supercond. Sci. Technol.*, 2009, **22**, 085001.

324. J. Ballato, J. S. Lewis III and P. Holloway. Display Applications of Rare-Earth-Doped Materials. *MRS Bulletin*, 1999, **24**, 51-56.

325. J. Meyer and F. Tappe. Photoluminescent Materials for Solid-State Lighting: State of the Art and Future Challenges. *Adv. Opt. Mater*. 2015, **3**, 424-430.

326. G. Blasse and B. C. Grabmaier, A General Introduction to Luminescent Materials. In: Luminescent Materials. Springer, Berlin, Heidelberg. 1994.

327. Q. Xu, T. Kuang, Y. Liu, L. Cai, X. Peng, T. Sreenivasan Sreeprasad, P. Zhao, Z. Yu and N. Li, Heteroatom-doped carbon dots: synthesis, characterization, properties, photoluminescence mechanism and biological applications, *J. Mater. Chem. B Mater. Biol. Med.*, 2016, **4**, 7204–7219.

328. W. R. Algar, M. Massey, K. Rees, R. Higgins, K. D. Krause, G. H. Darwish, W. J. Peveler, Z. Xiao, H.-Y. Tsai, R. Gupta, K. Lix, M. V. Tran and H. Kim, Photoluminescent nanoparticles for chemical and biological analysis and imaging, *Chem. Rev.*, 2021, **121**, 9243–9358.

329. K. Y. Zhang, Q. Yu, H. Wei, S. Liu, Q. Zhao and W. Huang, Long-lived emissive probes for time-resolved photoluminescence bioimaging and biosensing, *Chem. Rev.*, 2018, **118**, 1770–1839.

330. T. Lu, Z. Ma, C. Du, Y. Fang, H. Wu, Y. Jiang, L. Wang, L. Dai, H. Jia, W. Liu and H. Chen, Temperature-dependent photoluminescence in light-emitting diodes, *Sci. Rep.*,2014,**4**,6131.

331. S. Kaur, H. Kaur, A. S. Rao and G. V. Prakash, A review on photoluminescence phosphors for biomedical, temperature sensing, photovoltaic cell, anti-counterfeiting and white LED applications, *Physica B Condens. Matter*, 2024, **690**, 416224.

332. J. Meyer and F. Tappe, Photoluminescent materials for solid-state lighting: State of the art and future challenges, *Adv. Opt. Mater.*, 2015, **3**, 424–430.

333. X.-L. Shi, J. Zou and Z.-G. Chen. Advanced Thermoelectric Design: From Materials and Structures to Devices. *Chem. Rev.* 2020, **120**, 15, 7399–7515

334. S. D. N. Luu and P. Vaqueiro, Thermoelectric properties of $BiOCu_{1-x}M_xSe$ (M = Cd and Zn). *Semicond. Sci. Technol.*, 2014, **29**, 064002.

335. L.-D. Zhao, J. He, D. Berardan, Y. Lin, J.-F. Li, C.-W. Nan and N. Dragoe, BiCuSeO oxyselenides: new promising thermoelectric materials. *Energy Env. Sci.*, 2014, **7**, 2900–2924.

336. T. Suzuki, M. S. Bahramy, R. Arita, Y. Taguchi and Y. Tokura, Doping control and thermoelectric properties in $R_{1-x}A_xZnSbO$ (R = La, Ce; A = Ca, Sr). *Phys. Rev. B*, 2011, **83**. 035204.

337. K. Chatterjee and S. E. Skrabalak. Durable Metal Heteroanionic Photocatalysts. *ACS Appl. Mater. Interfaces*. 2021, **13**, 36670-36678.

338. J. T. Incorvati, L. F. Wan, B. Key, D. Zhou, C. Liao, L. Fuoco, M. Holland, H. Wang, D. Prendergast, K. R. Poeppelmeier and J. T. Vaughey, Reversible Magnesium Intercalation into a Layered Oxyfluoride Cathode. *Chem. Mater.* 2016, **28,** 17– 20.

339. B. Marr, How much data do we create every day? The mind-blowing stats everyone should read, https://bernardmarr.com/how-much-data-do-we-create-every-day-the-mind-blowing-stats-everyone-should-read/, (accessed September 3, 2024).

340. J. F. Scott, Multiferroic memories, *Nat. Mater.*, 2007, **6**, 256–257.

341. R. Tahir, S. Fatima, S. A. Zahra, D. Akinwande, H. Li, S. H. M. Jafri and S. Rizwan, Multiferroic and ferroelectric phases revealed in 2D $Ti_3C_2T_x$ MXene film for high performance resistive data storage devices, *Npj 2D Mater. Appl.*,2023,**7**,7.

342. F. Yang, M. H. Tang, Z. Ye, Y. C. Zhou, X. J. Zheng, J. X. Tang, J. J. Zhang and J. He, Eight logic states of tunneling magnetoelectroresistance in multiferroic tunnel junctions, *J. Appl. Phys.,*2007,***102***,*044504.

343. S. Manipatruni, D. E. Nikonov, C.-C. Lin, T. A. Gosavi, H. Liu, B. Prasad, Y.-L. Huang, E. Bonturim, R. Ramesh and I. A. Young, Scalable energy-efficient magnetoelectric spin–orbit logic, *Nature*, 2019, **565**, 35–42.

344. L. Keeney, T. Maity, M. Schmidt, A. Amann, N. Deepak, N. Petkov, S. Roy, M. E. Pemble and R. W. Whatmore, Magnetic field-induced ferroelectric switching in multiferroic Aurivillius phase thin films at room temperature, *J. Am. Ceram. Soc.*, 2013, **96**, 2339–2357.

345. M. M. Vopson, E. Zemaityte, M. Spreitzer and E. Namvar, Multiferroic composites for magnetic data storage beyond the super-paramagnetic limit, *J. Appl. Phys.*, 2014,**116**, 113910.

346. M. M. Vopson, Fundamentals of multiferroic materials and their possible applications, *Crit. Rev. Solid State Mater. Sci.*, 2015, **40**, 223–250.

347. R. Jasrotia, Suman, R. Khargotra, A. Verma, I. Sharma and R. Verma, in *Engineering Materials*, Springer Singapore, Singapore, 2021, pp. 195–213.

348. S. Sharma, A. Paliwal, M. Tomar and V. Gupta, Multiferroic BFO/BTO multilayer structures based magnetic field sensor, *Physica B Condens. Matter*, 2019, **571**, 1–4.

349. G. Yuan, R. Xu, H. Wu, Y. Xing, C. Yang, R. Zhang, W. Tang, Y. Wang and Y. Wang, High-temperature multiferroic magnetoelectric sensors, *Appl. Phys. Lett.*,2022,**121**,192903.

350. B.Stojanovic, *Magnetic, Ferroelectric, and Multiferroic Metal Oxides*; Korotcenkov, G., Series Ed.; Elsevier Science Publishing: Philadelphia, PA, 2018, pp-658.

351. M. Trassin, Low energy consumption spintronics using multiferroic heterostructures, *J. Phys. Condens. Matter*, 2016, **28**, 033001.

352. H. Wu, A. Tatarenko, M. I. Bichurin and Y. Wang, A multiferroic module for biomechanical energy harvesting, *Nano Energy*, 2021, **83**, 105777.

353. N. A. Spaldin, S.-W. Cheong and R. Ramesh, Multiferroics: Past, present, and future, *Phys. Today*, 2010, **63**, 38–43.

354. T.-D. Onuta, Y. Wang, C. J. Long and I. Takeuchi, Energy harvesting properties of all-thin-film multiferroic cantilevers, *Appl. Phys. Lett.,* 2011,**99**,203506.

355. J. F. Scott, Room-temperature multiferroic magnetoelectrics, *NPG Asia Mater.*, 2013, **5**, e72–e72.

356. M. Liu and N. X. Sun, Voltage control of magnetism in multiferroic heterostructures, *Philos. Trans. A Math. Phys. Eng. Sci.*, 2014, **372**, 20120439.

357. J. Yang, W. Bai, Y. Zhang, C.-G. Duan, J. Chu and X. Tang, Dielectric phenomena of multiferroic oxides at acoustic- and radio-frequency, *J. Phys. Condens. Matter*, 2023, **35**, 463001.

358. H. Lin, Y. Gao, X. Wang, T. Nan, M. Liu, J. Lou, G. Yang, Z. Zhou, X. Yang, J. Wu, M. Li, Z. Hu and N. X. Sun, Integrated magnetics and multiferroics for compact and power-efficient sensing, memory, power, RF, and microwave electronics, *IEEE Trans. Magn.*, 2016, **52**, 1–8.

359. V. A. Khomchenko, D. A. Kiselev, I. K. Bdikin, V. V. Shvartsman, P. Borisov, W. Kleemann, J. M. Vieira and A. L. Kholkin, Crystal structure and multiferroic properties of Gd-substituted $BiFeO_3$, *Appl. Phys. Lett.*,2008,**93**,262905.

360. T. Lottermoser and D. Meier, A short history of multiferroics, *Phys. Sci. Rev.*, 2021,**6**, 20200032.

361. M. Fiebig, T. Lottermoser, D. Meier and M. Trassin, The evolution of multiferroics, *Nat. Rev. Mater.*,2016,**1**,16046.

362. N. A. Spaldin and R. Ramesh, Advances in magnetoelectric multiferroics, *Nat. Mater.*, 2019, **18**, 203–212.

363. P. Barone, B. Sanyal and S. Picozzi,Multiferroics: Theory, Mechanisms, and Materials, in *Science and Technology of Atomic, Molecular, Condensed Matter & Biological Systems*, Elsevier, 2012, pp. 129–161.

364. W. Eerenstein, N. D. Mathur and J. F. Scott, Multiferroic and magnetoelectric materials, *Nature*, 2006, **442**, 759–765.

365. C.-W. Nan and J.-M. Liu, Multiferroics: a beautiful but challenging multi-polar world, *Natl. Sci. Rev.*, 2019, **6**, 620–620.

366. Y. Gao, M. Gao and Y. Lu, Two-dimensional multiferroics, *Nanoscale*, 2021, **13**, 19324–19340.

367. D. Khomskii, Classifying multiferroics: Mechanisms and effects, *Physics.,2009,***2***,*20.

368. S.-W. Cheong and M. Mostovoy, Multiferroics: a magnetic twist for ferroelectricity, *Nat. Mater.*, 2007, **6**, 13–20.

369. N. A. Spaldin, Multiferroics beyond electric-field control of magnetism, *Proc. Math. Phys. Eng. Sci.*, 2020, **476**, 20190542.

370. S. Dong, J.-M. Liu, S.-W. Cheong and Z. Ren, Multiferroic materials and magnetoelectric physics: symmetry, entanglement, excitation, and topology, *Adv. Phys.*, 2015, **64**, 519–626.

371. S.-W. Cheong, D. Talbayev, V. Kiryukhin and A. Saxena, Broken symmetries, non-reciprocity, and multiferroicity, *Npj Quantum Mater.,* 2018,**3**,19.

372. H. Liu and X. Yang, A brief review on perovskite multiferroics, *Ferroelectrics*, 2017, **507**, 69–85.

373. C. Lu, M. Wu, L. Lin and J.-M. Liu, Single-phase multiferroics: new materials, phenomena, and physics, *Natl. Sci. Rev.*, 2019, **6**, 653–668.

374. T. Jia, Z. Cheng, H. Zhao and H. Kimura, Domain switching in single-phase multiferroics, *Appl. Phys. Rev.*, 2018, **5**, 021102.

375. R. Ramesh and N. A. Spaldin, Multiferroics: progress and prospects in thin films, *Nat. Mater.*, 2007, **6**, 21–29.

376. L. W. Martin, S. P. Crane, Y.-H. Chu, M. B. Holcomb, M. Gajek, M. Huijben, C.-H. Yang, N. Balke and R. Ramesh, Multiferroics and magnetoelectrics: thin films and nanostructures, *J. Phys. Condens. Matter*, 2008, **20**, 434220.

377. S. Roy and S. B. Majumder, Recent advances in multiferroic thin films and composites, *J. Alloys Compd.*, 2012, **538**, 153–159.

378. C. Lu, W. Hu, Y. Tian and T. Wu, Multiferroic oxide thin films and heterostructures, *Appl. Phys. Rev.*,2015, **2** , 021304.

379. J. S. Andrew, J. D. Starr and M. A. K. Budi, Prospects for nanostructured multiferroic composite materials, *Scr. Mater.*, 2014, **74**, 38–43.

380. C.-W. Nan, M. I. Bichurin, S. Dong, D. Viehland and G. Srinivasan, Multiferroic magnetoelectric composites: Historical perspective, status, and future directions, *J. Appl. Phys.*,2008, **103**, 031101.

381. C. W. Nan, Y. Lin and J. H. Huang, Magnetoelectricity of multiferroic composites, *Ferroelectrics*, 2002, **280**, 153–163.

382. W. Qin, B. Xu and S. Ren, An organic approach for nanostructured multiferroics, *Nanoscale*, 2015, **7**, 9122–9132.

383. X.-L. Liu, D. Li, H.-X. Zhao, X.-W. Dong, L.-S. Long and L.-S. Zheng, Inorganic–organic hybrid molecular materials: From multiferroic to magnetoelectric, *Adv. Mater.*,2021,**33**, 2004542.

384. Y. Yang, J. Ji, J. Feng, S. Chen, L. Bellaiche and H. Xiang, Two-dimensional organic–inorganic room-temperature multiferroics, *J. Am. Chem. Soc.*, 2022, **144**, 14907–14914.

385. Z. Hu, H. Zhao, Z. Cheng, J. Ding, H. Gao, Y. Han, S. Wang, Z. Xu, Y. Zhou, T. Jia, H. Kimura and M. Osada, van der Waals force layered multiferroic hybrid perovskite $(CH_3NH_3)_2CuCl_4$ single crystals, *Phys. Chem. Chem. Phys.*, 2020, **22**, 4235–4239.

386. K. Aizu, Possible species of ferromagnetic, ferroelectric, and ferroelastic crystals, *Phys. Rev.*, 1970, **2**, 754–772.

387. I. E. Dzyaloshinskii, On the Magneto-Electrical Effect in Antiferromagnets, *Sov Phys JETP*, 1960, **10**, 628–629.

388. D. C. Freitas, R. Weht, A. Sulpice, G. Remenyi, P. Strobel, F. Gay, J. Marcus and M. Núñez-Regueiro, Ferromagnetism in layered metastable 1*T*-$CrTe_2$, *J. Phys. Condens. Matter*, 2015, **27**, 176002.

389. Y. Liu, S. Kwon, G. J. de Coster, R. K. Lake and M. R. Neupane, Structural, electronic, and magnetic properties of $CrTe_2$, *Phys. Rev. Mater.*, 2022,**6**, 084004.

390. Y. Ou, W. Yanez, R. Xiao, M. Stanley, S. Ghosh, B. Zheng, W. Jiang, Y.-S. Huang, T. Pillsbury, A. Richardella, C. Liu, T. Low, V. H. Crespi, K. A. Mkhoyan and N. Samarth, $ZrTe_2/CrTe_2$: an epitaxial van der Waals platform for spintronics, *Nat. Commun.*,2022,**13**, 2972.

391. S. V. Kiselev, R. P. Ozerov and G. S. Zhdanov, Detection of Magnetic Order in Ferroelectric $BiFeO_3$ by Neutron Diffraction, *Sov Phys Dokl.*1963,**7**, 742.

392. S. A. Fedulov, Determination of Curie Temperature for $BiFeO_3$ Ferroelectric, *Dokl Akad Nauk SSSR*, 1961, **139**, 1345–1346.

393. B. Ji, F. Wang, K. Wu, B. Zhang and J. Wang, d^6*versus* d^{10}, which is better for second harmonic generation susceptibility? A case study of $K_2TGe_3ch_8$ (T = Fe, Cd; Ch = S, Se), *Inorg. Chem.*, 2023, **62**, 574–582.

394. B. Ji, K. Pandey, C. P. Harmer, F. Wang, K. Wu, J. Hu and J. Wang, Centrosymmetric or noncentrosymmetric? Transition metals talking in $K_2TGe_3S_8$(T = co, Fe), *Inorg. Chem.*, 2021, **60**, 10603–10613.

395. Y. N. Venevtsev, G. S. Zhdanov, E. V. Bezus and V. V. Ivanova, Crystal Chemical Studies of Substances with Perovskite-Type Structure and Special Dielectric Properties, *Kristallografiya*, 1960, **5**, 620–626.

396. E. F. Bertaut, F. Forrat and P. Fang, Les Manganites de Terres Rares et d'ytrium: Une Nouvelle Classe de Ferroélectriques, *Comptes Rendus Acad Sci*, 1963, **256**, 1958–1961.

397. L. N. Kholodkovskaya, V. A. Dolgikh and B. A. Popovkin, The crystal structure of the new pyroelectric phase $Bi_4Te_2O_9Br_2$, *J. Solid State Chem.*, 1995, **116**, 406–408.

398. E. Ascher, H. Rieder, H. Schmid and H. Stössel, Some properties of ferromagnetoelectric nickel-iodine boracite, $Ni_3B_7O_{13}I$, *J. Appl. Phys.*, 1966, **37**, 1404–1405.

399. V. E. Wood and A. E. Austin, Possible Applications for Magnetoelectric Materials, *Int J Magn*, 1974, **5**, 303–315.

400. L. Zhao, M. T. Fernández-Díaz, L. H. Tjeng and A. C. Komarek, Oxyhalides: A new class of high- *T C* multiferroic materials, *Sci. Adv.*,2016,**2**,e1600353.

401. M. Markov, L. Alaerts, H. P. C. Miranda, G. Petretto, W. Chen, J. George, E. Bousquet, P. Ghosez, G.-M. Rignanese and G. Hautier, Ferroelectricity and multiferroicity in anti–Ruddlesden–Popper structures, *Proc. Natl. Acad. Sci. U. S. A.*, 2021,**118**,e2026020118.

402. J. Young, P. Lalkiya and J. M. Rondinelli, Design of noncentrosymmetric perovskites from centric and acentric basic building units, *J. Mater. Chem. C Mater. Opt. Electron. Devices*, 2016, **4**, 4016–4027.

The authors confirm that the data supporting the findings of this study are available within the article and its supplementary materials.